

THE INFLUENCE OF SOUTHERN OCEAN SHORTWAVE CLOUD FEEDBACKS
ON THE COUPLED CLIMATE SYSTEM

by

WILLIAM RAYMOND FREY

B.S., University of Michigan, 2005

M.A., University of Oklahoma, 2011

M.S., Air Force Institute of Technology, 2013

A thesis submitted to the
Faculty of the Graduate School of the
University of Colorado in partial fulfillment
of the requirements for the degree of
Doctor of Philosophy
Department of Atmospheric and Oceanic Sciences

2018

This thesis entitled:
The influence of Southern Ocean shortwave cloud feedbacks on the coupled climate system
written by William Raymond Frey
has been approved for the Department of Atmospheric and Oceanic Sciences

Prof. Jennifer E. Kay

Prof. Kristopher B. Karnauskas

Prof. Ben Livneh

Dr. Brian Medeiros

Dr. Isla R. Simpson

Date_____

The final copy of this thesis has been examined by the signatories, and we find that both the content and the form meet acceptable presentation standards of scholarly work in the above mentioned discipline.

Abstract

Frey, William R. (Ph.D., Atmospheric and Oceanic Sciences)

The Influence of Southern Ocean Shortwave Cloud Feedbacks on the Coupled Climate System

Thesis directed by Assistant Professor Jennifer E. Kay

The Southern Ocean, a unique region where clouds, ocean dynamics and sea ice interact to influence climate, has historically been poorly modeled and observed. Here, we improve a global climate model and use newly-available surface-independent cloud observations to establish how Southern Ocean cloud feedbacks impact global climate change. We modify the Community Earth System Model (CESM) by increasing supercooled cloud liquid to better match observations over the Southern Ocean. In the modified model, two extratropical cloud feedbacks cause equilibrium climate sensitivity (ECS, the equilibrium warming in response to doubled CO₂) to increase from 4.1 K in the control to 5.6 K. First, reduced conversion of cloud ice to liquid at high southern latitudes decreases the magnitude of a negative cloud phase feedback. Second, warming is amplified in the mid-latitudes by a larger positive shortwave cloud cover feedback. Despite the 1.5 K ECS increase, transient 21st century warming hardly increases in the modified model over the control because ocean heat uptake moves heat input by extratropical cloud feedbacks to depth. Persistent extratropical ocean heat uptake implies that extratropical cloud biases may not be as important to 21st century warming as biases in other regions. Next, we determine how interactions with sea ice impact Southern Ocean cloud feedbacks. We use surface-independent cloud observations to diagnose how present-day sea ice–cloud interactions during spring and summer impact top-of-atmosphere albedo. Observed low cloud cover and opacity are larger over open

water compared to over sea ice. The cloud opacity increase is due to an ice-toward-liquid cloud phase shift with no change in air-sea coupling. Even with the cloud response, top-of-atmosphere albedo decreases as sea ice retreats. In CESM, the cloud and albedo responses to sea ice variability are of the same sign but larger in magnitude than the observed responses. The modeled cloud opacity increase is linked to strengthened air-sea coupling rather than a cloud phase shift. Strengthened air-sea coupling with decreasing sea ice could impact model-predicted cloud feedbacks in a way inconsistent with observations. Our results highlight how Southern Ocean shortwave cloud feedbacks influence climate change in the coupled climate system.

Acknowledgements

Chapters 2, 3, and 4 are versions of the following articles, respectively, and should be cited as follows:

Frey, W. R., & Kay, J. E. (2018). The influence of extratropical cloud phase and amount feedbacks on climate sensitivity. *Climate Dynamics*, 50, 3097-3116. <https://doi.org/10.1007/s00382-017-3796-5>

Frey, W. R., Maroon, E. A., Pendergrass, A. G., & Kay, J. E. (2017). Do Southern Ocean cloud feedbacks matter for 21st century warming? *Geophysical Research Letters*, 44, 12,447–12,456. <https://doi.org/10.1002/2017GL076339>

Frey, W. R., Morrison, A. L., Kay, J. E., Guzman, R., & Chepfer, H. (2018). The combined influence of observed Southern Ocean clouds and sea ice on top-of-atmosphere albedo. *Journal of Geophysical Research: Atmospheres*, 123, 4461–4475. <https://doi.org/10.1029/2018JD028505>

This dissertation is the result of collaborations with many people who have graciously devoted their time and effort and greatly enhanced the quality of my work. I give sincere thanks to:

- Professor Jen Kay for her constant assistance and encouragement. With her guidance and support, I have learned more in my three years of graduate school than I ever thought possible.
- Current and past members of the Kay Group at CU including Matt Gentry, Elizabeth Maroon, Nate Miller, Ariel Morrison, Angie Pendergrass, Joe Sedlar, and Vineel Yettella, for their feedback and friendship.
- Kris Karnauskas, Ben Livneh, Brian Medeiros, and Isla Simpson for agreeing to be on my Ph.D. committee and for many helpful discussions along the way.
- Helene Chepfer and Rodrigo Guzman for their expertise which was essential in my efforts to understand and use CALIPSO cloud observations.
- U.S. Air Force Weather and the Air Force Institute of Technology, for providing me the opportunity, funding, and time to earn a Ph.D. in the midst of my ongoing career.

Finally, and most importantly, I thank my family. Thanks to my wife, Kelly, for her love and support and to my kids, Ella, Luke, Clara, and Jacob for their curiosity and perspective. Thanks to my parents, Pat and Roger, for nurturing my interest in weather and for their continuing encouragement and love.

The views expressed in this thesis are those of the authors and do not reflect the official policy or position of the United States Air Force, Department of Defense, or the U.S. Government.

Table of Contents

1	Introduction	1
1.1	Climate Change and Radiative Feedbacks.....	1
1.2	Climate Models.....	3
1.2.1	Types of Climate Models.....	3
1.2.2	The Community Earth System Model.....	4
1.2.3	Hierarchy of Model Configurations.....	5
1.2.4	Climate Change Scenarios and Metrics.....	6
1.3	Cloud Feedbacks Predicted by Climate Models.....	7
1.4	The Southern Ocean’s Importance to Global Climate.....	8
1.5	Synopsis.....	9
2	The Influence of Extratropical Cloud Phase and Amount Feedbacks on Climate Sensitivity	11
2.1	Abstract.....	11
2.2	Introduction.....	12
2.3	Model Description and Methods.....	16
2.3.1	Model Configuration.....	16
2.3.2	Model Runs.....	19
2.3.3	Analysis Techniques.....	21
2.4	Results.....	23
2.4.1	Impact of Model Cloud Changes on Climate Sensitivity.....	23
2.4.2	Comparison of the Negative Shortwave Cloud Feedback.....	25
2.4.3	Comparison of the Positive Shortwave Cloud Feedback.....	29
2.4.4	Identification of Sea Surface Temperature as the Primary Control on the Positive Mid-Latitude Feedback.....	32
2.4.5	Evidence for a Proposed Mechanism Underlying SST-Cloud Feedback.....	37
2.4.6	The Impact of Ocean Heat Uptake on Surface Warming and Cloud Feedbacks.....	39
2.5	Discussion.....	43
2.6	Summary.....	47
2.7	The Impact of Model Tuning on Shortwave Cloud Feedbacks.....	49
3	Do Southern Ocean Cloud Feedbacks Matter for 21st Century Warming?	53
3.1	Abstract.....	53
3.2	Introduction.....	53
3.3	Model Description.....	56
3.4	Results.....	57
3.4.1	Surface Warming.....	57
3.4.2	Radiative Feedback Analysis.....	59
3.4.3	Ocean Heat Uptake.....	61
3.4.4	Ocean Dynamics.....	62
3.5	Discussion.....	64
3.6	Conclusion.....	68

4	The Combined Influence of Observed Southern Ocean Clouds and Sea Ice on Top-of-Atmosphere Albedo	70
4.1	Abstract.....	70
4.2	Introduction.....	71
4.3	Data and Methods.....	74
4.3.1	Data.....	74
4.3.2	Methods.....	78
4.4	Results.....	79
4.4.1	Seasonal Sea Ice Concentration and Low Cloud Cover.....	79
4.4.2	Spring and Summer Low Cloud Cover across the Sea Ice Edge.....	80
4.4.3	Spring and Summer Low Cloud Cover Response to Sea Ice Variability.....	81
4.4.4	Spring and Summer Cloud Opacity Response to Sea Ice Variability.....	84
4.4.5	Combined Impact of Sea Ice Variability and Cloud Response on Top-of-Atmosphere Albedo.....	87
4.4.6	Insensitivity of Results to the Definitions of Sea Ice and Open Water.....	88
4.5	Discussion.....	91
4.5.1	Cloud and Albedo Response to Sea Ice Variability Revealed with Surface-Independent Observations.....	91
4.5.2	Potential Mechanisms for Increasing Opaque Cloud Fraction.....	91
4.5.3	Influence of Sea Ice on Southern Ocean Shortwave Cloud Radiative Feedbacks.....	93
4.6	Summary and Conclusions.....	94
5	The Combined Influence of Southern Ocean Clouds and Sea Ice on Top-of-Atmosphere Albedo in the Community Earth System Model	96
5.1	Introduction.....	96
5.2	Model and Methods.....	97
5.2.1	Model Set Up.....	97
5.2.2	Methods.....	98
5.3	Spring and Summer Cloud and Albedo Response to Sea Ice Variability in CESM Compared with Observations.....	98
5.3.1	Low Cloud Cover.....	98
5.3.2	Opaque Cloud Fraction.....	101
5.3.3	Top-of-Atmosphere Albedo.....	101
5.4	Discussion.....	102
5.4.1	Cloud and Albedo Response to Sea Ice Variability in CESM.....	102
5.4.2	Mechanisms for Increasing Opaque Cloud Fraction in CESM Compared to Observations.....	102
5.4.3	Influence of Sea Ice on Southern Ocean Shortwave Cloud Radiative Feedbacks in CESM.....	103
5.5	Summary.....	104
6	Conclusions and Future Work	106
6.1	Synopsis.....	106

6.2 How Southern Ocean Cloud Phase Impacts Cloud Feedbacks and Climate Change
Projections in a Global Climate Model 106

6.3 The Observed and Modeled Influence of Sea Ice Variability on Southern Ocean Clouds
and Top-of-Atmosphere Albedo 108

6.4 Concluding Thoughts 111

Bibliography **112**

List of Tables

2.1	Description of model runs.....	21
2.2	Global annual mean 2xCO ₂ forcing, surface warming, and feedbacks.....	25
2.3	Difference in shortwave cloud feedbacks between the slab ocean experiment and control	45
2.4	Description of atmosphere-only model runs.....	51
4.1	Summer cruises of the icebreaker Polarstern used in this study.....	77
4.2	Summary of main findings	89
5.1	CESM results within the intermittent mask.....	99

List of Figures

1.1	Cloud feedbacks in CMIP5 models.....	8
2.1	Annual zonal mean absorbed shortwave radiation bias (model minus observations).....	19
2.2	Change in global annual mean surface temperature between 2xCO ₂ and 1xCO ₂ runs....	24
2.3	Annual mean shortwave cloud feedback normalized by the annual global mean change in surface temperature between 2xCO ₂ and 1xCO ₂ model runs.....	26
2.4	Comparison of annual and zonal-mean cloud properties and feedbacks in slab ocean model runs.....	28
2.5	Change in annual mean low cloud fraction between 2xCO ₂ and 1xCO ₂ slab ocean model runs.....	31
2.6	Annual mean change in Estimated Inversion Strength, Sea Surface Temperature, and 700 hPa Vertical Velocity in slab ocean model runs.....	34
2.7	Joint frequency distributions created with data from SOM1xExp over the Southern Ocean region between 30 and 60 degrees south latitude	35
2.8	Probability distribution functions of 700 hPa vertical velocity, sea surface temperature, and estimated inversion strength paired with mean low cloud fraction.....	37
2.9	Vertical profiles of cloud fraction and relative humidity	38
2.10	Change in surface warming pattern.....	41
2.11	Annual mean difference in surface heat flux, zonally integrated surface heat flux, and ocean heat content.....	42
2.12	Annual mean difference in sea surface temperature and low cloud fraction.....	43
2.13	Shortwave cloud feedbacks and change in low cloud fraction	51
3.1	Relationship between equilibrium climate sensitivity (ECS) and transient 21 st century warming in global climate models.....	55
3.2	Surface warming above pre-industrial (1850-1899)	58
3.3	21 st century radiative feedbacks (2091-2100 minus 1996-2005).....	60

3.4	21 st century ocean heat uptake (OHU) anomalies compared to pre-industrial (1850-1899)	62
3.5	21 st century ocean heat content and meridional overturning circulation (MOC) streamfunction compared to pre-industrial (1850-1899)	63
4.1	CALIPSO-GOCCP data demonstration	76
4.2	Seasonal Antarctic sea ice and low cloud cover	80
4.3	Spring and Summer Low Cloud Cover and Sea Ice Concentration as a function of meridional distance from the sea ice edge	81
4.4	Low cloud cover within the intermittent mask	82
4.5	Ship-Based cloud observations	83
4.6	Ship-Based meteorological profiles	85
4.7	Opaque cloud fraction within the intermittent mask	86
4.8	Probability density functions of the altitude of CALIPSO LIDAR signal attenuation	87
4.9	Top-of-Atmosphere all-sky albedo within the intermittent mask	89
4.10	CALIPSO low cloud cover, CALIPSO opaque cloud fraction, and CERES top-of-atmosphere all-sky albedo as a function of NSIDC sea ice concentration	90
5.1	CESM CALIPSO-simulated low cloud cover, opaque cloud fraction, and CESM top-of-atmosphere all-sky albedo as a function of sea ice concentration	100

Chapter 1

Introduction

1.1 Climate Change and Radiative Feedbacks

Earth's climate state is determined by an energy balance between incoming solar radiation and outgoing longwave radiation (OLR). When a forcing is imposed that upsets the energy balance, the climate responds through a variety of feedbacks until a new energy balance is reached. One such forcing is anthropogenic emission of CO₂, a greenhouse gas. Increased concentration of atmospheric CO₂ causes OLR to decrease, creating a positive energy imbalance with more energy coming into the Earth system than going out. The primary feedback that acts to restore energy balance is the negative temperature feedback. In response to the positive energy imbalance, the Earth warms. OLR is strongly linked to temperature, so as Earth warms OLR increases until a new, warmer, climate state is reached that again balances incoming solar radiation with OLR. In the absence of any other feedbacks, the temperature feedback alone would bring Earth back to an equilibrium with a warming of about 1K after a doubling of CO₂ (Mauritsen et al., 2013).

Current best estimates of the warming caused by a doubling CO₂ are much greater than 1K (2.1 - 4.7 K, Flato et al. (2013)) because the climate system includes other positive and negative feedbacks in addition to the temperature feedback (e.g. Coleman, 2003; Mauritsen et al., 2013). The negative temperature feedback described above can be broken into two components. The first component of the temperature feedback is the Planck feedback, which describes the radiative response to a vertically uniform temperature change equal to the change in surface temperature. Because the upper atmosphere radiates to space more effectively from the surface, the deviation from vertically uniform warming is also important. Thus, the second component of the temperature

feedback is the lapse rate feedback, which describes the radiative response due to the deviation from vertically uniform warming. As the atmosphere warms it is able to hold more water vapor, a strong greenhouse gas, creating a positive feedback (e.g. Manabe & Wetherald, 1967; Dessler et al., 2008). Increased water vapor concentration decreases OLR and pushes the system further from energy balance, thus increasing warming. Other feedbacks impact the amount of solar, or shortwave, radiation being absorbed by the system. One example of a shortwave feedback is the positive surface albedo feedback (e.g. Budyko, 1969; Sellers, 1969; Hall, 2004). Increased temperatures cause land and sea ice to melt and snow cover to shrink, decreasing surface albedo and allowing more shortwave radiation to be absorbed.

Feedbacks related to clouds are one of the most uncertain aspects of climate change in part because of the many ways clouds impact Earth's radiation budget. The longwave and shortwave radiative effect of clouds is largely determined by cloud cover, optical depth, and altitude. Cloud cover defines the areal extent of clouds while optical depth quantifies how much radiation is transmitted through a cloud compared to the incident radiation. Cloud optical depth depends on both the amount of water in the cloud and how that water is partitioned between ice and liquid because of differences in ice and liquid cloud particle size. Changes in cloud cover, optical depth, and altitude with warming modify the radiative effect of clouds and create cloud radiative feedbacks (e.g. Schneider, 1972; Schneider & Dickinson, 1974; Zelinka et al., 2012a).

Clouds impact Earth's radiation budget by decreasing the amount of longwave radiation emitted to space (a warming effect) and increasing the amount of solar shortwave radiation reflected back to space (a cooling effect). An increase in cloud cover with warming enhances these impacts and would create a positive longwave feedback and a negative shortwave feedback. A decrease in cloud cover with warming would have the opposite effects. Changes in cloud optical

depth create a feedback because cloud optical depth determines cloud emissivity and albedo. An increase in cloud optical depth with warming would enhance the greenhouse effect of the cloud and create a positive longwave feedback. At the same time, an increase in cloud optical depth with warming would increase cloud albedo and produce a negative shortwave feedback. Changes in cloud altitude create a longwave feedback because cloud altitude is closely linked to cloud temperature. As the climate warms, clouds are expected to rise in altitude while maintaining a constant temperature. Because the cloud top temperature remains constant, the radiation emitted by clouds remains constant even as the climate warms and creates a positive feedback (Hartmann & Larson, 2002). Changes in cloud altitude have a small shortwave effect because cloud albedo is largely independent of cloud altitude.

1.2 Climate Models

1.2.1 Types of Climate Models

The varied and interconnected feedbacks involved in climate change necessitate a comprehensive modeling approach that takes into account the entire Earth system. Techniques used to model climate have advanced substantially over the last half century. Manabe and Wetherald (1967) pioneered climate modeling by using a one-dimensional radiative-convective equilibrium model to show that a doubling of CO₂ along with a water vapor feedback consistent with a constant relative humidity atmosphere would result in a warming of 2.3 K. Rapid advancements followed, resulting in coupled general circulation models (GCMs), which solve the equations of motion to represent the 3-dimensional climate. The first GCM to include both the atmosphere and the ocean was developed by Manabe and Bryan (1969) before a cryosphere component was added (Manabe & Wetherald, 1975). Models showing the impact of cloud

feedbacks arrived in the 1980s. Cloud cover feedbacks were demonstrated in a 1-D radiative convective equilibrium model (Hansen et al., 1984) and later a GCM (Wetherald & Manabe, 1988) while Roeckner et al. (1987) modeled a cloud optical depth feedback related to changes in cloud liquid water path.

More physical processes have continued to be added to models as understanding and computing power has increased. Currently, there are two main types of climate models used to simulate climate change. The first type of climate model, atmosphere-ocean general circulation models (AOGCMs), include atmosphere, ocean, land, and sea ice components which are all coupled together to produce one self-consistent representation of the climate. Changes in greenhouse gases can be prescribed to an AOGCM to make climate projections. One limitation to standard AOGCMs is that they do not include an interactive carbon cycle. Because carbon exchange between the atmosphere, land, and ocean may be changed in a warmer world (e.g. Friedlingstein et al., 2006), the ability to include an interactive carbon cycle is important to climate change projections. The second type of climate model, Earth System Models (ESMs), incorporate an interactive carbon cycle as well as many other biogeochemical processes that may be important in determining the climate response to forcing (Flato, 2011).

1.2.2 The Community Earth System Model

The modeling portion of this dissertation focuses on one such ESM, the Community Earth System Model, version 1 (CESM1) (Hurrell et al., 2013). CESM can be run in several different configurations depending on the goals of a modeling experiment (Hurrell et al., 2013). We use the version of the model from the CESM Large Ensemble (LE) project (Kay et al., 2015). The LE version of CESM includes the Community Atmosphere Model, version 5 (CAM5), the Parallel

Ocean Program, version 2 (POP2, Smith et al., 2010), the Community Land Model, version 4 (CLM4, Lawrence et al., 2011), and the Los Alamos National Laboratory Community Ice Code, version 4 (CICE4, Hunke & Lipscomb, 2010). All components are run at approximately 1 degree horizontal resolution. There are 60 vertical levels in the ocean and 30 vertical levels in the atmosphere. CAM5 includes improved cloud parameterizations, notably a two-moment microphysical scheme (Morrison & Gettelman, 2008) and an updated shallow convection scheme (Park & Bretherton, 2009), which determine the phase partitioning in clouds and impact the cloud feedbacks predicted by the model (e.g. Gettelman et al., 2012).

1.2.3 Hierarchy of Model Configurations

CESM1 (CAM5) is a fully-coupled ESM that includes a full-depth ocean that is dynamically and thermodynamically coupled to the other components of the climate system. A fully-coupled model is the most realistic representation of the climate system but a fully-coupled model also has disadvantages. Most notably, fully-coupled models are computationally expensive and they take many centuries to reach a new equilibrium after an external forcing (such as increased greenhouse gases) due to the millennial timescales involved with deep ocean circulation. To surmount these limitations and to provide a framework useful for hypothesis testing, a hierarchy of simplified configurations can be used to estimate the behavior of the fully-coupled model and/or isolate the roles of various parts of the climate system.

In our modeling experiments we use two simplified model configurations. In the first simplified configuration, the full-depth ocean is replaced by a mixed-layer, or “slab”, ocean. The slab ocean is thermodynamically coupled to the atmosphere while ocean dynamics and heat transport are prescribed. The chief benefit of the slab ocean model is that it reaches equilibrium

quickly after an imposed forcing (within decades) because the deep ocean response is not included. In the second simplified configuration, no ocean model is included at all. Instead, sea surface temperatures and sea ice conditions are prescribed as boundary conditions for the atmosphere model. Because surface conditions are prescribed, the atmosphere model can be modified in ways that do not conserve energy without causing a runaway climate. As a result, atmosphere-only configurations can be used to identify the impact of individual changes to the atmosphere model without the need for model tuning to maintain energy balance.

1.2.4 Climate Change Scenarios and Metrics

The above-described hierarchy of models is used to understand climate change in response to anthropogenic greenhouse gas emissions. One of the most common metrics used to quantify climate change is climate sensitivity. In general, climate sensitivity refers to the global, annual mean surface warming in response to a forcing. Because the forcing resulting from anthropogenic emissions is itself uncertain, historically the standard forcing of a doubling of atmospheric CO₂ concentration from preindustrial values has been used (e.g. Charney et al., 1979). The climate sensitivity in response to a doubling of CO₂ is referred to as equilibrium climate sensitivity (ECS). ECS is commonly estimated using both slab ocean (e.g. Meehl et al., 2007) and fully-coupled (Gregory et al., 2004) model configurations.

Though ECS is a useful metric that enables comparison between different versions, generations, and types of climate models, it has limitations. Notably, an instantaneous doubling of atmospheric CO₂ is not a realistic real-world forcing and as a result ECS is not always directly related to more realistic climate change projections (as will be discussed further in Chapter 3). Therefore, to produce 21st century climate projections, fully coupled models are forced with

realistic projected anthropogenic emissions and land use changes. In the current generation of climate models (the Climate Model Intercomparison Project, version 5 (CMIP5, Taylor et al., 2012)), 21st century forcing is described by representative concentration pathway (RCP) scenarios (Meinshausen et al., 2011). Despite considerable progress in climate science, uncertainty remains in both ECS and 21st Century climate projections (Flato et al., 2013).

1.3 Cloud Feedbacks Predicted by Climate Models

The continued uncertainty in climate change projections is primarily due to cloud feedbacks (e.g. Flato et al., 2013; Vial et al., 2013; Webb et al., 2013). CMIP5 models generally agree on the pattern of cloud feedbacks, with positive net (longwave plus shortwave) cloud feedbacks over most of the globe with the notable exceptions of the Arctic and the Southern Ocean (Figure 1.1a). Both shortwave and longwave feedbacks contribute to the positive feedbacks over much of the globe but the negative feedback over the Southern Ocean (poleward of ~50°S) is driven entirely by the shortwave component (Figure 1.1b). The negative shortwave cloud feedback over the Southern Ocean is driven by optical depth changes (Figure 1.1d) with comparatively very small contributions from changes in cloud cover (Figure 1.1 c).

The negative shortwave cloud optical depth feedback over the Southern Ocean is important to climate change projections for several reasons. First, many climate models, including CESM, poorly represent the clouds in this Southern Ocean region (Trenberth & Fasullo, 2010; Grise et al., 2015; Kay et al., 2016a) which calls the modeled cloud feedbacks into question. Second, the cloud optical depth feedback over the Southern Ocean has a strong influence on model projections of ECS (Tan et al., 2016). Finally, the negative shortwave cloud optical depth feedback is important

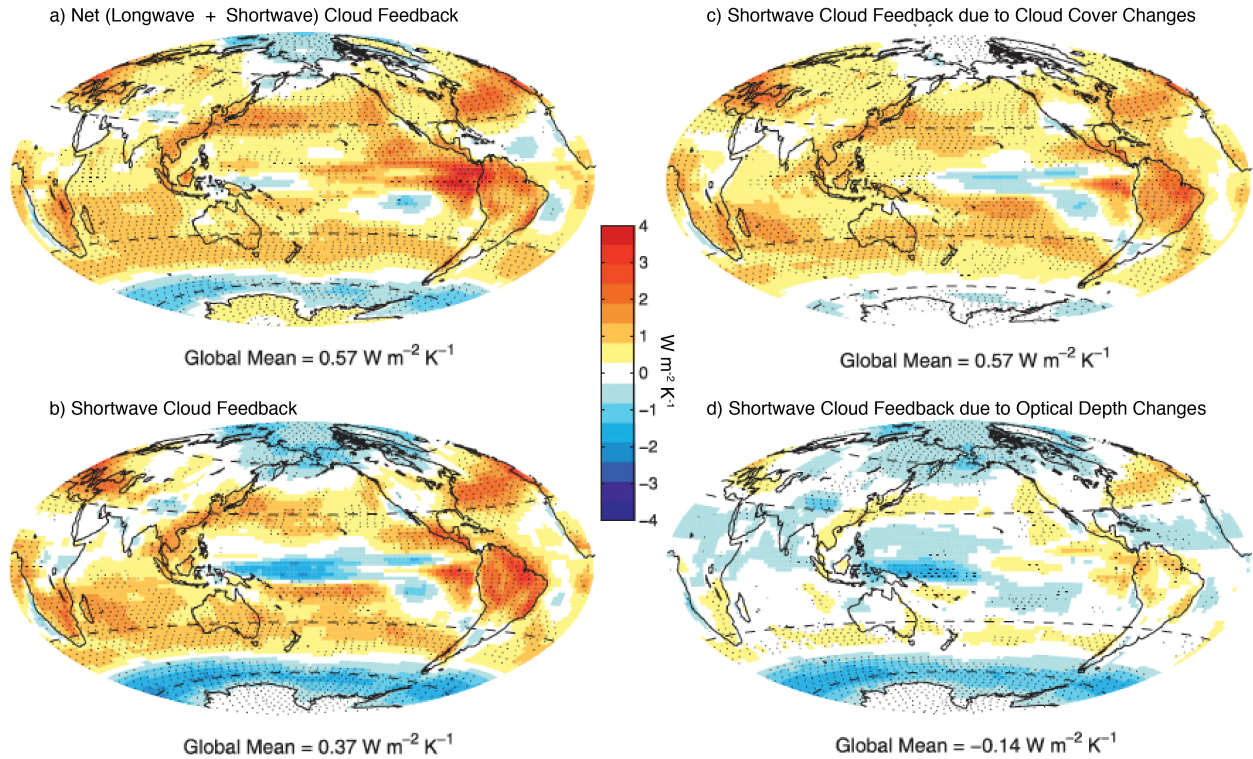


Figure 1.1: Cloud Feedbacks in CMIP5 models. Annual and ensemble mean (a) net cloud feedback, (b) shortwave cloud feedback and components of the shortwave cloud feedback due to (c) change in cloud cover and (d) change in cloud optical depth. Feedbacks normalized by global, annual mean warming. Stippling indicates regions where $\geq 75\%$ of the models agree on the sign of the feedback plotted. Figure and caption adapted from Zelinka et al. (2012a).

because it occurs over the Southern Ocean, a unique region where clouds, ocean circulation, and sea ice interact to influence local and global climate.

1.4 The Southern Ocean's Importance to Global Climate

The Southern Ocean region is an important region for climate because of its local characteristics and its connections to the global climate system. Locally, the Southern Ocean region contains a year-round storm track and is one of the cloudiest regions on the planet. Relative to the amount of solar insolation, Southern Ocean clouds have a larger impact on the shortwave energy budget than any other region of the globe (Tsushima et al., 2006). The high latitude

Southern Ocean (poleward of 60°S) is also seasonally covered with sea ice which itself has a strong impact on albedo (Qu & Hall, 2005) and may interact with the atmosphere to impact cloud properties.

Unique dynamics in the Southern Ocean link the region to the global climate system. Strong westerly winds circle the globe over the Southern Ocean, driving the Antarctic Circumpolar Current (AAC) and inducing northward Ekman flow. This divergent Ekman flow causes upwelling from depth along sloped isopycnals, bringing cool water to the surface and providing closure for the global Meridional Overturning Circulation (MOC) (Marshall & Speer, 2012). Because of the long (millennial) timescale of the MOC, the upwelled water has not been at the surface for centuries. As a result, the upwelled water is very effective at taking up heat (Armour et al., 2016) and anthropogenic CO₂ (Mikaloff-Fletcher et al., 2006; Khatiwala et al., 2009) from the atmosphere. In fact, the Southern Ocean accounts for roughly half of global ocean CO₂ uptake and three quarters of global ocean heat uptake (Frölicher et al., 2015). Persistent upwelling causes the Southern Ocean to warm more slowly than the global mean under the influence of greenhouse gas forcing (Armour et al., 2016). Because ocean heat uptake slows surface warming, it may impact clouds and cloud feedbacks which in many cases are closely linked to sea surface temperatures.

1.5 Synopsis

The primary goal of this dissertation is to establish the impact of Southern Ocean shortwave cloud feedbacks on climate change projections. This goal is accomplished using both a climate model (including novel model runs using CESM) and multiple observational data sets. The next four chapters of this dissertation each address a unique aspect of how Southern Ocean cloud feedbacks impact climate:

- Chapter two identifies the influence of improved Southern Ocean cloud phase parameterization in CESM on cloud feedbacks and shows how the modified cloud feedbacks increase ECS (Frey & Kay, 2018).
- Chapter three shows that the modifications to CESM that produce a large increase in ECS produce almost no change in model projections of 21st Century warming because of persistent Southern Ocean heat uptake (Frey et al., 2017).
- Chapter four identifies the observed cloud and top-of-atmosphere albedo response to Southern Ocean sea ice variability and demonstrates that sea ice loss with warming will likely not directly impact shortwave cloud optical depth feedbacks (Frey et al., 2018).
- Chapter five compares the cloud response to Southern Ocean sea ice variability in CESM to the observed response identified in chapter four.

Finally, Chapter six summarizes the key conclusions of this dissertation and provides suggestions for future work.

Chapter 2

The Influence of Extratropical Cloud Phase and Amount Feedbacks on Climate Sensitivity

2.1 Abstract

Global coupled climate models have large long-standing cloud and radiation biases, calling into question their ability to simulate climate and climate change. This study assesses the impact of reducing shortwave radiation biases on climate sensitivity within the Community Earth System Model (CESM). The model is modified by increasing supercooled cloud liquid to better match absorbed shortwave radiation observations over the Southern Ocean while tuning to reduce a compensating tropical shortwave bias. With a thermodynamic mixed-layer ocean, equilibrium warming in response to doubled CO₂ increases from 4.1 K in the control to 5.6 K in the modified model. This 1.5 K increase in equilibrium climate sensitivity is caused by changes in two extratropical shortwave cloud feedbacks. First, reduced conversion of cloud ice to liquid at high southern latitudes decreases the magnitude of a negative cloud phase feedback. Second, warming is amplified in the mid-latitudes by a larger positive shortwave cloud feedback. The positive cloud feedback, usually associated with the subtropics, arises when sea surface warming increases the moisture gradient between the boundary layer and free troposphere. The increased moisture gradient enhances the effectiveness of mixing to dry the boundary layer, which decreases cloud amount and optical depth. When a full-depth ocean with dynamics and thermodynamics is included, ocean heat uptake preferentially cools the mid-latitude Southern Ocean, partially inhibiting the positive cloud feedback and slowing warming. Overall, the results highlight strong

connections between Southern Ocean mixed-phase cloud partitioning, cloud feedbacks, and ocean heat uptake in a climate forced by greenhouse gas changes.

2.2 Introduction

Clouds exert a powerful influence on the present climate, producing a net cooling effect of approximately -20 W m^{-2} in the global mean (Boucher et al., 2013). Due to their large impact on Earth's radiation budget, quantifying how clouds change in response to greenhouse warming is critical to accurately assessing the climate's overall response to increased greenhouse gas forcing. In fact, cloud feedbacks remain the largest source of uncertainty in model estimates of climate sensitivity (Boucher et al., 2013; Vial et al., 2013). Nevertheless, climate models robustly agree on the sign and location of some cloud feedbacks. For example, tropical anvil clouds rise in all climate models leading to a positive longwave cloud feedback (Zelinka and Hartmann, 2010; Zelinka et al., 2012a). Shortwave cloud feedbacks are more uncertain, with competing contributions from changes in cloud amount, optical depth and geographic location. Globally, the net cloud feedback remains unknown but a recent assessment suggested the net cloud feedback is “likely positive” (Boucher et al., 2013).

The only region with a robust negative shortwave cloud feedback is the oceanic mid-to-high latitudes, especially over the Southern Ocean (Zelinka et al., 2012a). This robust negative shortwave cloud feedback arises from cloud albedo increases due in part to changes in cloud phase from ice to liquid with warming. The potential for this negative cloud phase feedback has been known for decades (Mitchell et al., 1989). Climate models have also long been known to be sensitive to cloud phase parameterizations. For example, one modeling study showed modifying the threshold converting cloud liquid to ice changed the sign of the net global cloud feedback from

negative to positive (Li and Le Treut, 1992). Despite these early studies with important implications for climate sensitivity, relatively few studies on mid-latitude cloud phase feedbacks have followed, perhaps in part due to robust agreement among climate models that such a feedback exists and is negative in sign.

More recent work has highlighted that robust model agreement should not be immediately equated to credible model behavior. Indeed, Trenberth and Fasullo (2010) pointed out that large, long-standing, and ubiquitous biases in shortwave radiation are co-located with robust model-predicted negative shortwave cloud feedbacks. While many of the relationships found in Trenberth and Fasullo (2010) have since been revisited for CMIP5 models (Grise et al., 2015), the collocation of shortwave radiation biases and negative cloud feedbacks still remains in some models (for example, see Kay et al., 2014). Zelinka et al. (2012a) highlighted the role of optical depth increases as a potential explanation for the negative shortwave cloud feedback over the Southern Ocean. This optical depth increase arises primarily from increased cloud liquid water path with warming in mixed-phase clouds. As clouds warm, temperature-dependent microphysical processes which tend to deplete cloud liquid are suppressed leading to increased cloud liquid in mixed-phase clouds (Mitchell et al., 1989; Klein et al., 2009; Ceppi et al., 2016a; McCoy et al., 2016). When cloud temperatures exceed the melting point, the cloud ceases to be mixed-phase and becomes all liquid. As a result, the warmed climate supports fewer mixed-phase clouds and more all liquid clouds (Tsushima et al., 2006; McCoy et al., 2014; Gordon and Klein, 2014; Storelvmo et al., 2015). Cloud water droplets are much smaller than cloud ice crystals which means that increasing cloud liquid at the expense of ice increases optical depth and albedo (Storelvmo et al., 2015 and references therein). Because it is influenced by conversion of cloud ice to liquid, the magnitude of

this negative cloud phase feedback is strongly controlled by the amount of cloud ice present in the mean state climate (Tsushima et al., 2006; Choi et al., 2014; McCoy et al., 2014).

Determining the phase of cloud particles is complicated by the fact that the freezing point of a cloud particle varies widely between the homogenous freezing temperature of roughly 235 K and the thermodynamic freezing temperature of 273 K based on its size and the availability of ice nuclei (McCoy et al., 2015). As a consequence, the amount of cloud ice in the mean state is determined by the widely varying parameterizations used in models to simulate the complex physics of mixed-phase clouds. For example, the temperature at which ice and liquid are equally mixed varies by as much as 40 K between models (McCoy et al., 2015). These varying parameterizations create intermodel differences in the optical depth increases which accompany warming (McCoy et al., 2015) which in turn cause differences in the magnitude of the cloud phase feedback (Ceppi et al., 2016a; McCoy et al., 2016).

Evidence for a negative cloud phase feedback has also been shown in observations (for example, Ceppi et al., 2016b). However, other observational evidence has cast doubt on the magnitude of the negative cloud phase feedback predicted by models. Cyclone compositing studies have shown that the positive absorbed shortwave radiation bias over the Southern Ocean identified by Trenberth and Fasullo (2010) arises primarily from low shallow convective clouds in post-cold-front regimes (Bodas-Salcedo et al., 2012; Williams et al., 2013; Bodas-Salcedo et al., 2014). Within these mixed-phase clouds, insufficient supercooled liquid and excessive ice lowers albedo and produces the positive shortwave radiation bias (Kay et al., 2016a). Since the magnitude of the negative cloud phase feedback depends in part on the amount of cloud ice in the mean state, the fact that model clouds have excessive ice calls the magnitude of the negative cloud phase feedback into question (Gordon and Klein, 2014; Kay et al., 2016b).

The above-described links between cloud phase partitioning, radiation biases, and cloud phase feedbacks in both observations and models motivate a hypothesis: Climate models overestimate the magnitude of the negative cloud phase feedback at extratropical southern latitudes because they overestimate the amount of cloud ice present in the mean state. Further, since negative feedbacks reduce warming, models with negative cloud phase feedbacks that are too large may underestimate the amount of warming resulting from greenhouse gas forcing, quantified by their equilibrium climate sensitivity. Recent work with the Community Earth System Model (CESM) showed that perturbing microphysics parameters to bring mean state cloud phase partitioning closer to observations does in fact decrease the magnitude of the negative cloud phase feedback over the Southern Ocean and increase equilibrium climate sensitivity by up to 1.3 K (Tan et al., 2016).

It makes sense that modifying mean state phase partitioning in mixed phase clouds directly impacts the negative cloud phase feedback. Yet, such a large increase in equilibrium climate sensitivity is surprising given the relatively small spatial extent of mixed-phase low clouds. Here we explore the possibility that a weaker negative cloud phase feedback might also impact other cloud feedbacks. More explicitly - a weaker negative cloud phase feedback increases warming and this additional warming could be amplified by other cloud-circulation-climate feedbacks. For example, warming has been linked to Hadley cell expansion (Lu et al., 2007) which may impact cloud radiative effects by altering subsidence patterns (Myers and Norris, 2013; Tselioudis et al., 2016). Increased sea surface temperatures also modify the boundary layer which may decrease low cloud fraction and further amplify warming (Rieck et al., 2012; Brient and Bony, 2013; Qu et al., 2014). Indeed, we expect these additional feedbacks could cause more warming overall than the cloud phase feedback itself since they are not spatially limited to the domain of mixed-phase low

clouds. Further, the ability of the Southern Ocean to modify warming patterns through heat uptake and transport (Senior and Mitchell, 2000; Winton et al., 2010; Rose et al., 2014; Armour et al., 2016) suggests that interactions between ocean dynamics and cloud feedbacks could be important in the Southern Hemisphere extratropics. In short, the impacts of a decreased negative cloud phase feedback on the climate system remain relatively unexplored.

In this study, we assess the impact of reducing the absorbed shortwave radiation bias over the Southern Ocean on climate sensitivity in a global climate model. Consistent with previous work, we find an increase in equilibrium climate sensitivity of 1.5 K. However, increased climate sensitivity is not solely caused by a reduced negative feedback at high southern latitudes. Unlike previous work, we find evidence for an increased positive feedback over the mid-latitude Southern Ocean that amplifies warming. Finally, we isolate the impact of ocean heat uptake and show that ocean dynamics weaken the positive feedback in the mid-latitudes under transient climate change.

This paper is organized as follows: Section two describes methods including the changes made to the model to reduce the absorbed shortwave radiation bias over the Southern Ocean and the model runs used in this study. Next, section three presents results which document how cloud feedbacks produce the increase in equilibrium climate sensitivity resulting from the model changes. Section four discusses the results in the context of previous work and finally section five summarizes key conclusions.

2.3 Model Description and Methods

2.3.1 Model Configuration

We use the code base from the Community Earth System Model Large Ensemble project (CESM-LE) (Kay et al., 2015) with the Community Atmosphere Model, version five (CAM5) for

all model runs in this study. CESM (CAM5) is a global coupled climate model which was a participant in phase five of the Coupled Model Intercomparison Project (CMIP5) (Taylor et al., 2012). CESM (CAM5) is described in a special edition of *Journal of Climate* including a description of the cloud processes relevant to this study (Park et al., 2014).

Motivated by observations showing that CAM5 shallow convective clouds over the Southern Ocean contain too little supercooled liquid and too much ice (Kay et al., 2016a), we follow Kay et al. (2016b) and modify the shallow convective detrainment scheme in CAM5 to increase supercooled liquid at the expense of ice. The CAM5 shallow convection scheme prescribes the phase of detrained condensate via a piecewise function depending on temperature:

$$\begin{aligned}
 f &= 0; \text{ for } T > T_{ice} \\
 f &= \frac{(T_{ice}-T)}{30}; \text{ for } 238.15 \text{ K} < T < T_{ice} \\
 f &= 1; \text{ for } T < 238.15 \text{ K}
 \end{aligned}
 \tag{Eq (1)}$$

where f is the cloud ice fraction (unitless), T is temperature (Kelvin), and T_{ice} is a constant. The default version of CAM5 sets $T_{ice} = 268$ K which results in all condensate cooler than 268 K containing at least some ice while all condensate warmer than 268 K is pure liquid. To better match observations showing supercooled liquid dominating at temperatures below 268 K in mixed-phase clouds (Hu et al., 2010; Morrison et al., 2011; Huang et al., 2012; Cesana and Chepfer, 2013; Chubb et al., 2013; Bodas-Salcedo et al., 2016), we follow Kay et al (2016b) and change T_{ice} from 268 to 253 K resulting in more detrained supercooled liquid and less ice at temperatures between 268 and 238.15 K. Unlike previous work (Tan et al., 2016), we leave the microphysics scheme unmodified. In CAM5 process ordering, the shallow convective detrainment scheme operates before microphysics (Park et al., 2014). Therefore, modifying the shallow convection scheme as we have here to detrain more liquid at colder temperatures allows the microphysics scheme to

determine the how cloud phase evolves in time. In contrast, when more ice is detrained, as in the default version of CAM5, clouds remain dominated by ice because the microphysics scheme cannot change ice to liquid at the sub-freezing temperatures pervasive in Southern Ocean mixed-phase clouds.

Though there are potentially many ways to modify CAM5 to increase supercooled liquid in clouds over the Southern Ocean, modifying the shallow convection scheme, as we have here, has three primary positive attributes. First, it only impacts clouds with cloud-top temperatures below 268 K leaving tropical and subtropical low clouds unaffected. Second, the change primarily impacts regions where shallow convective clouds dominate. Therefore, the change has a large impact over the Southern Ocean, where shallow convective clouds are prevalent, while leaving other cold areas such as the Arctic, with much less shallow convection, unaffected. Different methods of changing the relative proportions of ice and liquid not targeted at a specific regime could have undesirable impacts in other areas with extensive cold clouds. Third, changing T_{ice} to 253 K is consistent with the original shallow convection formulation by Park and Bretherton (2009) though it was not adopted for the default version of CESM (CAM5) during development.

Due to the impact of increased supercooled liquid and the accompanying increase in albedo over the Southern Ocean, tuning is required to maintain radiative equilibrium and avoid a “snowball Earth” climate. Again following Kay et al. (2016b), we modify the threshold relative humidity for low cloud formation (rh_{minl}) by increasing it from 0.8925 to 0.9175 and setting its value equal over ocean and over land. Combining the changes to the shallow convective detrainment scheme and rh_{minl} results in a stable climate with reduced absorbed shortwave radiation biases over both the Southern Ocean and the tropics (Figure 2.1). Kay et al. (2016b) provides a full discussion of the impact these changes have on the current climate. Here we focus

Absorbed Shortwave Radiation Bias: Model minus Observations

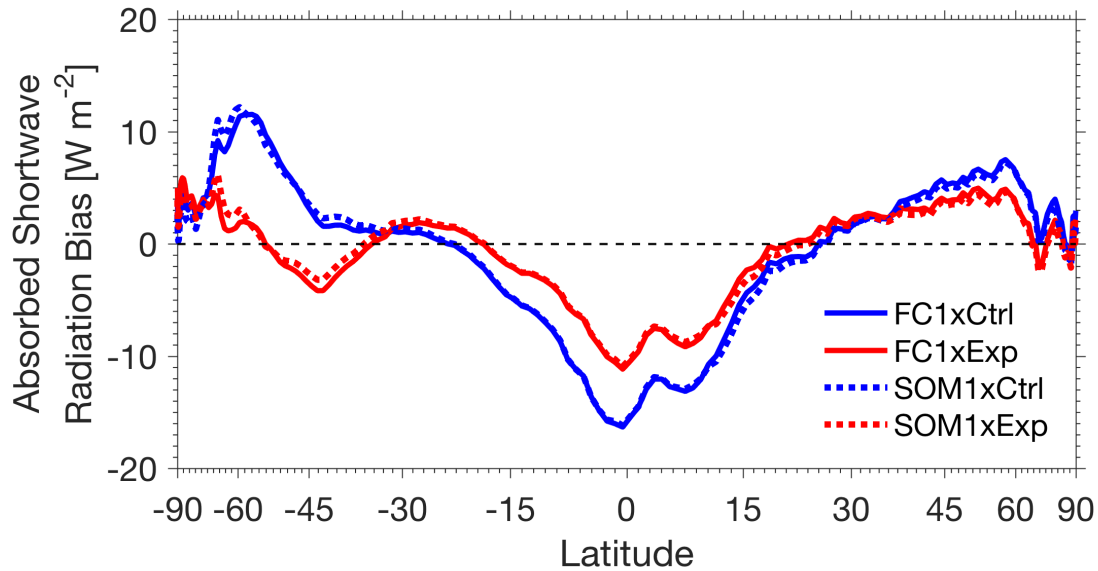


Figure 2.1: Annual zonal mean absorbed shortwave radiation bias (model minus observations). Fully coupled (solid) and slab ocean runs (dotted) for the default (control) version of CESM-CAM5 (blue) and the modified (experiment) version of the model (red). Observations are from CERES-EBAF v2.8 (Loeb et al., 2009) from years 2000–2016. See Table 2.1 for a description of model runs.

on the implications of reducing the Southern Ocean absorbed shortwave radiation bias in the context of greenhouse gas-driven warming.

2.3.2 Model Runs

To investigate the response of the modified model (hereafter called experiment model) to greenhouse gas forcing and compare to the default model (hereafter called control model) response, we utilize a series of model run pairs with different greenhouse gas levels in two ocean model configurations. First, we include only a thermodynamic mixed layer, or “slab”, ocean model (SOM) where ocean circulation is fixed. Second, we include a full-depth ocean model which is fully coupled to the atmosphere including both thermodynamics as well as dynamic ocean

transport. Using this hierarchy of models, we can not only use the mixed layer model as a way to estimate equilibrium climate sensitivity (Danabasoglu and Gent, 2009) but also, when compared with full-depth dynamic ocean runs, we can use it to isolate the impact of ocean circulation on climate (Deser et al., 2016; Kay et al., 2016b).

We begin by running the control model in both thermodynamic-only (SOM) and full-depth, fully-coupled (FC) ocean configurations forced with pre-industrial CO₂ levels (1xCO₂) and CO₂ instantaneously doubled from pre-industrial levels (2xCO₂) resulting in four runs (SOM1xCtrl, SOM2xCtrl, FC1xCtrl, and FC2xCtrl). To generate experiment model runs for comparison, we first run the fully-coupled ocean experiment model forced with 1xCO₂ levels (FC1xExp) for 200 years until the ocean heat fluxes have reached an equilibrium with the atmosphere (Kay et al., 2016b). We use years 150 - 200 from FC1xExp to prescribe ocean heat fluxes and mixed-layer depth to our SOM experiment runs (SOM1xExp and SOM2xExp). Finally, after year 200 of FC1xExp we double CO₂ and run a further 200 years providing the fully coupled doubled CO₂ experiment run (FC2xExp). Slab ocean runs were continued for 60 years, which enabled the 2xCO₂ runs to reach a new equilibrium state. The reduction in absorbed shortwave radiation biases seen in the FC1xExp model compared to FC1xCtrl (Kay et al., 2016b) was maintained in the slab ocean framework (Figure 2.1). Finally, to analyze the mechanism responsible for changes in mid-latitude cloud amount and liquid water path, we extended the SOM1xExp and SOM2xExp runs for five additional years, saving high frequency instantaneous output every 25 hours. Saving output every 25 hours allows sampling of the entire diurnal cycle at each grid point. All model runs were completed at 0.9° latitude x 1.25° longitude horizontal resolution with 30 vertical levels. Table 2.1 summarizes the eight model runs used for this study.

Name	Length (yrs)	CO ₂ Concentration (ppm)	Description
FC1xCtrl	200	284.7	Fully coupled CESM-LE (Kay et al. 2015) pre-industrial 1850 control run (b.e11.B1850C5CN.f09_g16.005), years 400-599.
FC2xCtrl	200	569.4	Fully coupled control run with CO ₂ doubled from pre-industrial concentration. Initial condition 1 Jan, year 402 of FC1xCtrl.
FC1xExp	200	284.7	Fully coupled experiment run ($T_{ice} = 253K$) with pre-industrial CO ₂ concentration. Initial condition 1 Jan, year 402 of FC1xCtrl.
FC2xExp	200	569.4	Fully coupled experiment run ($T_{ice} = 253K$) with CO ₂ doubled from pre-industrial concentration. Initial condition 1 Jan, year 201 of FC1xExp.
SOM1xCtrl	60	284.7	Slab ocean control run with prescribed ocean heat transport and mixed-layer depths from years 402-1510 of the fully-coupled CESM-LE pre-industrial control run (b.e11.B1850C5CN.f09_g16.005) and pre-industrial CO ₂ concentration. Initial condition 1 Jan, year 402 of FC1xCtrl.
SOM2xCtrl	60	569.4	Slab ocean control run with prescribed ocean heat transport and mixed-layer depths from years 402-1510 of the fully-coupled CESM-LE pre-industrial control run (b.e11.B1850C5CN.f09_g16.005) and CO ₂ doubled from pre-industrial concentration. Initial condition 1 Jan, year 402 of FC1xCtrl.
SOM1xExp	65	284.7	Slab ocean experiment run with prescribed ocean heat transport and mixed-layer depths from years 150-200 of FC1xExp and pre-industrial CO ₂ concentration. Initial condition 1 Jan, year 402 of FC1xCtrl.
SOM2xExp	65	569.4	Slab ocean experiment run with prescribed ocean heat transport and mixed-layer depths from years 150-200 of FC1xExp and CO ₂ doubled from pre-industrial concentration. Initial condition 1 Jan, year 402 of FC1xCtrl.

Table 2.1: Description of model runs. All runs use the Community Earth System Model with the Community Atmosphere Model, version 5 [CESM(CAM5)] at one-degree horizontal resolution. Monthly average output saved for all runs with the exception of years 61 through 65 of SOM1xExp and SOM2xExp, when instantaneous output was saved every 25 hours.

2.3.3 Analysis Techniques

We applied several analysis techniques to understand the cloud changes resulting from greenhouse gas forcing in our model results. The interpretation of the impact of clouds on changes in top-of-atmosphere shortwave fluxes is complicated by changes in surface albedo and/or clear air that might also influence flux values (Soden et al., 2004). To separate the impact of clouds from

surface and clear air changes we use the Approximate Partial Radiative Perturbation (APRP) method (Taylor et al., 2007) to estimate the shortwave cloud feedback. The APRP method allows us to identify the negative shortwave cloud feedback at high southern latitudes even though changes in surface albedo cause the overall change in absorbed shortwave radiation to be positive.

Another central theme of our analysis is identifying potential causes of cloud amount and liquid water path decreases over the mid-latitude Southern Ocean. Here we draw useful techniques from the large body of literature that has analyzed how low cloud amount changes, primarily in subtropical subsidence regions, are influenced by sea surface temperatures, vertical velocity, and/or stability (i.e. Bretherton, 2015; McCoy et al., 2017). Specifically, we investigate the influence of stability on low clouds with the Estimated Inversion Strength (EIS) parameter from Wood and Bretherton (2006). We follow Myers and Norris (2013) and construct joint frequency distributions with EIS, sea surface temperatures and vertical velocity to isolate the influence of each variable on low cloud amount in the presence of internal climate variability. To analyze high frequency output from the end of the SOM1xExp and SOM2xExp runs we construct probability distribution functions of EIS, sea surface temperature and vertical velocity along with accompanying mean low cloud fraction, as in Bony et al. (2004).

Our experimental design allows us to isolate the role of ocean dynamics in the climate system by comparing full depth ocean runs to their mixed-layer counterparts (Deser et al., 2016). We use methods from Armour et al. (2016) to calculate surface heat flux anomalies as well as ocean heat uptake and storage as a function of latitude. Anomalies in these quantities are used to show where the mixed-layer ocean and fully coupled experiments differ and we attribute the differences to ocean dynamics.

2.4. Results

2.4.1 Impact of Model Cloud Changes on Climate Sensitivity

We begin with the difference in global annual mean surface temperature between the 2xCO₂ and 1xCO₂ runs as a function of time (Figure 2.2). In the slab ocean configuration, both the experiment and the control reach a new equilibrium temperature after about 40 years (Figure 2.2a). The equilibrium climate sensitivity, defined as the global annual mean surface temperature warming from years 41 through 60 of the 2xCO₂ run, is 5.6 K in the experiment model compared with 4.1 K in the control, an increase of 1.5 K. The temporal evolution of warming has also been modified in the experiment. The experiment model warms an additional 0.9 K after year 20 while the control warms less than 0.25 K after the same time. This is likely in part due to the fact that Southern Ocean mixed-layer depth, which is prescribed in slab ocean runs based on the corresponding fully-coupled runs, is deeper in the experiment slab ocean model compared to the control (not shown). As expected, the fully coupled model (Figure 2.2b) warms more slowly than the slab ocean model as the deep ocean is allowed to take up heat. While initially the warming in the fully coupled experiment looks similar to the control, after year 100 a Student's t-test shows that the experiment is warming more than the control at a 99% significance level.

The increased warming in the experiment compared with the control, in both the slab ocean and fully coupled model configurations, is primarily a result of shortwave cloud feedbacks. Global mean feedback values (Table 2) show that the difference in shortwave feedback between the experiment and control versions of the model is an order of magnitude larger than the difference in longwave feedback. The bulk of the difference between the experiment and control comes from the shortwave cloud feedback for both the slab ocean and fully coupled modeling frameworks

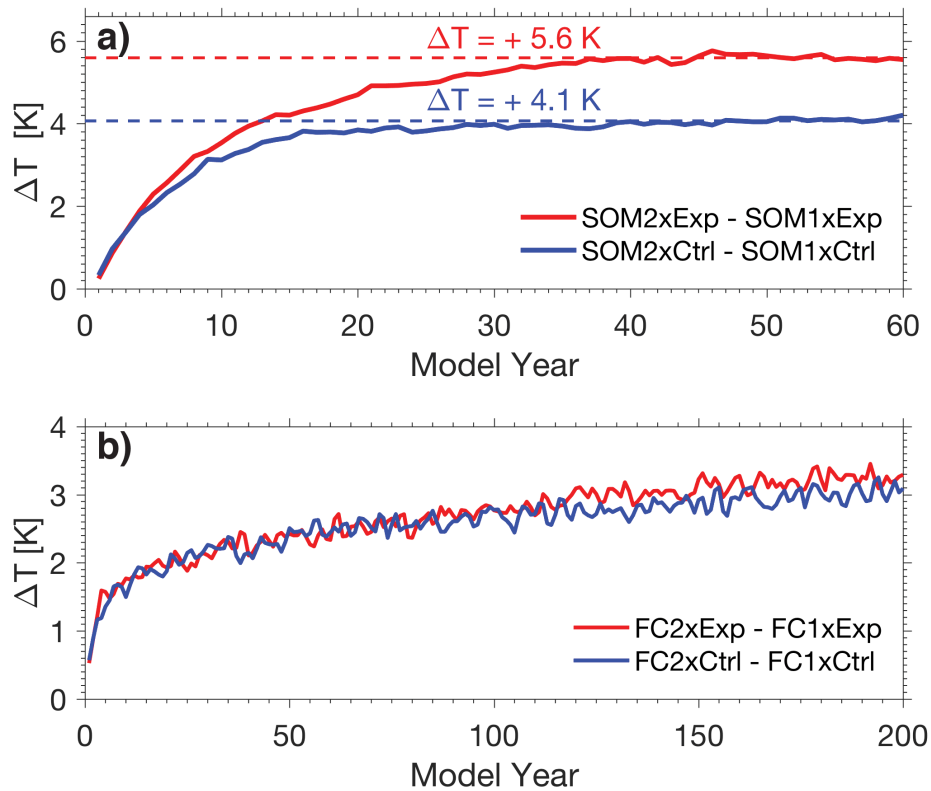


Figure 2.2: Change in global annual mean surface temperature between 2xCO₂ and 1xCO₂ runs. a) slab ocean models and b) fully coupled models. Control model (blue) and experiment model (red). Temperature change is calculated by subtracting the mean of the entire 1xCO₂ run from each year of the corresponding 2xCO₂ run. Dashed lines and text in a indicate the equilibrium climate sensitivity values, defined as the global annual mean warming from years 41 through 60 of the 2xCO₂ runs. Note the difference in both the time and temperature axis scales between a and b. See Table 2.1 for a description of model runs.

(Table 2.2). The spatial pattern of the shortwave cloud feedback is similar in both the slab ocean and fully coupled configurations (Figure 2.3). For each configuration, the largest differences between the control and experiment models is in the extratropics, primarily in the Southern Hemisphere (Figure 2.3c and f). We have verified that the tuning change made to the experiment model, namely adjusting the relative humidity threshold for low cloud formation, does not impact the cloud feedbacks shown in the experiment model (see section 2.7). Since the cloud feedbacks

	SOM Exp	SOM Ctrl	FC Exp	FC Ctrl
Forcing due to doubled CO ₂ (W m ⁻²)	3.8	3.8	3.8	3.8
Surface Warming (K)	5.6	4.1	3.2	3.0
Total Feedback (W m ⁻² K ⁻¹)	-0.58	-1.23	-0.83	-1.00
Longwave Feedback	-2.08	-2.07	-2.16	-2.13
Longwave Clear Air feedback	-1.79	-1.79	-1.79	-1.79
Longwave Cloud Feedback	-0.29	-0.28	-0.37	-0.34
Shortwave Feedback	1.50	0.84	1.33	1.13
Shortwave Surface Feedback	0.44	0.38	0.52	0.62
Shortwave Clear-Sky Feedback	0.05	0.03	0.03	0.03
Shortwave Cloud Feedback	1.01	0.43	0.78	0.48
Shortwave Cloud Amount Feedback	0.68	0.38	0.57	0.48
Shortwave Cloud Scattering Feedback	0.42	0.10	0.28	0.07
Shortwave Cloud Absorption Feedback	-0.08	-0.05	-0.07	-0.07

Table 2.2: Global annual mean 2xCO₂ forcing, surface warming, and feedbacks. Surface warming and feedbacks calculated by differencing the last 20 years of each 2xCO₂ run and their 1xCO₂ counterpart and then averaging. All feedbacks (W m⁻² K⁻¹) normalized by global annual mean surface warming. Forcing due to doubled CO₂ and longwave feedbacks diagnosed using model fluxes following Kay et al. (2012). Shortwave feedbacks estimated with the APRP method following Taylor et al. (2007).

are similar in both the slab ocean and fully coupled configurations, we will take advantage of the larger signal provided by the slab ocean models to examine the mechanisms behind the cloud feedbacks.

2.4.2 Comparison of the Negative Shortwave Cloud Feedback

We expect a weaker negative cloud phase feedback in the experiment compared with the control because our experiment model has less ice and more supercooled liquid in the mean state (Figure 2.4a). The negative feedback appears at high southern latitudes, over ocean from the

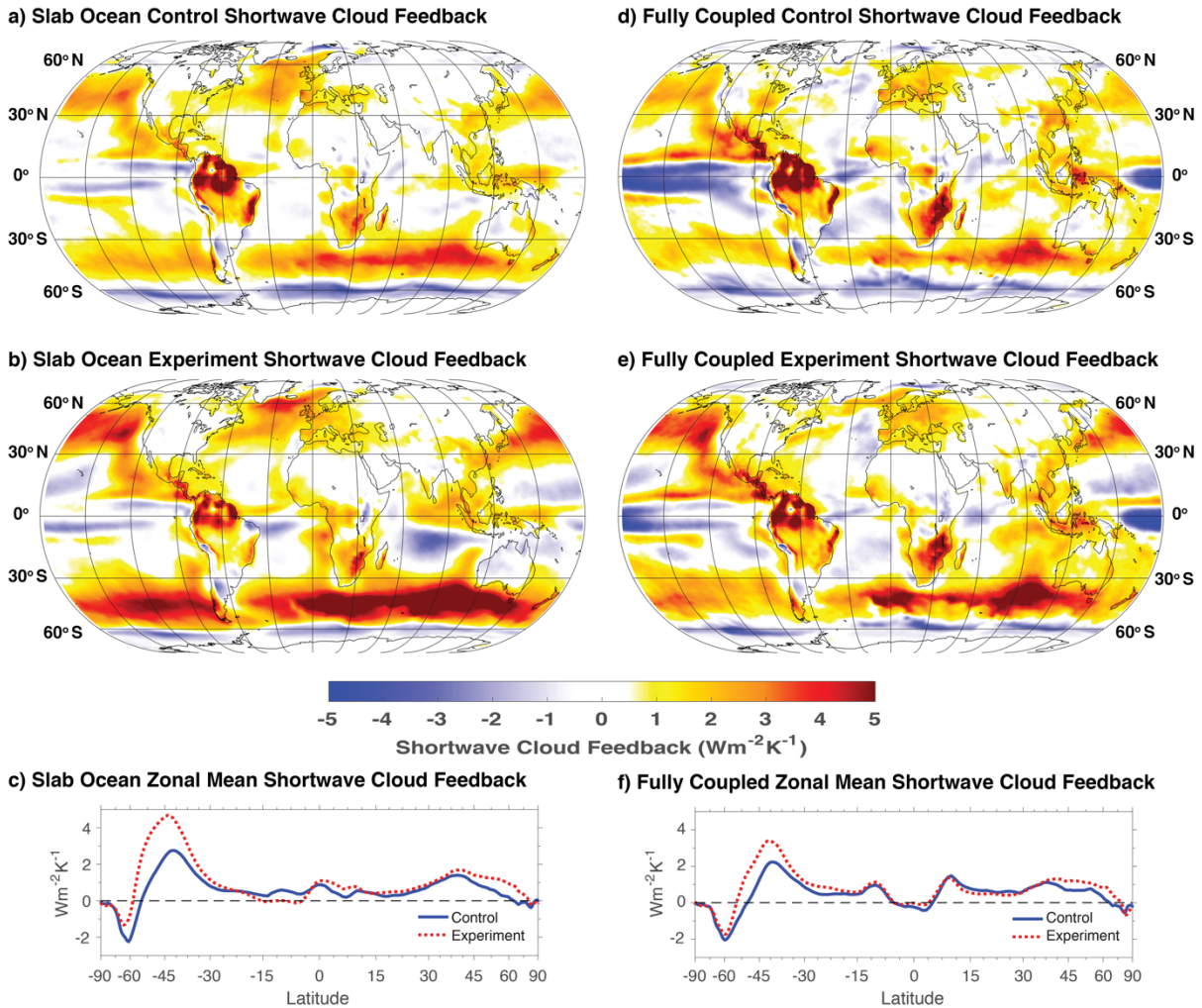


Figure 2.3: Annual mean shortwave cloud feedback normalized by the annual global mean change in surface temperature between 2xCO₂ and 1xCO₂ model runs. a) Slab ocean control, b) Slab ocean experiment, c) Slab ocean zonal means, d) Fully coupled control, e) Fully coupled experiment, and f) Fully coupled zonal means. In c) and f), control (solid blue) and experiment (dotted red). The average of the last 20 years is used for the 2xCO₂ runs (years 41- 60 for SOM2xExp and SOM2xCtrl, years 181- 200 for FC2xExp and FC2xCtrl), while an average of the entire run is used for the 1xCO₂ runs. Shortwave cloud feedbacks calculated using the approximate partial radiation perturbation method (Taylor et al. 2007).

Antarctic coast north to near 55° south in the control (Figure 2.3a) and 59° south in the experiment (Figure 2.3b) model. We define these regions as the negative feedback region for each model. As expected, the negative feedback is smaller in the experiment compared with the control (Figure 2.3c). In the fully coupled version of the model, the difference in maximum magnitude between

the experiment and control is much smaller than in the slab ocean model (compare Figure 2.3c to 3f). In both the fully-coupled and slab ocean frameworks the meridional extent of the Southern Hemisphere negative shortwave cloud feedback is reduced in the experiment compared with the control. Since a negative feedback acts to slow warming, a smaller negative feedback in the experiment contributes to more warming (Figure 2.2).

The negative feedback at high southern latitudes is caused primarily by changes in the scattering properties of clouds, rather than cloud amount (Figure 2.4). Where the total shortwave cloud feedback is negative the scattering component is strongly negative and partly counteracted by a weakly positive cloud amount feedback (Control Figure 2.4b, Experiment Figure 2.4c). Within the Southern Hemisphere negative feedback region, the negative feedback is caused by increased liquid water path (Figure 2.4e) shown by Ceppi et al. (2016a) to be partly caused by suppression of microphysical liquid water sinks with warming. In our runs the microphysics schemes have been left unaltered between the experiment and control. As such, poleward of 60 degrees South, where in-cloud temperatures remain predominately below freezing, the liquid water path increase is similar in magnitude between the two versions of the model when normalized by the local temperature change (Figure 2.4e). Further equatorward, though, the liquid water path increase in the control model is larger than in the experiment. Here the increased liquid water path is partly a result of a decrease in ice water path as more cloud temperatures exceed the freezing level and mixed-phase clouds become all liquid. In the control model, this ice water path decrease has a larger magnitude than the experiment (Figure 2.4f): a direct result of the changes made to the shallow convection scheme to reduce ice content in the experiment model clouds (Figure 2.4a).

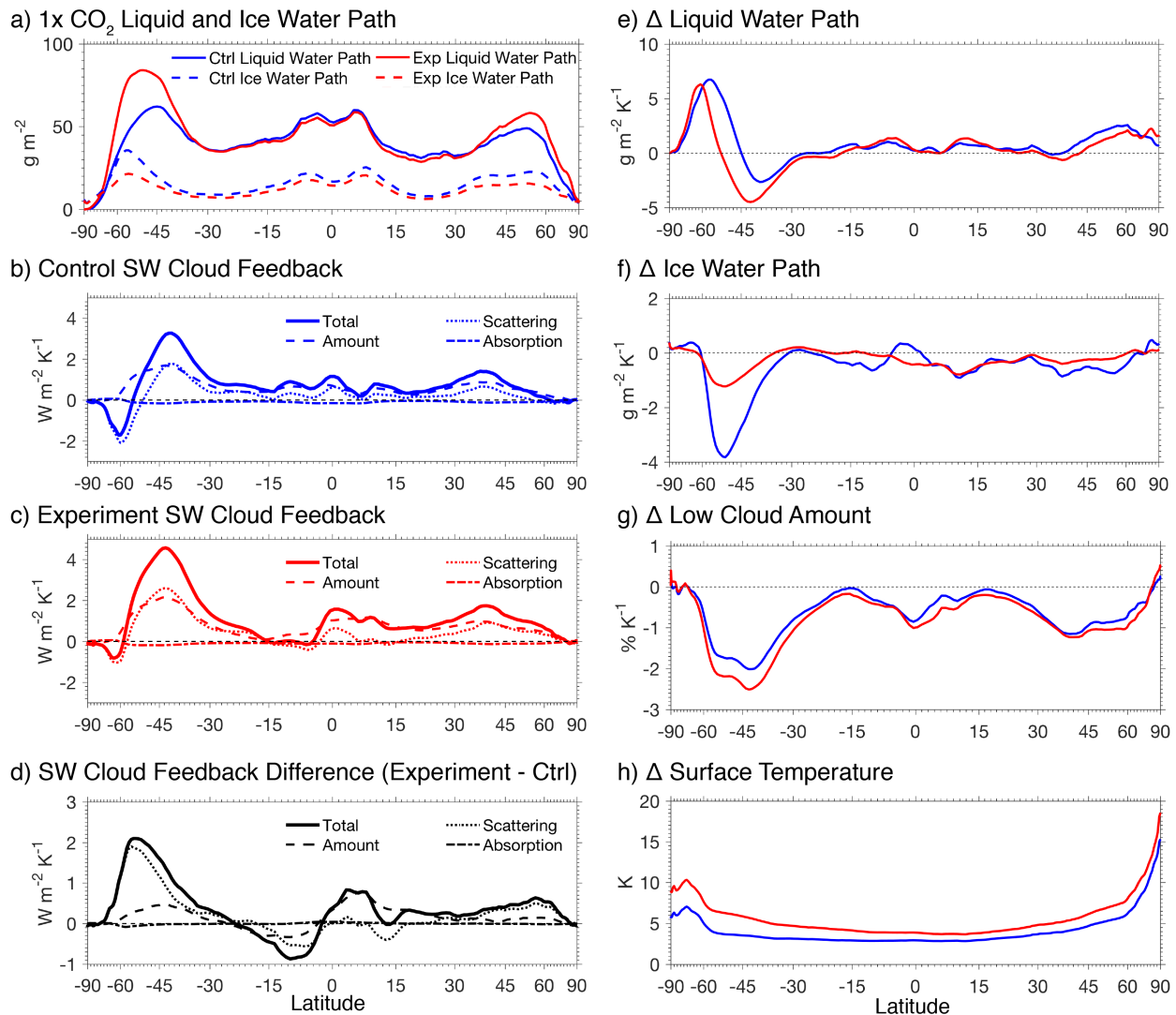


Figure 2.4: Comparison of annual and zonal-mean cloud properties and feedbacks in slab ocean model runs. a) Total grid box liquid (solid) and ice (dashed) water path from SOM1xCtrl (blue) and SOM1xExp (red). Zonal and annual mean shortwave cloud feedbacks: b) Control, c) Experiment, d) Difference, Experiment minus Control. Change due to doubled CO₂ in: e) total grid box liquid water path, f) total grid box ice water path, g) low cloud amount and h) surface temperature. SOM Control (blue) and SOM Experiment (red). Quantities in (b) through (g) are normalized by the local surface temperature change shown in (h). Feedbacks (b through d) are decomposed into feedbacks due to cloud amount (dashed), scattering (dotted), and absorption (dash-dot) which together sum to the total shortwave cloud feedback (solid). Feedbacks calculated using the approximate partial radiation perturbation method (Taylor et al. 2007). Change in total grid box liquid (e) and ice (f) water path is normalized by total cloud fraction before differencing to partly remove the impact of cloud amount changes on results. Low cloud amount (g) is defined here and throughout the paper as the vertically-integrated cloud fraction between the surface and 700 hPa. The average of the last 20 years is used for the 2xCO₂ runs (years 41- 60 for SOM2xExp and SOM2xCtrl), while an average of the entire run is used for the 1xCO₂ runs.

While many CMIP5 models exhibit a negative shortwave optical depth (scattering) feedback at mid-to-high latitudes in both the northern and southern hemispheres (Zelinka et al., 2012a), in our runs it is only apparent in the southern hemisphere (Figure 2.4b and c). We expect that the lack of a corresponding feedback in the northern hemisphere is related to the fact that much of the northern hemisphere is land or seasonally varying sea ice rather than ocean at these high latitudes. In addition, hemispheric differences in mid-to-high latitude cloud phase partitioning seen in observations (Hu et al., 2010; Morrison et al., 2011; Chubb et al., 2013) and in CESM (Kay et al., 2016a) may also play a role in the differing northern and southern hemisphere feedbacks. A more thorough analysis of the hemispheric differences is beyond the scope here, but we note that we have targeted our model changes at shallow convective clouds which are more prevalent over the Southern Ocean than at similar northern latitudes. This suggests that we should expect larger differences between the experiment and control in the southern rather than northern hemisphere as we see in Figure 2.4.

2.4.3 Comparison of the Positive Shortwave Cloud Feedback

The differences in cloud feedbacks leading to increased climate sensitivity are not confined to the high-latitude negative feedback region. In fact, large differences exist into the mid-latitudes where both the experiment and the control exhibit positive feedbacks. This difference is most apparent in the Southern Hemisphere between 30 to 55 °S in the control model and 59 °S in the experiment (Figure 2.3c). We define these regions as the positive feedback region for each model. Here, the magnitude of the positive feedback is greater in the experiment than in the control (Figure 2.3c, Figure 2.4d). There is a similar positive feedback over oceans in the Northern hemisphere mid-latitudes (Figure 2.3).

The shortwave cloud feedback in the positive feedback region is the sum of contributions from both cloud amount and cloud scattering properties (Figure 2.4 b and c). In both the experiment and the control, the cloud amount feedback is positive over the entire southern hemisphere mid-latitude region (30 – 60 degrees South). This is consistent with the change in low cloud amount (Figure 2.4g zonal means, Figure 2.5 map) which is negative over this entire region. The mechanism linking low cloud amount to absorbed shortwave radiation is straightforward: Decreased cloud amount decreases albedo and allows more shortwave radiation to be absorbed. As a consequence, areas with larger cloud amount decreases (Figure 2.5) correspond with areas which exhibit larger positive shortwave cloud amount feedbacks (Figure 2.4 b and c). The time evolution of low cloud amount decrease also closely follows the evolution of warming, with cloud fraction continuing to decrease until year 40 in the slab ocean runs (not shown).

The scattering component of the shortwave cloud feedback is related to changes in liquid water path. On the poleward edge of the positive feedback region the scattering component is negative as a result of increased liquid water path, decreasing the magnitude of the overall positive feedback (Figure 2.4b, c and e). The scattering component remains negative from the South Pole to 51 °S in the control compared to 57 °S in the experiment. Further equatorward, the scattering feedback becomes positive in both the experiment and the control as liquid water path decreases, amplifying the positive feedback from decreased cloud amount. While we expect liquid and ice water paths to decrease as cloud amount decreases, the liquid and ice water path changes shown in Figure 2.4e and f are normalized by total cloud fraction and thus partly independent of cloud amount decreases. Ceppi et al (2016a) similarly found that cloud water changes were not primarily caused by cloud amount changes in their analysis.

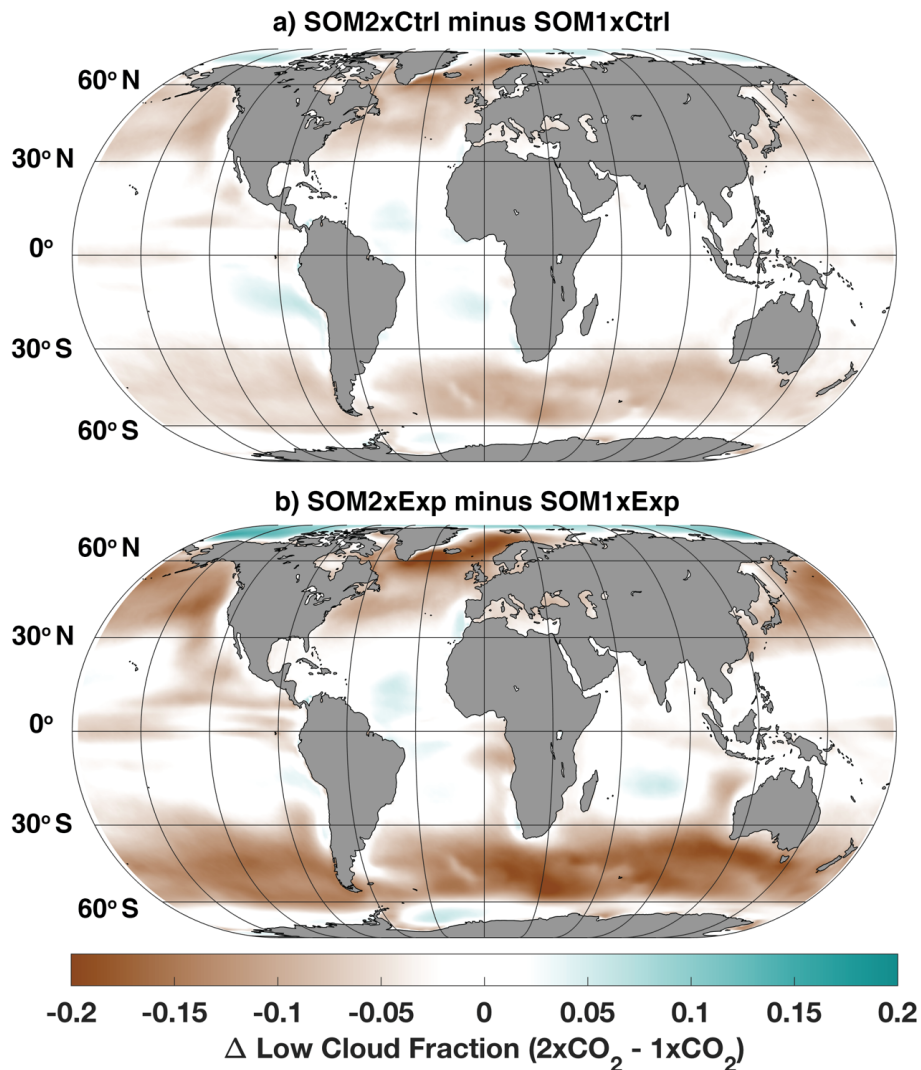


Figure 2.5: Change in annual mean low cloud fraction between $2xCO_2$ and $1xCO_2$ slab ocean model runs. a) Control and b) Experiment. The average of the last 20 years is used for the $2xCO_2$ runs (years 41- 60), while an average of the entire run is used for the $1xCO_2$ runs. Low cloud fraction is defined here and throughout the paper as the vertically-integrated cloud fraction between the surface and 700 hPa.

The fact that the scattering feedback is different (either more negative or less positive, depending on latitude) in the control compared to the experiment (Figure 2.4 b-d) can be plausibly explained by the difference in in-cloud ice to liquid conversion. In the control model, more ice is available to melt into liquid (Figure 2.4a) increasing liquid water path at the expense of ice (Figure

2.4 e and f). This phase change in isolation produces a negative feedback. In the negative feedback region, it magnifies the negative feedback related to increased liquid water path and in the positive feedback region it partially counteracts the positive feedback due to cloud amount decrease and cloud thinning.

In sum, the positive shortwave cloud feedback in the mid-latitudes is the result of both cloud amount decreases and reduced liquid water path or cloud thinning partly counteracted by in-cloud ice to liquid conversion. It is plausible that similar mechanisms could both reduce cloud amount (Figure 2.4g) and thin clouds (Figure 2.4e) (i.e. Tsushima et al., 2006; Bretherton & Blossey, 2014; Sherwood et al., 2014; Bretherton, 2015; Gettelman & Sherwood, 2016). For example, a drying mechanism could gradually thin a cloud and reduce its liquid water path before the cloud ultimately disappears. If this mechanism acts over large areas cloud amount would decrease as some clouds disappear. At the same time the cloud that is left may have a reduced liquid water path due to the drying process. Therefore, to investigate the mechanism leading to the positive shortwave cloud feedback seen in our model runs, we consider three variables which have been linked to low cloud amount feedbacks in previous literature. In sections 2.4.4 and 2.5.5 we present results from the experiment model only. Similar relationships are found in the control model as well but are not shown for brevity.

2.4.4 Identification of Sea Surface Temperature as the Primary Control on the Positive Mid-Latitude Feedback

Much research has been devoted to the change in subtropical low cloud feedbacks in weak subsidence regimes as these regions are thought to explain much of the spread in equilibrium climate sensitivity amongst global climate models (Bony & Dufresne, 2005; Webb et al., 2006; Webb et al., 2013). Decreases in subtropical low cloud amount have been attributed to decreased

stability (Wood & Bretherton, 2006), increased subsidence (Myers & Norris, 2013), and changes in the boundary layer driven by sea surface temperatures (Rieck et al., 2012; Brient & Bony, 2013; Qu et al., 2014). Here we find techniques used previously to investigate the subtropics useful in understanding mid-latitude low cloud changes in our experiments. Over the mid-latitude Southern Ocean, stability, quantified by Wood and Bretherton's (2006) estimated inversion strength (EIS), decreases (Figure 2.6a) while sea surface temperature (SST) increases (Figure 2.6b), with larger increases occurring further poleward. Subsidence changes as well, though there are areas where it decreases, most notably on the northern edge of the mid-latitudes, and others where it increases (Figure 2.6c). Similar changes in each parameter are seen in the control model (not shown), though the magnitude of each change is smaller.

To determine which variable or variables might be important in controlling low cloud changes over the Southern Hemisphere mid-latitudes, we first consider how each varies with low cloud amount in the presence of internal climate variability. We find that changes in sea surface temperature have a stronger impact on low cloud amount than either stability or vertical velocity. Following Myers and Norris (2013), we construct joint frequency distributions of SST paired with EIS (Figure 2.7a) and SST paired with vertical velocity at the 700mb level (ω_{700}) (Figure 2.7b) for the ocean region between 30 and 60° south. For constant EIS, increasing SST leads to decreased low cloud amount (Figure 2.7a). Conversely, when SST is held constant an increase or decrease in EIS leads to a minimal change in low cloud amount. Similarly, for constant ω_{700} increasing SST leads to decreased low cloud amount (Figure 2.7b). When SST is held constant, changes in ω_{700} have little impact on low cloud amount, even when motion changes from ascent to subsidence or from subsidence to ascent.

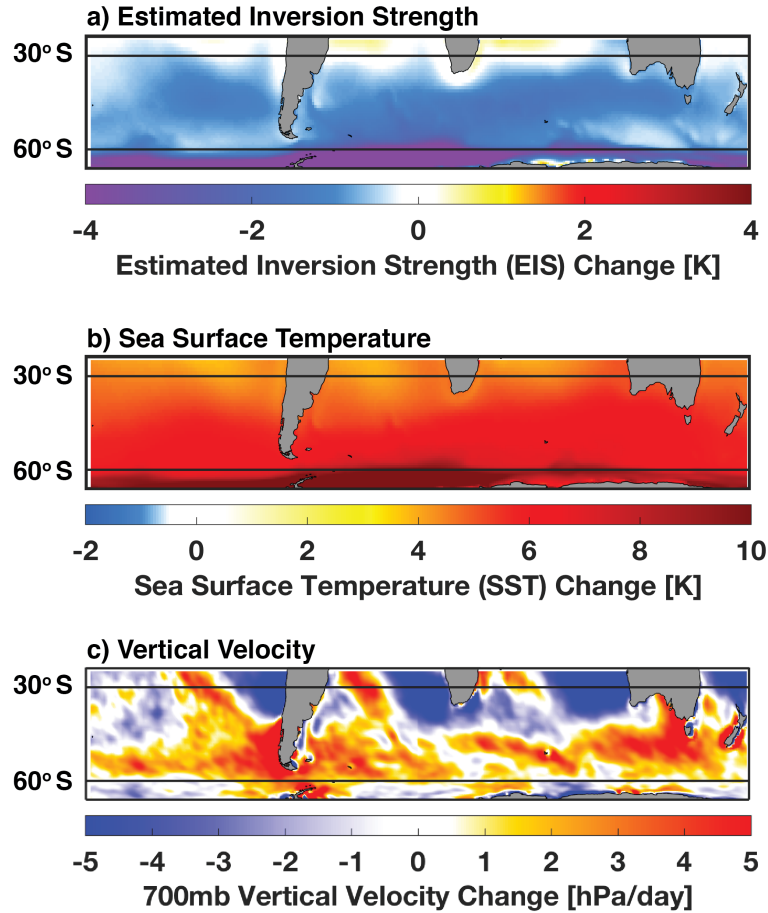


Figure 2.6: Annual mean change (SOM2xExp minus SOM1xExp) in: a) Estimated Inversion Strength, b) Sea Surface Temperature, and c) vertical velocity at 700 mb. The average of the last 20 years is used for SOM2xExp (years 41- 60), while an average of the entire run is used for SOM1xExp.

A similar analysis using grid cell by grid cell interannual anomalies in SST, EIS, ω_{700} , and low cloud amount (Figure 2.7 c, d) yields a slightly more complex picture. Both SST and EIS anomalies appear to influence cloud fraction anomalies (Figure 2.7c). Namely, for a given EIS anomaly, positive SST anomalies lead to negative low cloud amount anomalies and likewise for a given SST anomaly negative EIS anomalies lead to negative cloud amount anomalies. Even when anomalies are considered, ω_{700} appears unimportant compared to SST in controlling low cloud fraction (Figure 2.7d). The relationships shown for SOM1xExp hold for the SOM1xCtrl,

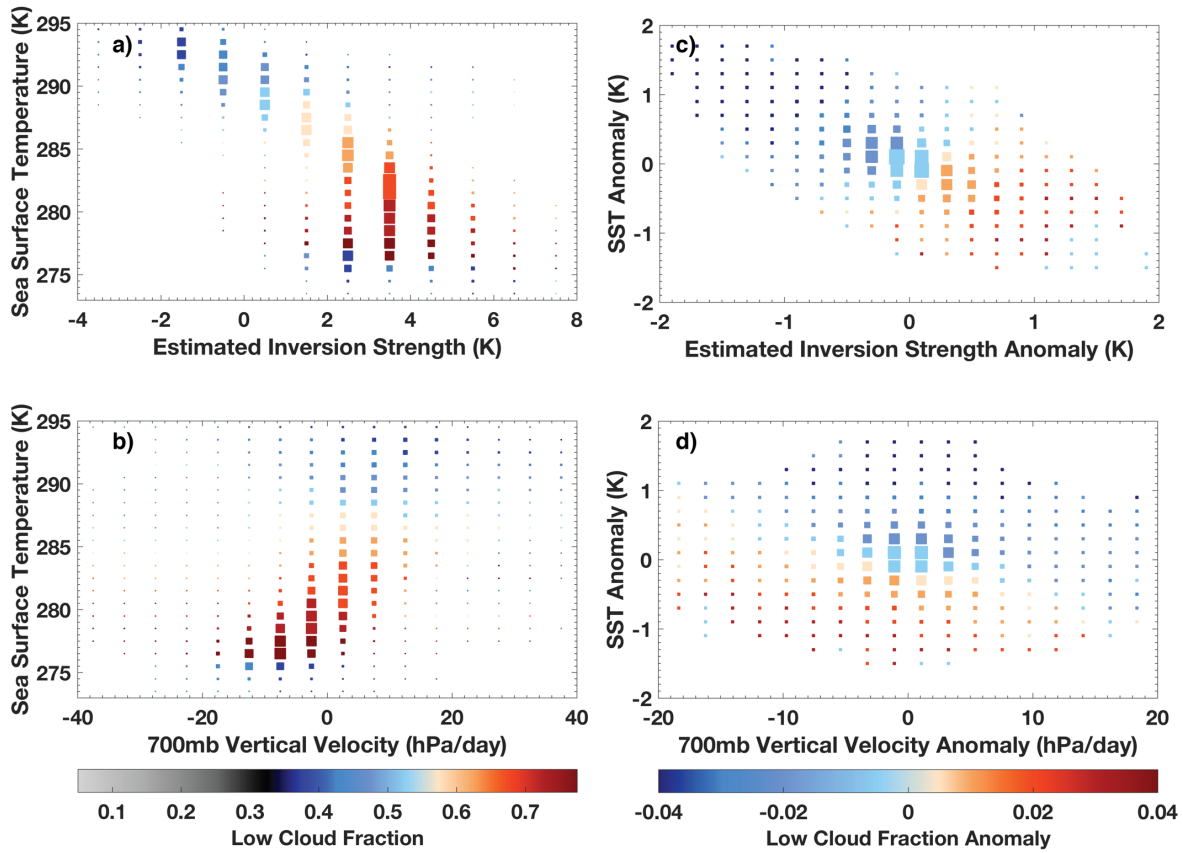


Figure 2.7: Joint frequency distributions created with data from SOM1xExp over the Southern Ocean region between 30 and 60 degrees south latitude. Annual mean values (a, b) and interannual anomalies (c, d). a and c: Estimated inversion strength paired with sea surface temperature. b and d: 700mb vertical velocity paired with sea surface temperature. The size of the block within each bin is proportional to the number of data points in the bin and the block is colored according to the low cloud fraction mean (a, b) or the low cloud fraction anomaly (c, d) within the bin.

FC1xCtrl, and FC1xExp runs (not shown). These results motivate a more thorough investigation to understand how sea surface temperatures and/or stability changes lead to decreased low cloud amount over the mid-latitude Southern Ocean.

As such, we extended the SOM1xExp and SOM2xExp runs for an additional five years and saved instantaneous output every 25 hours. Consistent with the relationships shown for internal variability in Figure 2.7, the decrease in southern hemisphere mid-latitude low cloud amount (Figure 2.5) cannot be explained by the change in ω_{700} between the SOM2xExp and

SOM1xCtrl runs. Probability distribution functions of ω_{700} reveal a modified circulation (Figure 2.8a). The SOM2xExp run exhibits a stronger peak in the weak subsidence regime (0 to +50 hPa/day) at the expense of both strong subsidence (+100 to +200 hPa/day) and strong ascent (-100 to -200 hPa/day). For any given ω_{700} value, the warmer SOM2xExp run has decreased low cloud fraction compared with the cooler SOM1xExp run (Figure 2.8d) and the difference is largest in subsidence regimes (positive ω_{700}).

When sea surface temperatures and stability are considered, we see the expected shift towards higher temperatures and decreased stability when comparing probability distribution functions of SST (Figure 2.8b) and EIS (Figure 2.8c) between the SOM2xExp and SOM1xExp runs. For a given SST there is little change in mean low cloud amount between SOM1xExp and SOM2xExp (Figure 2.8e), even though stability and vertical velocity may be changing. However, increasing SST results in decreased low cloud amount in both the SOM1xExp and SOM2xExp runs. In contrast, we see that at a given EIS level low cloud amount is decreased in SOM2xExp compared to SOM1xExp (Figure 2.8f). Taken together, Figure 2.8 suggests that the increase in SST is more responsible for the decrease in low cloud amount from SOM1xExp to SOM2xExp than either the decrease in stability or change in subsidence. While Figures 2.7 and 2.8 display data from a rather wide latitude band (30 to 60 degrees South) comprising a diverse region from the subtropics to the Southern Hemisphere storm track, the relationships identified hold even when smaller, more homogeneous latitude bands, such as 30 to 40 or 50 to 60 degrees South, are considered in isolation.

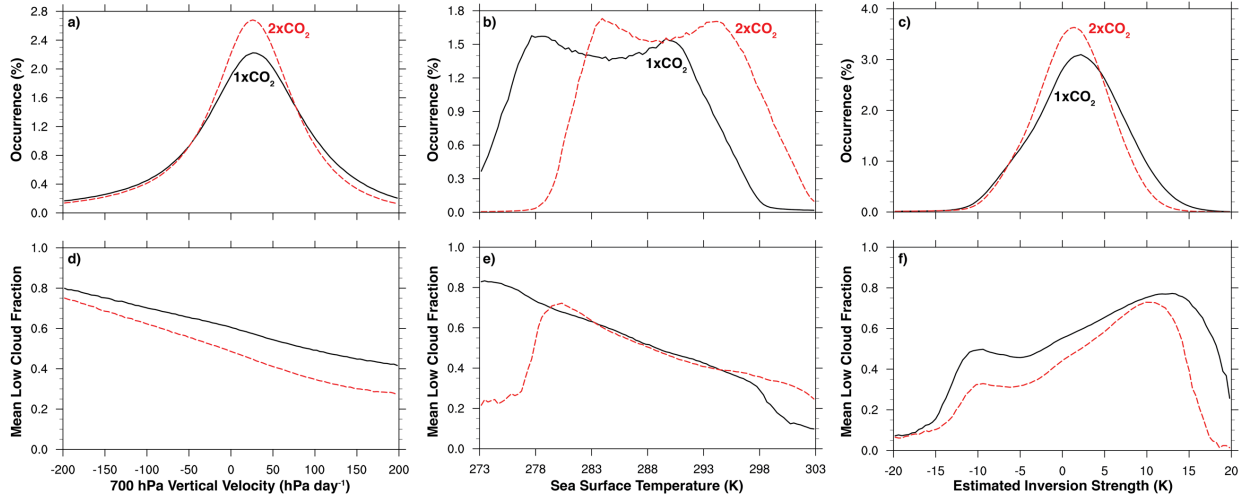


Figure 2.8: Probability distribution functions of a) 700 mb vertical velocity, b) sea surface temperature and c) estimated inversion strength paired with mean low cloud fraction in each d) vertical velocity bin, e) sea surface temperature bin and f) estimated inversion strength bin. SOM1xExp (solid black) and SOM2xExp (dashed red). Distributions created with instantaneous model output over the Southern Ocean region between 30 and 60 degrees south latitude from years 61 to 65 of each model run.

2.4.5 Evidence for a Proposed Mechanism Underlying SST-Cloud Feedback

While many mechanisms have been proposed leading to decreased low cloud amount and optical depth with warming (Bretherton, 2015 and references therein), our results support a thermodynamic mechanism where increased SSTs increase vertical moisture gradients and enhance the effectiveness of mixing to decrease cloud amount and thin clouds (Rieck et al., 2012; Brient & Bony, 2013; Qu et al., 2014). To investigate the potential thermodynamic mechanism for decreased cloud amount and cloud thinning in the mid-latitudes we control for subsidence and divide our data into three ω_{700} regimes: weak subsidence (0 to +50 hPa/day), strong subsidence (+100 to +200 hPa/day) and strong ascent (-100 to -200 hPa/day). In cloud fraction profiles it is again clear that within a given subsidence regime, the SOM2xExp run, with higher surface temperatures, has lower cloud fraction than the SOM1xExp run (Figure 2.9a). Relative humidity profiles (Figure 2.9b) illustrate a potential mechanism resulting in the smaller low cloud fractions

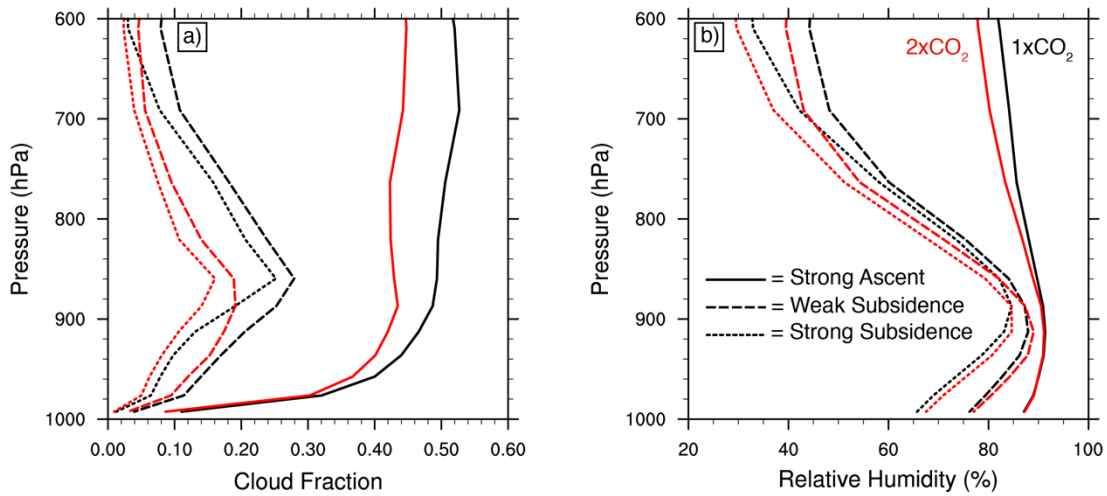


Figure 2.9: Vertical profiles. a) cloud fraction and b) relative humidity separated into strong ascent (solid lines, ω_{700} from -100 to -200 hPa/day), weak subsidence (dashed lines, ω_{700} from 0 to +50 hPa/day), and strong subsidence (dotted lines, ω_{700} from +100 to +200 hPa/day) regimes. SOM1xExp (black) and SOM2xExp (red). Profiles created with instantaneous model output over the Southern Ocean region between 30 and 60 degrees south latitude from years 61 to 65 of each model run.

and reduced cloud liquid water path. The top of the boundary layer is near the peak in relative humidity, between 800 and 900 hPa. Below this level, in the boundary layer, the ocean surface provides a ready moisture source and as the climate warms moisture evaporates into the boundary layer to increase specific humidity. As a result, the SOM2xExp run maintains or increases relative humidity compared to SOM1xExp as it warms. Above the boundary layer in the free troposphere, where the ocean is not as readily available as a moisture source, specific humidity does not increase enough as the climate warms to maintain relative humidity. As a result, relative humidity decreases in the SOM2xExp run as it warms compared with SOM1xExp. Turbulent mixing across the top of the boundary layer entrains free troposphere air into the boundary layer. This mixing may be more effective at drying the boundary layer in the SOM2xExp run because the moisture gradient between the moist boundary layer and the free troposphere is stronger than in the SOM1xExp run

(Figure 2.9b). This mixing process dries the boundary layer which reduces cloud fraction (Figure 2.4g) and reduces liquid water path in the clouds that remain (Figure 2.4e) in the SOM2xExp run compared with the SOM1xExp run.

The warmer sea surface temperatures in the SOM2xExp run are linked to the changes in relative humidity just discussed (Figure 2.9b). From the Clausius-Clapeyron relationship, we know that saturation vapor pressure scales exponentially with temperature. In the boundary layer, the air is able to maintain an approximately stable relative humidity as it warms because the ocean is available as a moisture source. Above the boundary layer, especially in subsidence regimes prevalent in this region (Figure 2.8a), access to the ocean as a moisture source is reduced so relative humidity may decrease as the temperature warms. Therefore, boundary layers over higher sea surface temperatures may have a greater moisture contrast with the free troposphere and mixing from the free troposphere is more effective at thinning boundary layer clouds which decreases liquid water path (Figure 2.4e) and cloud amount (Figure 2.4g). This process, identified previously in the subtropics (Rieck et al., 2012; Brient & Bony, 2013; Qu et al., 2014), is proposed here to act in the mid-latitudes. Since the experiment model warms more initially, the positive cloud feedback is enhanced in the experiment compared with the control which further amplifies warming.

2.4.6 The Impact of Ocean Heat Uptake on Surface Warming and Cloud Feedbacks

We have used slab ocean model results to identify mechanisms leading to the shortwave cloud feedbacks that increase climate sensitivity (Sections 2.4.2-2.4.5). Now, we turn to our fully-coupled model runs to investigate the finding that warming with a fully-coupled dynamic ocean was much slower than warming with a mixed-layer “slab” ocean (Figure 2.2). In the FC2xExp model, ocean circulation is allowed to evolve and change the spatial patterns of surface heat flux

while in the SOM2xExp, fluxes are prescribed based on the ocean circulation in the FC1xExp run. Changes in ocean circulation and ocean heat uptake are expected to change the pace and pattern of warming seen in the FC2xExp run compared with SOM2xExp. The SOM experiment run exhibits a polar amplified warming pattern in the Southern hemisphere compared to the control (Figure 2.10a). Stated another way, the Southern hemisphere mid and high latitudes warmed more, compared to global mean warming, in the SOM experiment run than the SOM control run. In contrast, the fully-coupled runs do not exhibit a similar southern hemisphere polar amplification (Figure 2.10b). Instead, there is comparatively little difference in warming amplification between the experiment and control from the sea ice edge to the equator, with the exception of a band near 45 degrees South most notably in the South Atlantic (Figure 2.10b). The fully-coupled ocean appears to dampen the warming in the Southern hemisphere mid-latitudes compared to the slab ocean runs.

To interrogate why this might be the case, we follow Armour et al. (2016) and consider the change in surface heat flux (SHF) between FC2xExp and FC1xExp (Figure 2.11a). Surface heat flux is defined here as positive into the ocean. A band of positive SHF anomaly is seen over the Southern Ocean, near 60° south, with a large area of negative SHF anomaly further north in the South Atlantic. Integrating surface heat flux over time and longitude produces a total heat uptake anomaly as a function of latitude, per century (Figure 2.11b). The heat uptake pattern is consistent with the surface heat flux anomaly, with a maximum between 50 – 60° south (the ocean takes up more heat in FC2xExp compared with FC1xExp) and a minimum near 45° south. Total ocean heat content (Figure 2.11b), however, peaks around 45° south, equatorward of the peak in heat uptake. This pattern is caused by the upwelling branch of the deep ocean meridional overturning

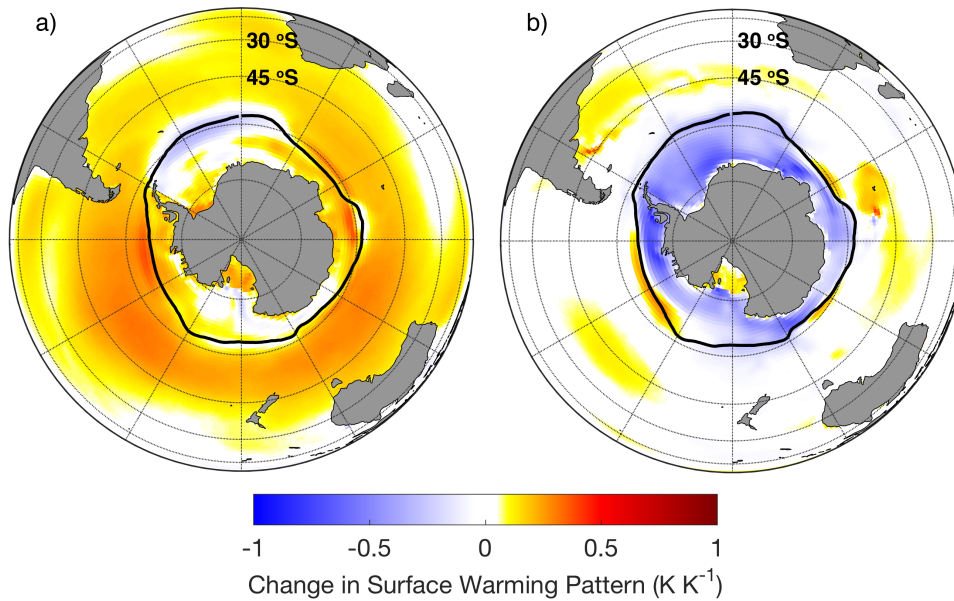
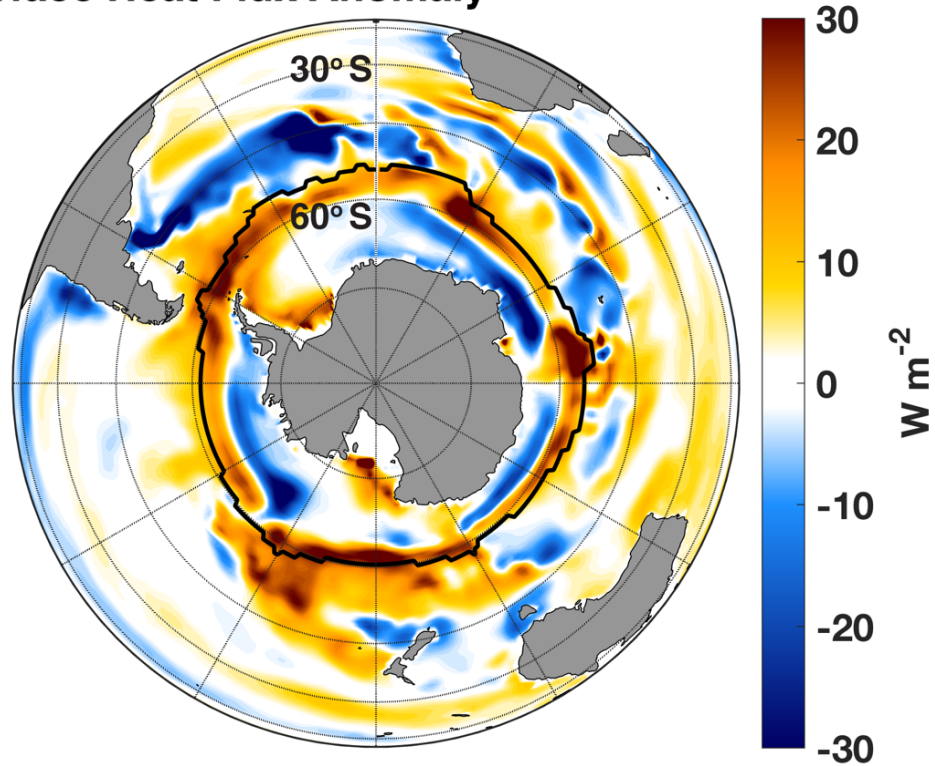


Figure 2.10: Change (experiment minus control) in surface warming pattern (K K^{-1}). Slab ocean models (a) and fully coupled models (b). Warming pattern computed for each model run pair by calculating the annual mean warming due to doubled CO_2 at each grid cell and then normalizing by the global annual mean warming. Change in warming pattern calculated by subtracting the warming pattern in control run from the warming pattern in experiment run. The average of the last 20 years is used for the $2\times\text{CO}_2$ runs, while an average of the entire run is used for $1\times\text{CO}_2$ runs. The black line shows annual mean sea ice extent from the $1\times\text{CO}_2$ control run.

circulation which draws in heat at high southern latitudes near the peak in heat uptake and transports it equatorward (Armour et al., 2016).

Ocean heat transport in the fully coupled runs not only delays warming by moving heat away from the surface, but also by altering the spatial pattern of surface warming and weakening the positive shortwave cloud feedback over the Southern Ocean. In areas where the ocean is taking up excess heat in FC2xExp (positive SHF anomaly, Figure 2.11a), sea surface temperatures in FC2xExp are lower when compared with SOM2xExp, most notably between $50 - 60^\circ$ southeast of New Zealand (Figure 2.12a). This decreased sea surface temperature weakens the positive shortwave cloud feedback. In areas where the sea surface temperatures are cooler, FC2xExp has larger low cloud fraction than SOM2xExp (Figure 2.12b) which further delays warming.

a) Surface Heat Flux Anomaly



b)

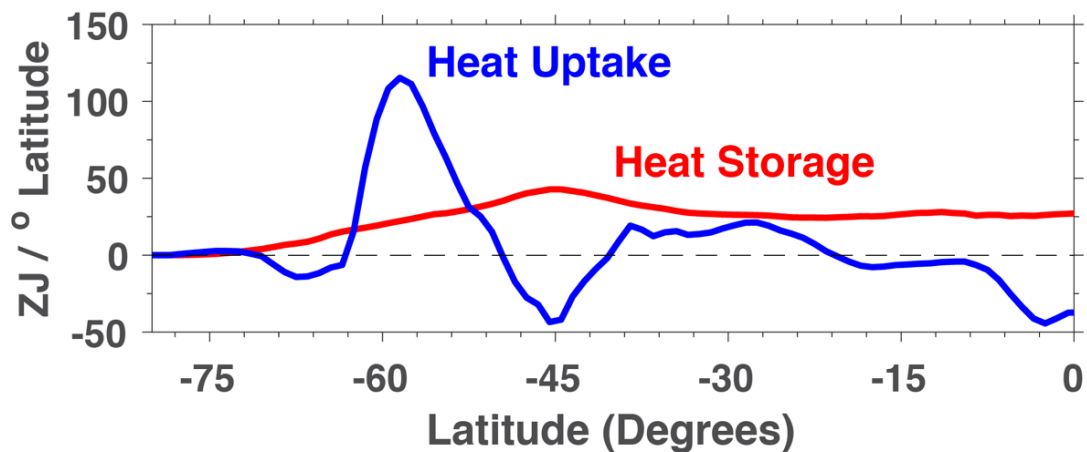


Figure 2.11: Annual mean difference between FC2xExp and FC1xExp: a) surface heat flux (SHF) and b) zonally integrated SHF (blue, per century) and full-depth ocean heat content (red). Positive SHF defined downward (into the ocean). The average of the last 20 years is used for FC2xExp (years 181- 200), while an average of the entire run is used for FC1xExp. The black line shows maximum winter sea ice extent from FC1xExp.

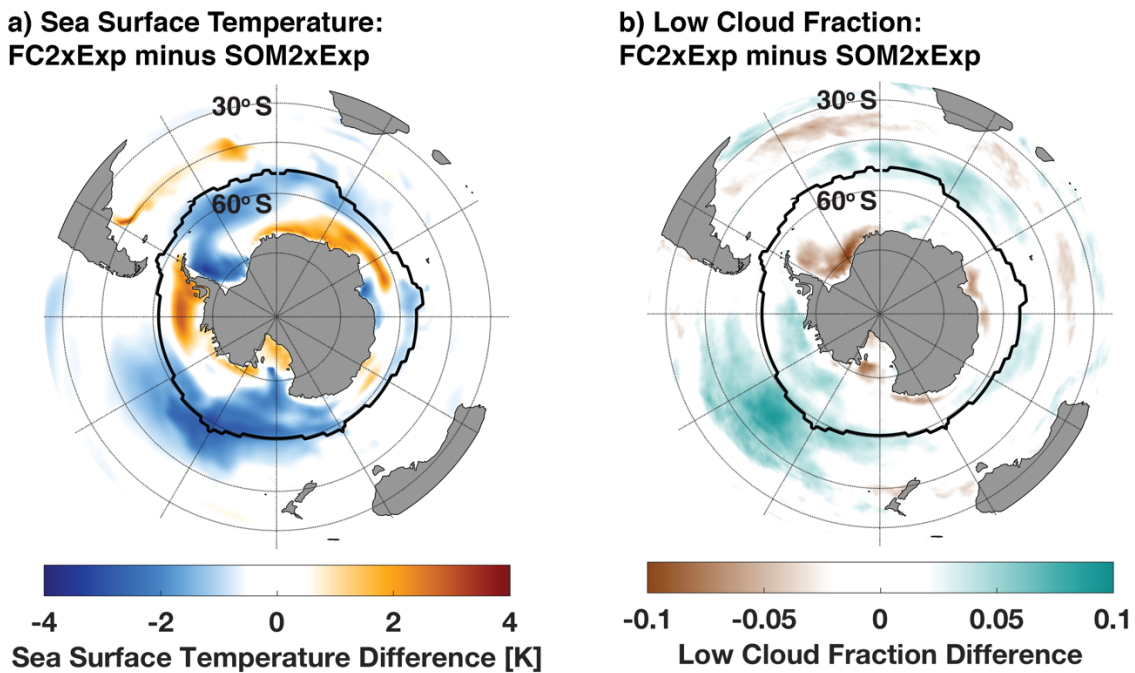


Figure 2.12: Annual mean difference between FC2xExp and SOM2xExp: a) sea surface temperature and b) low cloud fraction. Years 181-200 are used for FC2xExp, while years 8-9 are used for SOM2xExp. SOM2xExp years selected to match global annual mean warming from the FC2xExp time period. The black line shows maximum winter sea ice extent from FC1xExp.

2.5 Discussion

Consistent with previous work (Tan et al., 2016), we find reducing cloud liquid biases and associated absorbed shortwave radiation biases in a climate model coupled to a thermodynamic mixed-layer (slab) ocean increases equilibrium climate sensitivity by 1.5 K. Indeed, this work shows increased climate sensitivity is robust to the method of increasing supercooled liquid in mixed-phase clouds. Yet, this study goes well beyond previous work in two key ways. First, we identify potential feedback mechanisms responsible for increased climate sensitivity, and second, we identify the role of a fully coupled ocean in the warming response to greenhouse gas increases.

The first key result of this paper is that changing the negative cloud phase feedback in mixed-phase clouds cannot fully explain increased equilibrium climate sensitivity. Indeed, our

work identifies a large amplifying feedback for the warming: a positive shortwave cloud feedback over the mid-latitude oceans. Decreasing mean state cloud ice increases warming *initially* due to a smaller negative cloud phase feedback, but importantly, this initial warming is *amplified* in the mid-latitudes by a positive shortwave cloud feedback. Interestingly, the positive mid-latitude feedback contributes to warming more than the changed negative high-latitude feedback because it acts over a larger geographic area. Simply put, the increased positive feedback contributes more than five times more energy to the system than the decreased negative feedback magnitude (Table 2.3).

We find evidence for a thermodynamic mechanism linking increased sea surface temperature with decreased cloud amount and optical depth as the likely cause of the positive mid-latitude cloud feedback. Yet, our work does not conclusively tie our findings to this mechanism. Indeed, many other plausible mechanisms have been suggested in the literature. Sherwood et al. (2014) suggested that intermodel differences in lower-tropospheric mixing at both local and regional scales could be responsible for intermodel differences in low cloud feedbacks and climate sensitivity estimates. A recent review by Bretherton (2015) presented four potential mechanisms governing low cloud changes at low latitudes. 1) The radiative mechanism: increased downwelling longwave radiation at the top of the boundary layer decreases entrainment, thinning low cloud (Christensen et al., 2013). 2) The stability mechanism: decreasing stability allows more mixing into the boundary layer, decreasing cloud amount (Wood & Bretherton, 2006; Kamae & Watanabe, 2012). 3) The dynamic mechanism: increased subsidence leads to decreased low cloud amount (Myers & Norris, 2013). And 4) The thermodynamic mechanism: increased moisture difference between the free troposphere and the boundary layer decreases low cloud amount (Rieck et al., 2012; Brient & Bony, 2013; Qu et al., 2014). Our results (Figures 2.7 and 2.8) suggest support for

	SW Cloud Feedback Component	Δ Area Average Feedback SOM Exp minus Ctrl ($\text{W m}^{-2} \text{K}^{-1}$)	Δ Area Integrated Feedback SOM Exp minus Ctrl (10^{12}W K^{-1})
Negative Feedback Region	Total	0.39	20.77
90 degrees south to:	Amount	-0.14	-6.72
55 degrees south (Ctrl)	Scattering	0.51	27.20
59 degrees south (Exp)	Absorption	0.02	0.29
Positive Feedback Region	Total	0.97	106.96
30 degrees south to:	Amount	0.27	36.21
55 degrees south (Ctrl)	Scattering	0.73	73.76
59 degrees south (Exp)	Absorption	-0.02	-3.01

Table 2.3: Difference in shortwave cloud feedbacks between the slab ocean experiment and control. Area average feedbacks ($\text{W m}^{-2} \text{K}^{-1}$) calculated over the last 20 years of the $2\times\text{CO}_2$ runs and normalized by local annual mean surface warming averaged over the same period. Area integrated feedback (W K^{-1}) calculated by multiplying feedback in each grid cell by its area and then summing over the region of interest. Shortwave cloud feedback components estimated with the APRP method (Taylor et al., 2007).

the thermodynamic mechanism given that sea surface temperature increases appear more related to low cloud amount in our model runs than either stability or subsidence.

Much of the increase in warming we have shown is due to decreased in-cloud ice to liquid conversion with warming, which impacts the scattering component of the shortwave cloud feedback. In fact, the change in the scattering component is larger than the change in the cloud amount component at both mid and high Southern latitudes (Table 2.3 and Figure 2.4d). In the high latitude negative feedback region, decreased in-cloud ice to liquid conversion makes the scattering feedback less negative (Figure 2.4 b-d). In the middle latitude positive feedback region, decreased ice to liquid conversion more weakly opposes the positive feedbacks from cloud amount and cloud thinning and produces a larger overall feedback (Figure 2.4 b-d). Cloud phase has a large impact on cloud feedbacks into the mid-latitudes and subtropics.

The second key finding of this paper is that Southern Ocean heat uptake mitigates much of the excess surface warming related to our model modifications on human timescales (as in Senior & Mitchell, 2000; Raper et al., 2002; Winton et al., 2010). The upwelling branch of the meridional

overturning circulation takes up heat and preferentially cools the southern hemisphere mid-latitudes which weakens the positive shortwave cloud feedback (Figures 2.11 and 2.12). This is consistent with previous work (Rose et al., 2014; Rose & Rayborn, 2016) which identified high latitude ocean heat uptake as particularly effective (compared to heat uptake in other regions) at delaying surface warming or, in their parlance, increasing climate sensitivity with time as ocean heat uptake decays to equilibrium. Though we show a large (1.5 K) increase in equilibrium climate sensitivity with a thermodynamic mixed-layer ocean (Figure 2.2a), the expected difference in warming over the first two centuries is comparatively small (Figure 2.2b). The high efficacy of ocean heat uptake to damp the impact of increased absorbed shortwave radiation in our study is a product of its geographical location over the Southern Ocean; precisely where ocean heat uptake is most effective at delaying surface warming.

The pattern of surface warming (Figure 2.10) is important because it controls the degree to which the positive shortwave cloud feedback over the mid-latitude Southern Ocean is activated. Warming in a different area might not be amplified by feedbacks in the same way. This is similar to the regional feedback framework advanced by Armour et al. (2013), which suggested that the pattern of warming influences the time variation in global climate feedback and effective climate sensitivity. In our study, ocean heat uptake inhibits amplified mid-latitude warming (Figures 2.10 and 2.11) and as a result the difference in warming is muted when a full-depth ocean with dynamics is included (Figure 2.2).

We hypothesize that this muted difference in warming is best interpreted as a “delay” in warming rather than a permanent effect. After a 200-year model run with a full-depth dynamic ocean, the linear regression technique of Gregory et al. (2004) yields equilibrium climate sensitivity (ECS) estimates of 3.9K for the default model compared with 4.4K in our modified

model, an increase of only 0.5K. While this increase is much smaller than the increase in ECS calculated with a thermodynamic mixed-layer ocean (Figure 2.2a), estimates of ECS calculated via linear fits (Gregory et al. 2004) are known to change with time (Williams et al., 2008; Andrews et al., 2012; Andrews et al., 2015; Knutti & Rugenstein, 2015; Gregory & Andrews, 2016). Importantly for our results, the spread in estimated ECS between the experiment model and the default model is increasing with time. For example, from year 100 to year 200 the spread in estimated ECS increases from 0.2K to 0.5K. We find no reason to be sure the spread will not continue to increase. Indeed, because the ocean heat uptake relevant in our study is expected to decay over millennia as the meridional overturning circulation equilibrates with the warmed atmosphere, we hypothesize that Southern Ocean surface warming may eventually “catch up” to mimic the pattern seen in the mixed-layer ocean model (Figure 2.10a). This could activate cloud feedbacks in this region (as in Armour et al., 2013) and produce a true ECS more in line with those estimated with a mixed-layer ocean model (Figure 2.2a). Given this, and the limits of linear ECS estimates (Knutti & Rugenstein, 2015), we have more confidence in our mixed-layer ocean estimates of ECS than those calculated via regression techniques for the models analyzed in this study.

2.6 Summary

This study highlights the impact of Southern Ocean cloud feedbacks and ocean heat uptake on climate sensitivity. We improved absorbed shortwave radiation in a global climate model by increasing supercooled liquid at the expense of ice in mixed-phase clouds and modifying the relative humidity threshold for low cloud formation to maintain global energy balance (Kay et al., 2016b). These changes caused equilibrium climate sensitivity to increase by 1.5 K in the slab ocean

modeling framework. Increased climate sensitivity was caused by changes in two shortwave cloud feedbacks. First, reduced low cloud ice content in the experiment model decreased the size of a negative cloud phase feedback at high southern latitudes, leading to excess warming. Second, this initial warming was amplified via a positive feedback over mid-latitude oceans related to decreased cloud amount and cloud thinning. We propose a mechanism for the positive mid-latitude feedback: Higher sea surface temperatures magnify the moisture gradient between the moist boundary layer and the dry free troposphere which causes mixing across the top of the boundary layer to be more effective at decreasing low cloud amount and optical depth (Rieck et al., 2012; Brient & Bony, 2013; Qu et al., 2014). Since the experiment model warmed more initially than the control, the positive shortwave cloud feedback in the mid-latitudes was larger in the experiment model which further amplified warming. When a full-depth dynamic ocean is included, ocean heat uptake and transport driven by the upwelling branch of the meridional overturning circulation preferentially cool the mid-latitude Southern Ocean which not only slows surface warming directly but also weakens the positive shortwave cloud feedback in the mid-latitudes. These effects mitigate much of the excess warming caused by our model modifications on human timescales underscoring the importance of Southern Ocean dynamics to climate change projections.

Since many global climate models suffer from radiation biases similar to the ones addressed in this study (i.e. Hwang & Frierson, 2013; Hawcroft et al., 2016), future work is needed to assess whether our results are robust across models or specific to the Community Earth System Model. Additionally, the impact of bias reductions on other aspects of climate under increased CO₂ forcing, such as atmospheric dynamics and precipitation, must still be addressed. Much remains to be done to fully understand the role of the Southern Ocean region in the climate system.

2.7 The Impact of Model Tuning on Shortwave Cloud Feedbacks

In this section, we show that the cloud feedbacks produced by the experiment model are unaffected by model tuning. There are two model changes differentiating our experiment model from the control: 1) We adjust the T_{ice} parameter in the shallow convection scheme to detrain more liquid and less ice in mixed-phase clouds (the T_{ice} change). And 2) We tune the model by adjusting the relative humidity for low cloud formation (the tuning change). The tuning change is necessary in both the slab ocean and fully coupled frameworks to maintain a stable climate. However, the tuning change impacts cloud amount in a given climate state and therefore it seems possible that the tuning change could impact the cloud feedbacks and cloud amount decreases produced by the experiment model.

To determine whether this is the case we use an AMIP (Atmospheric Model Intercomparison Project)-style, or atmosphere only, modeling framework where surface temperatures and sea ice are prescribed to the model in a repeating annual cycle. With this framework, we can run the model with only the T_{ice} change in isolation and not be concerned with global energy balance as the surface temperatures are prescribed. We prescribe sea surface temperatures and sea ice conditions to the AMIP model by taking averages of the monthly mean temperatures and sea ice conditions from 10 years of the SOM1xExp and SOM2xExp runs. We then run two AMIP runs for ten years each; one with pre-industrial CO_2 levels (AMIP1x T_{ice} Only) and one with doubled CO_2 levels. (AMIP2x T_{ice} Only). Both AMIP runs include the T_{ice} change and omit the tuning change. See Table 2.4 for a full description of the two AMIP runs.

Comparing the total cloud feedback between the SOM Experiment runs and the AMIP T_{ice} Only runs reveals almost no change in the cloud feedback when the T_{ice} change is made without the tuning change (Figure 2.13a). We also see that the change in low cloud fraction due to doubled

CO₂, which is responsible for part of the positive cloud feedback at mid-latitudes, is virtually unchanged between the SOM Experiment runs and AMIP T_{ice}Only runs (Figure 2.13b). Though inclusion of the tuning change does result in a lower cloud fraction in the SOM Experiment runs compared with the T_{ice}Only runs (not shown), this is true in both doubled CO₂ and preindustrial runs and the difference between the two remains unchanged. The difference in cloud feedbacks between our experiment and control (Figure 2.3) is primarily the result of our changes to shallow convective mixed-phase clouds (the T_{ice} change) and largely unaffected by our model tuning change.

Name	Length (yrs)	CO ₂ Concentration (ppm)	Description
AMIP1xT _{ice} Only	10	284.7	Atmosphere-only model run with pre-industrial CO ₂ levels. SST and Sea Ice prescribed as monthly averages from years 70 – 79 of SOM1xExp. Initial condition 1 Jan year 72 of SOM1xExp.
AMIP2xT _{ice} Only	10	569.4	Atmosphere-only model run with CO ₂ doubled from pre-industrial levels. SST and Sea Ice prescribed as monthly averages from years 68 - 77 of SOM2xExp. Initial condition 1 Feb year 71 of SOM2xExp.

Table 2.4: Description of atmosphere-only model runs. All runs use the Community Earth System Model with the Community Atmosphere Model, version 5 [CESM(CAM5)] at one-degree horizontal resolution. Both of these “T_{ice}Only” runs *include* the modified shallow convection scheme (T_{ice} parameter changed from 268 K to 253K) as in the “Experiment” runs from Table 1 but *omit* the tuning change to the rhminl threshold.

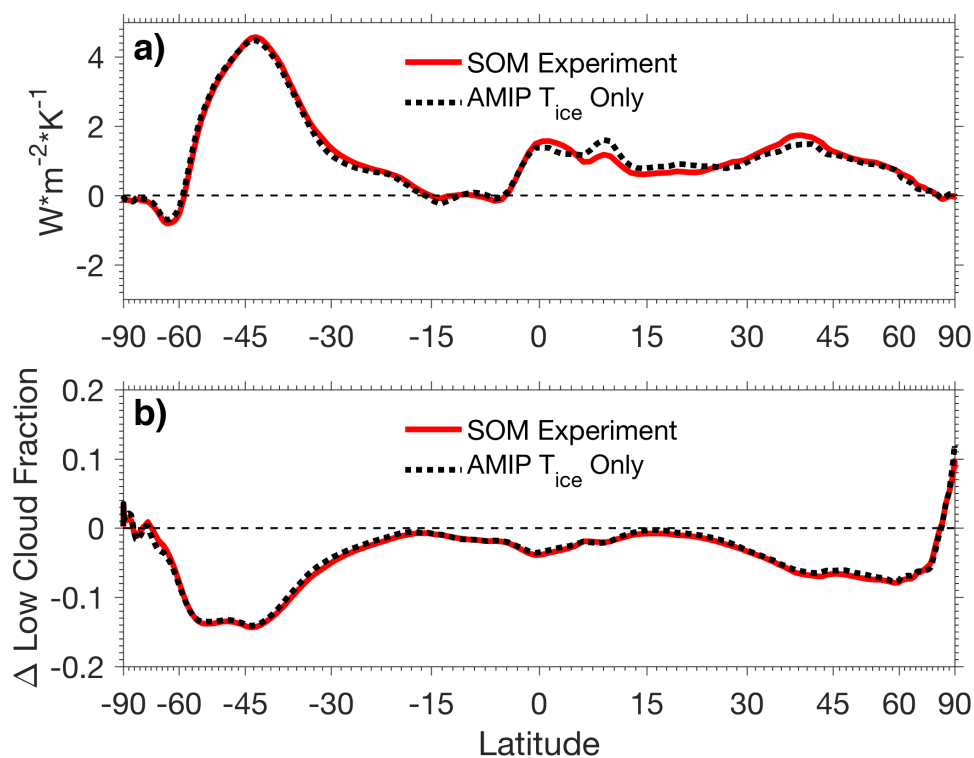


Figure 2.13: Shortwave cloud feedback (a) and change in low cloud fraction (b) resulting from a doubling of CO₂. Slab Ocean Experiment (solid red) and AMIP T_{ice}Only (dotted black). Shortwave cloud feedback estimated using the APRP method (Taylor et al. 2007) and normalized with the local surface warming. Feedback and low cloud fraction difference for SOM Experiment calculated using the average of the last 20 years of SOM2xExp (years 41- 60) and the average of the entire SOM1xExp run. Feedback and low cloud fraction difference for AMIPT_{ice}Only calculated using the average of years 1-10 of AMIP2xT_{ice}Only and AMIP1xT_{ice}Only.

Acknowledgements

We thank Brian Medeiros, Isla Simpson and Kris Karnauskas for helpful conversations related to this work and useful suggestions on the manuscript. We thank Dave Bailey and Bob Tomas for their help with setting up our model runs. We gratefully acknowledge high-performance computing support from Yellowstone ([ark:/85065/d7wd3xhc](https://doi.org/ark:/85065/d7wd3xhc)) provided by NCAR's Computational and Information Systems Laboratory, sponsored by the National Science Foundation. This work was supported by start-up funds awarded to J. E. Kay by the University of Colorado Cooperative Institute for Research in the Environmental Sciences and NSF award AGS 1554659. W. R. Frey is also supported by the Air Force Institute of Technology. The views expressed in this article are those of the authors and do not reflect the official policy or position of the United States Air Force, Department of Defense, or the U.S. Government.

Chapter 3

Do Southern Ocean Cloud Feedbacks Matter for 21st Century Warming?

3.1 Abstract

Cloud phase improvements in a state-of-the-art climate model produce a large 1.5 K increase in equilibrium climate sensitivity (ECS, the surface warming in response to instantaneously doubled CO₂) via extratropical shortwave cloud feedbacks. Here we show that the same model improvements produce only a small surface warming increase in a realistic 21st century emissions scenario. The small 21st century warming increase is attributed to extratropical ocean heat uptake. Southern Ocean mean-state circulation takes up heat while a slowdown in North Atlantic circulation acts as a feedback to slow surface warming. Persistent heat uptake by extratropical oceans implies that extratropical cloud biases may not be as important to 21st century warming as biases in other regions. Observational constraints on cloud phase and shortwave radiation that produce a large ECS increase do not imply large changes in 21st century warming.

3.2 Introduction

Equilibrium climate sensitivity (ECS), the global surface warming resulting from an instantaneous doubling of CO₂, is widely used for climate model intercomparison (i.e., Charney et al., 1979; Andrews et al., 2012). The range in ECS predicted by state-of-the-art climate models has remained consistent, evolving from 1.5–4.5 K (Charney et al., 1979) to 2.1–4.7 K in the Coupled Model Intercomparison Project Phase 5 (CMIP5) ensemble (Flato et al., 2013). Many processes impact ECS. In particular, observationally constrained cloud phase improvements in the

Community Earth System Model (CESM) aimed at rectifying a shortwave radiation bias common to many models (Trenberth & Fasullo, 2010) increase ECS by up to 1.5 K via more positive extratropical shortwave cloud feedback (Tan et al., 2016; Frey & Kay, 2018).

While ECS is important for model intercomparison and used in integrated assessment models, which estimate climate change impacts (Calel & Stainforth, 2017), the real-world significance of changes in ECS is unclear (Allen & Frame, 2007). Some have argued that intermodel ECS spread has a limited impact on climate change policy (Rogelj et al., 2014), while others argue that an ECS change of 0.5 K has important policy implications (Kaya et al., 2016). There is not a consistent relationship between ECS and transient warming quantified by transient climate response (TCR), an idealized transient warming metric (Cubasch et al., 2001), especially for high ECS values (Knutti et al., 2005; Meehl et al., 2007; Flato et al., 2013; Millar et al., 2015; Tsutsui, 2017). Many have argued that transient warming should not be inferred from ECS or vice versa (Wigley & Schlesinger, 1985; Senior & Mitchell, 2000; Allen et al., 2006; Armour et al., 2013; Rose et al., 2014; Andrews et al., 2015; Gregory et al., 2015; Gregory & Andrews, 2016; Zhou et al., 2016).

In addition, to idealized experiments used to estimate ECS and TCR, realistic 21st century forcing scenarios are applied to climate models to produce climate change projections (e.g., Representative Concentration Pathway (RCP) scenarios (Meinshausen et al., 2011)). Here we consider the relationship between ECS and 21st century warming. Among CMIP5 models (Forster et al., 2013) these quantities are positively correlated ($R^2 = 0.72$) though meaningful scatter exists (black dots in Figure 3.1). Some models separated by more than 1 K in ECS predict very similar transient warming. In short, based on existing literature, it remains unclear whether the large ECS

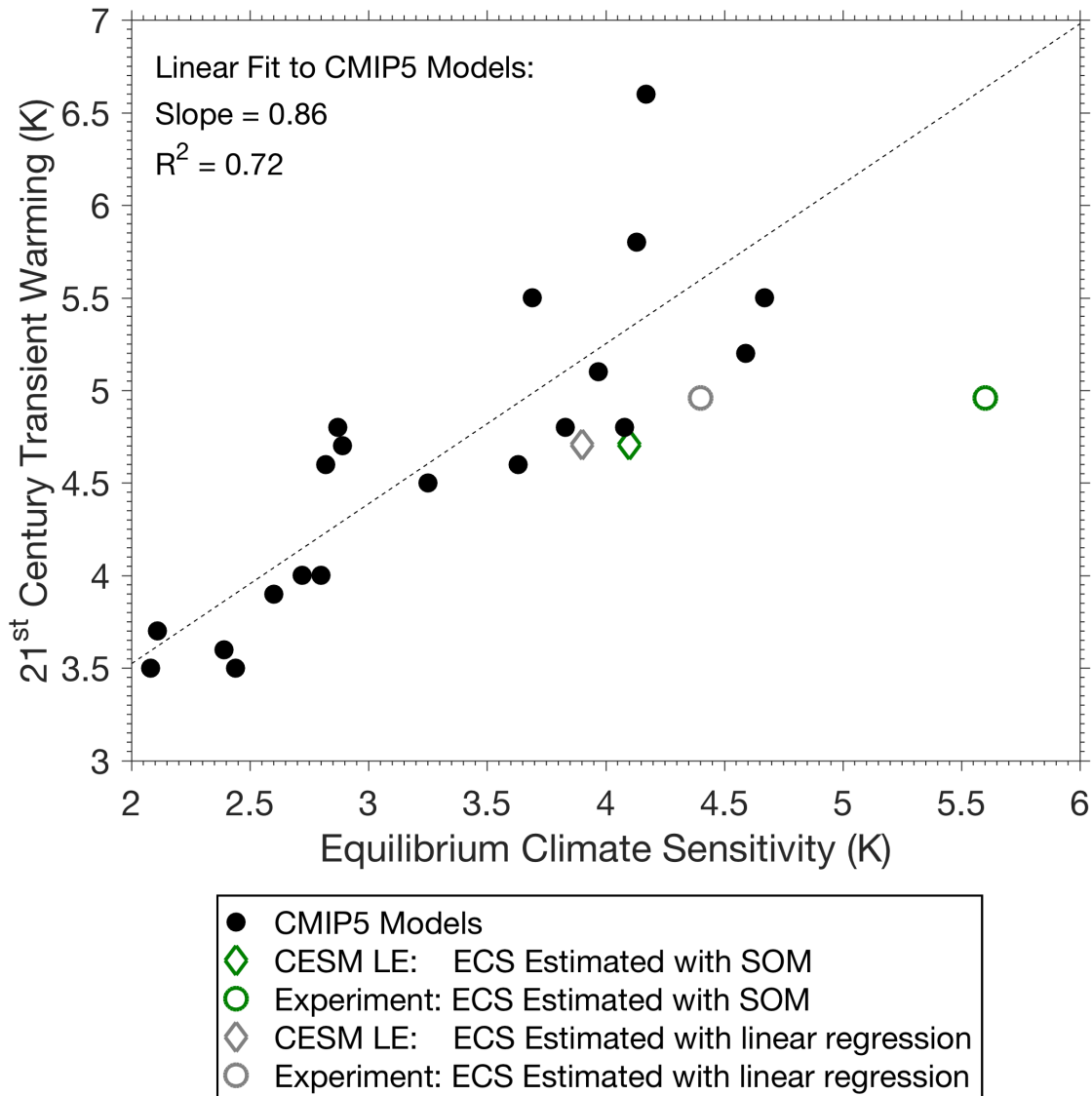


Figure 3.1: Relationship between Equilibrium Climate Sensitivity (ECS) and Transient 21st Century Warming in Global Climate Models. ECS plotted against the global mean warming over the last nine years (2091 through 2099) of the transient RCP8.5 forcing scenario relative to the pre-industrial period (1850-1899) for CMIP5 climate models (black dots) compared with the CESM Large Ensemble (diamonds) and our modified “Experiment” version of CESM (circles). *ECS and transient warming values for CMIP5 models taken from Forster et al. (2013) Table 1 (ECS) and Table 3 (transient warming). ECS estimated with slab ocean models (SOM) (green) and linear regression (gray) [Gregory et al., 2004] for the CESM Large Ensemble (diamonds) and the Experiment (circles) taken from Frey and Kay (2018). A best linear fit to the CMIP5 models is shown (dashed line) and text in the figure gives its slope and R^2 value.*

increase caused by improved model cloud phase over the Southern Ocean (Tan et al., 2016; Frey & Kay, 2018) is meaningful to projected transient 21st century warming.

Ocean heat uptake (OHU) is one of many factors influencing transient climate change (Hoffert et al., 1980; Raper et al., 2002; Manabe & Stouffer, 2007) in part by moving heat vertically (Gregory, 2000) to delay surface warming (Winton et al., 2010; Flato et al., 2013). OHU is not spatially uniform. Many models predict polar amplified OHU as the climate warms (Marshall et al., 2015). This extratropical (defined as poleward of 30° latitude) OHU is particularly effective at slowing surface warming because of its impact on radiative feedbacks (Winton et al., 2010; Bitz et al., 2012; Armour et al., 2013; Rose et al., 2014; Rose & Rayborn, 2016; Rugenstein et al., 2016a; Trossman et al., 2016).

The efficacy of extratropical OHU to delay surface warming has been demonstrated with a variety of idealized models (Winton et al., 2010; Rose et al., 2014; Armour et al., 2016; Rugenstein et al., 2016a; Trossman et al., 2016). Here we investigate the impact of OHU with a realistic model configuration including a full-depth dynamic ocean and a plausible forcing scenario. We show that model improvements that produce a large ECS increase produce only a small, though statistically significant, increase in 21st century warming under the RCP8.5 forcing scenario. Our results suggest that the effectiveness of OHU to slow transient warming in our experiment is linked to the collocation of increased positive shortwave cloud feedback, which drive the ECS increase, with areas of maximum OHU in the extratropics.

3.3 Model Description

We use the large ensemble (LE) version of CESM (Kay et al., 2015) based on CESM version 1 (Hurrell et al., 2013). Following Kay et al. (2016b) and Frey and Kay (2018), we modify

the Community Atmosphere Model version 5 to produce more liquid and less ice in extratropical shallow convective clouds. This improvement to cloud phase, along with tuning the threshold relative humidity for low cloud formation to maintain radiative equilibrium, reduces shortwave radiation biases over the Southern Ocean and tropics (Kay et al., 2016b). Starting at the end of a 200 year run forced with constant 1850 conditions (which allows upper ocean temperatures to reach a new equilibrium (Kay et al., 2016b)), we initialize a transient run with historical (1850–2005) and RCP8.5 (2006–2100) forcings (Riahi et al., 2011). Hereafter, we refer to this modified transient run as the “Experiment.”

We compare our Experiment with the CESM LE (Kay et al., 2015). The LE simulates the years 1920–2100 multiple times with small atmospheric initial condition differences using the same historical and RCP8.5 forcing as our Experiment. We use 38 of the 40 LE members, omitting 31 and 33, which were postprocessed in a way that may impact radiative feedback calculations (Baker et al., 2016). The LE allows for separation of internal variability from forced response and provides an ideal data set to identify the impact of our cloud phase improvement and tuning on transient warming.

3.4 Results

3.4.1 Surface Warming

We first examine global, annual mean surface warming (Figure 3.2a). During the historical period (1920–2005) Experiment warming is within the LE range and comparable to observations. In the RCP8.5 period (2006–2100) the Experiment warms more than the LE, but only slightly above the LE range. By the late 21st century (2081–2100) the Experiment has warmed by 4.78 K above the 1850–1899 baseline. For comparison, LE warming over the same period ranges from

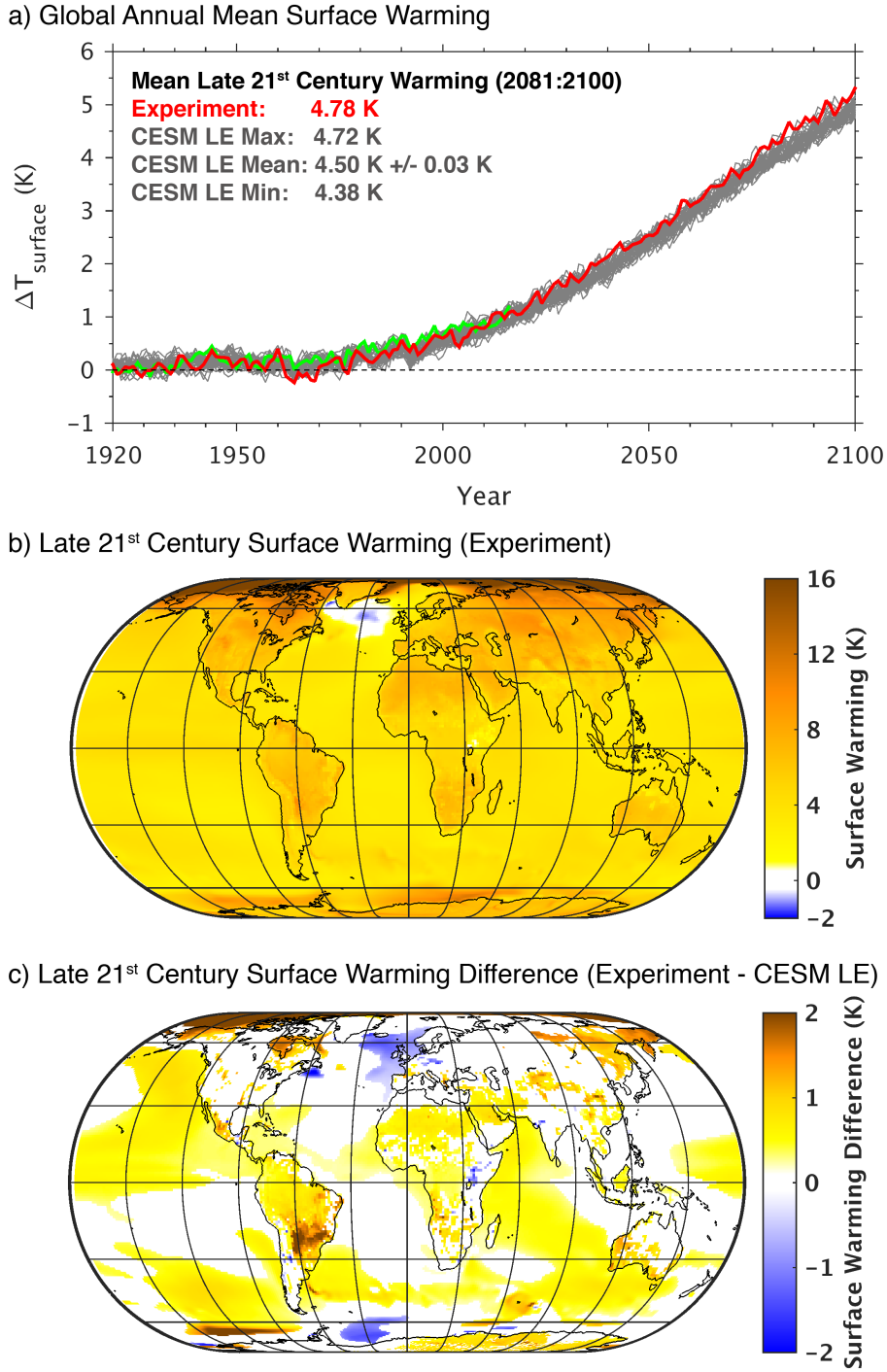


Figure 3.2: Surface warming above pre-industrial (1850-1899). a) Global annual mean surface warming: Experiment (red), CESM LE (gray), observations (green) [Hansen et al., 2010]. b) Late 21st century (2081-2100) annual mean surface warming (Experiment). c) Late 21st century annual mean surface warming difference (Experiment - CESM LE mean). *Text in (a) shows mean warming over the late 21st century with a 99% confidence interval calculated about the LE mean using the T-distribution. Differences colored in (c) are statistically significant (99% confidence) [Wilks, 2016]. Differences not statistically significant are white.*

4.38 to 4.72 K with a mean of 4.50 K. The 0.3 K difference in warming between the Experiment and LE mean is statistically significant (99% confidence level) but small compared with the 1.5 K ECS increase (Frey & Kay, 2018).

The Experiment spatial pattern of warming (Figure 3.2b) follows well-established patterns in response to greenhouse forcing: notably polar amplification and North Atlantic cooling. Comparing warming between the Experiment and LE (Figure 3.2c) reveals interesting extratropical patterns. In the North Atlantic, the Experiment warms less than the LE. In the southern extratropics, there is increased Experiment warming from roughly 30 to 50°S and less warming further poleward.

3.4.2 Radiative Feedback Analysis

To understand the drivers behind the small 21st century warming increase (Figure 3.2a) and the geographic differences in warming (Figure 3.2c) between the Experiment and LE, we analyze radiative feedbacks (Soden & Held, 2006). We find that the Experiment has more positive shortwave cloud feedback than the LE and this increase is not fully compensated by other feedbacks. In the global mean (Figure 3.3a), both the Experiment and LE exhibit positive shortwave feedback as a result of positive cloud and surface albedo feedbacks. In contrast, both the Experiment and LE exhibit negative longwave feedback dominated by a negative Planck feedback partly compensated by positive water vapor and cloud feedbacks. The difference in shortwave feedback between the Experiment and LE is more than double the difference in longwave and dominated by more positive cloud feedback (Figure 3.3b).

The increase in shortwave cloud feedback occurs entirely in the extratropics, primarily over the Southern Ocean (Figure 3.3c). In the tropics, the Experiment shortwave cloud feedback is

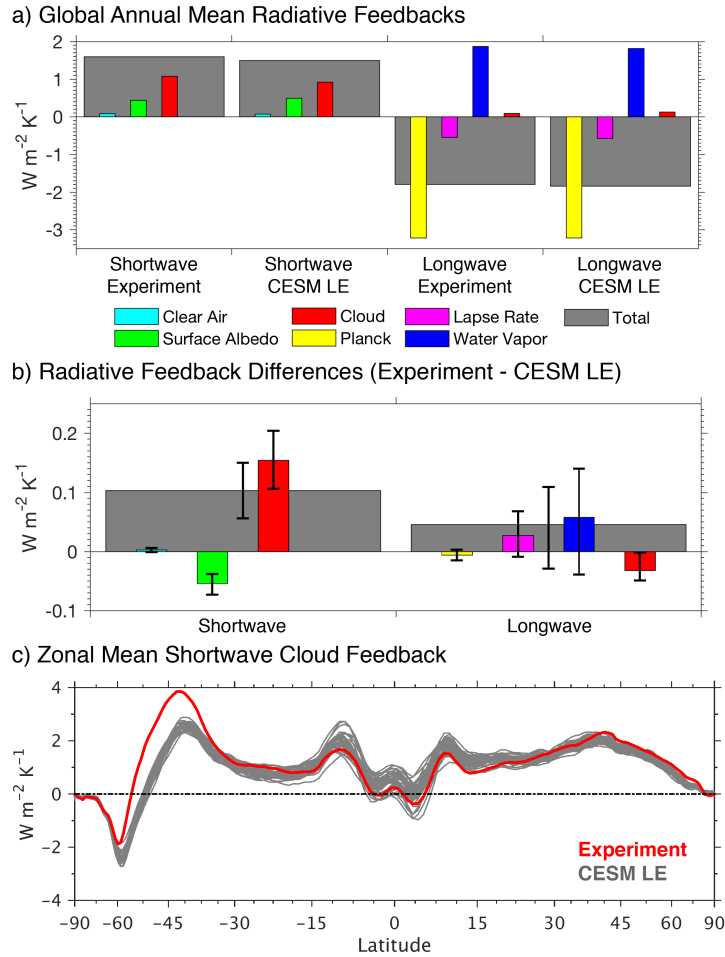


Figure 3.3: 21st century Radiative Feedbacks (2091-2100 minus 1996-2005). a) Global annual mean radiative feedbacks normalized by global annual mean surface temperature change. b) Radiative feedback differences (Experiment minus CESM LE mean); error bars show the range among CESM LE members. c) Zonal annual mean shortwave cloud feedback normalized by local surface temperature change: Experiment (red) and CESM LE members (gray). *Longwave feedbacks estimated using radiative kernels [Pendergrass et al., 2017]. Shortwave feedbacks estimated using the approximate partial radiative perturbation (APRP) method in order to separate cloud and surface feedbacks [Taylor et al., 2007].*

within the LE range. In the extratropics, the Experiment shortwave cloud feedback is either at the top of (Northern Hemisphere) or well above (Southern Hemisphere) the LE range. This pattern is caused by the cloud improvements in the Experiment, which impact the magnitude of shortwave cloud feedback due to phase changes with warming (Frey & Kay, 2018).

The shortwave cloud feedback difference between the Experiment and LE (Figure 3.3c) is similar to the pattern of difference shown in slab ocean model runs forced with doubled CO₂ used to estimate ECS in Frey and Kay (2018). Yet the increase in 21st century warming (Figure 3.2a) is much smaller than the ECS increase of 1.5 K in Frey and Kay (2018). Taken together, these results suggest that OHU mutes the surface warming caused by extratropical cloud feedback in the RCP8.5 run and causes the increase in transient warming between the Experiment and LE to be small.

3.4.3 Ocean Heat Uptake

In both the Experiment and LE, OHU occurs preferentially in the extratropics (Figures 3.4a and 3.4b). The Southern Ocean takes up heat over the entire RCP8.5 period maximizing near 60°S. Northern extratropical OHU is not present at the beginning of the run but develops over time. By 2100 there is a broad OHU maximum near 60°N. By the late 21st century (2081–2100) the area-integrated OHU anomaly in the northern extratropics in the Experiment (LE) averages to 782 TW (635 TW) compared with 610 TW (516 TW) in the southern extratropics and only 49 TW (130 TW) in the tropics. In the southern extratropics, the difference in OHU between the Experiment and LE is not uniform but is distributed longitudinally over the Southern Ocean, the same region containing large shortwave cloud feedback differences (Figures 3.4c and 3.4d). Northern extratropical differences in OHU between the Experiment and LE occur mainly in the Atlantic and are not collocated with shortwave cloud feedback differences. We next analyze the role of ocean circulation in producing extratropical OHU.

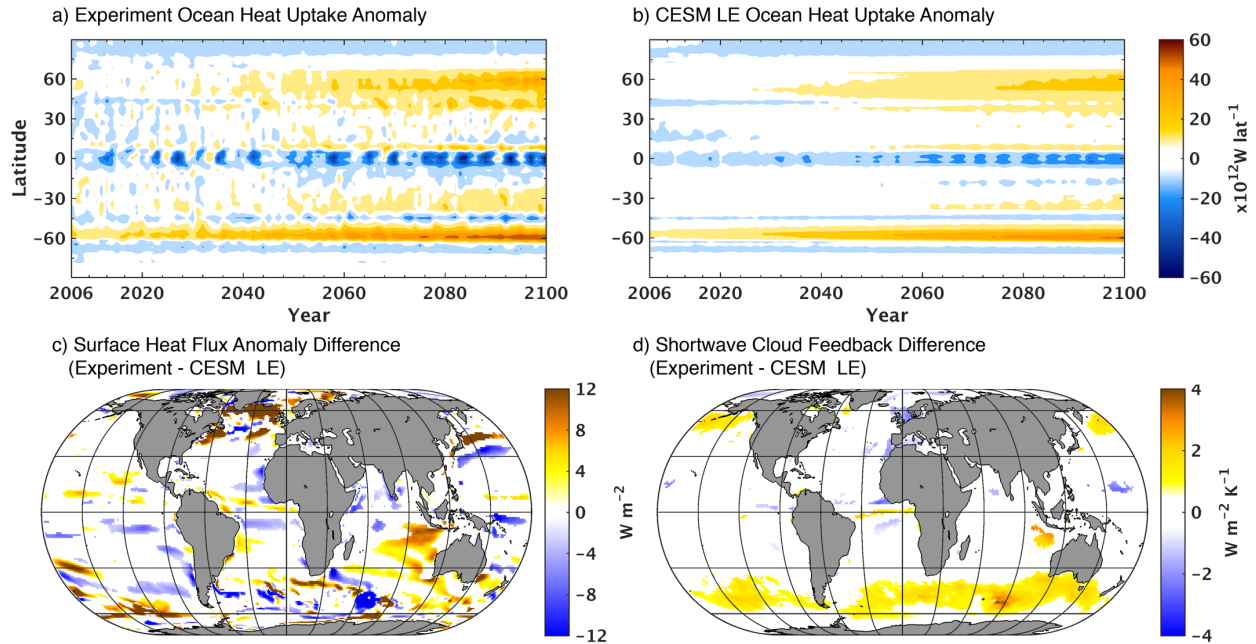


Figure 3.4: 21st century ocean heat uptake (OHU) anomalies compared to pre-industrial (1850-1899). a) Annual mean zonally integrated OHU anomaly for the Experiment. b) As in a) for the CESM LE mean. c) Late 21st century (2081-2100) surface heat flux anomaly difference (Experiment minus CESM LE mean). d) as in c) for shortwave cloud feedback. *Zonally integrated ocean heat uptake calculated by multiplying surface heat flux by grid cell area and summing zonally. Positive values indicate heat into the ocean. Differences colored in c) and d) are statistically significant (99% confidence) [Wilks, 2016]. Differences not statistically significant are white.*

3.4.4 Ocean Dynamics

In the Southern Ocean, positive heat content anomalies exist throughout the top 2,000 m (Figure 3.5a, colors). The heat content anomaly pattern is due to mean-state ocean circulation (Figure 3.5a, contours). The upwelling branch of the meridional overturning circulation (MOC) (Marshall & Speer, 2012) brings cool water to the surface where it gains heat from the atmosphere, producing maximum OHU near 60°S (Figure 3.4a). The circulation then brings this water equatorward before it sinks near 45°S, producing a heat content maximum and moving heat to depth (Figure 3.5a) (Armour et al., 2016). The circulation strength changes little over the RCP8.5

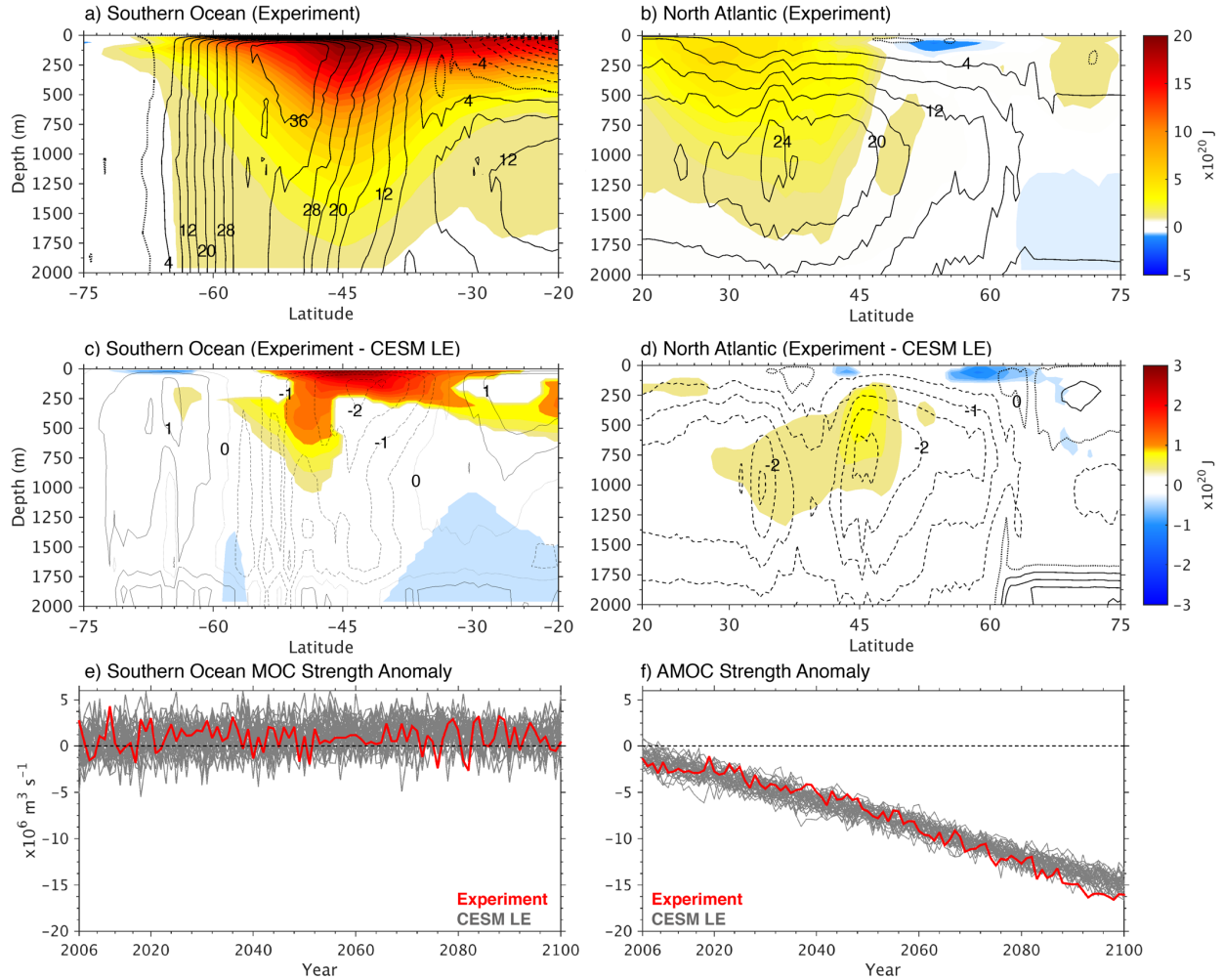


Figure 3.5: 21st century ocean heat content and meridional overturning circulation (MOC) streamfunction compared to pre-industrial (1850-1899). a) Experiment late 21st century (2081-2100) Southern Ocean zonally-integrated ocean heat content anomaly (colors) and pre-industrial MOC streamfunction (contours, $10^6 \text{ m}^3 \text{ s}^{-1}$). b) As in a) for the North Atlantic. c) Late 21st century difference (Experiment minus CESM LE mean) in Southern Ocean heat content anomaly (colors) and MOC streamfunction anomaly (contours, $10^6 \text{ m}^3 \text{ s}^{-1}$). d) as in c) for the North Atlantic. e) Southern Ocean and f) North Atlantic MOC strength anomaly. *Ocean heat content calculated by multiplying potential temperature by grid cell volume, a constant heat capacity for sea water ($3992 \text{ J Kg}^{-1} \text{ K}^{-1}$), and a constant sea water density (1035 Kg m^{-3}), as in Rugestein et al. [2013]. MOC strength defined as the maximum streamfunction between 30 and 60 degrees South (e) and North (f). Positive (negative) streamfunction, shown with solid (dashed) contours, indicates clockwise (counterclockwise) circulation. Differences colored in (c) and (d) are statistically significant (99% confidence) [Wilks, 2016]. Differences not statistically significant are white.*

period (Figure 3.5e). Southern Ocean heat uptake is enhanced in the Experiment compared to the LE due to greater heating at the surface from a more positive shortwave cloud feedback (Figure 3.4d). The Experiment warms more than the LE both at the surface and at depth at southern midlatitudes (Figure 3.5c).

In the North Atlantic, the mean-state Atlantic MOC (AMOC) brings water northward before sinking at higher latitudes (Figure 3.5b, contours). As the RCP8.5 scenario progresses the AMOC slows down (Figure 3.5f) (Stouffer & Manabe, 2003; Gregory et al., 2005; Weaver et al., 2012; Jahn & Holland, 2013; Rugenstein et al., 2016b;) and decreased high-latitude sinking results in less cool water descending and less warm surface water transported northward (Gregory, 2000; Banks & Gregory, 2006; Xie & Vallis, 2012). This produces high-latitude near-surface cooling and warming at depth (Figure 3.5b). The AMOC slows down more in the Experiment than the LE by the late 21st century (Figure 3.5f). As a result, heat content at depth increases and near-surface heat content decreases in the extratropical North Atlantic in the Experiment compared to the LE (Figure 3.5d).

3.5 Discussion

Compared to the LE, our Experiment takes up and stores more heat at depth in both the Southern Ocean and North Atlantic (Figures 3.4 and 3.5). Southern Ocean heat uptake does not require circulation changes (Marshall & Speer, 2012; Armour et al., 2016) and can be understood as a direct response acting to move heat input by cloud feedback to depth, slowing surface warming. Southern Ocean heat uptake is stronger in the Experiment than the LE not because of circulation differences (Figure 3.5e) but because more heat is available at the surface from more positive shortwave cloud feedback in the same region (Figure 3.4d). The efficacy of OHU to mute

the impact of increased shortwave cloud feedback over the Southern Ocean suggests that model biases in this region may be less important to 21st century warming than biases in regions without strong OHU. We cannot be sure whether the increase in Southern Ocean heat uptake in our Experiment has reached a limit or if OHU would increase further if the shortwave cloud feedback were even more positive.

In contrast, North Atlantic OHU develops as warming progresses (Figures 3.4a and 3.4b) and is not collocated with differences in shortwave cloud feedback between the Experiment and LE (Figure 3.3d). Circulation changes necessary for North Atlantic OHU (Gregory, 2000; Banks & Gregory, 2006; Xie & Vallis, 2012) result from an AMOC slowdown (Figures 3.5d and 3.5f), a consequence of increased warming (Gregory et al., 2005; Weaver et al., 2012; Jahn & Holland, 2013). In a sense, North Atlantic OHU acts like a negative feedback (Trossman et al., 2016; Winton et al., 2013). The Experiment warms more than the LE over time (Figure 3.2a), which causes the AMOC to slow more in the Experiment (Figure 3.5f). As a consequence, North Atlantic OHU increases more in the Experiment than the LE by the late 21st century (Figure 3.4c), slowing surface warming.

Improved cloud phase in CESM produces a large (1.5 K) increase in ECS (Frey & Kay, 2018) but only a small increase in 21st century warming (Figure 3.2a). While this is not astonishing, it is also not obvious based on comparison between ECS and 21st century warming among CMIP5 models (black dots in Figure 3.1). One difference between our models and the CMIP5 ensemble is the cause of intermodel ECS spread. Among modern ensembles, ECS spread has been attributed to tropical and subtropical feedbacks (Vial et al., 2013; Webb et al., 2013; Sherwood et al., 2014; Tian, 2015) while extratropical feedbacks drive the ECS increase in our Experiment (Figure 3.3). This geographical difference in feedbacks may be important because of

differences between tropical and extratropical OHU. Specifically, tropical OHU is important on short timescales (Clement et al., 1996; Held et al., 2010), but does not persist for long periods. Rose et al. (2014, Figure A1) show that in years 1–5 after quadrupling CO₂ OHU occurs in both the tropics and extratropics, but by years 96–105 tropical OHU is virtually zero while extratropical OHU persists (see also Marshall et al., 2015; Rugenstein et al., 2016a). Similarly, in transient runs OHU is much greater in the extratropics than tropics (Figure 3.4). When ECS increase is driven by feedbacks collocated with OHU in the southern extratropics, e.g., our Experiment, the ocean takes up heat and moves it to depth (Figure 3.5) slowing transient warming. In contrast, we hypothesize that tropical feedbacks contribute more to surface warming in transient runs because they are not collocated with persistent OHU. Therefore, ECS and transient warming may be more closely related for models which differ primarily in tropical shortwave feedbacks. Future work is required to determine whether collocation of feedbacks and OHU is necessary to slow transient warming and determine its relevance more generally.

Our work identifies interesting discrepancies in ECS estimates obtained with two common techniques. ECS is usually estimated rather than explicitly diagnosed due to the cost of running a fully coupled climate model to equilibrium. We estimate ECS for the Experiment and LE with mixed-layer “slab” ocean models (SOM) run to equilibrium with doubled CO₂. In contrast, CMIP5 ECS estimates use linear regression (Gregory et al., 2004) applied to fully coupled models with full-depth oceans. ECS is commonly estimated with both SOM (Meehl et al., 2007) and linear regression (Gregory et al., 2004; Andrews et al., 2012; Flato et al., 2013), and both techniques have been shown to produce reasonable estimates (Danabasoglu & Gent, 2009; Jonko et al., 2013; Li et al., 2013). Nevertheless, both methods have limitations. SOMs do not account for ocean circulation changes and produce different spatial patterns of feedback and warming compared with

fully coupled models (Boer & Yu, 2003; Williams et al., 2008; Jonko et al., 2013). Linear regression uses simulations that have not reached equilibrium and thus lack the Southern Ocean warming our SOM simulations achieve (Armour et al., 2013; Frey & Kay, 2018). As a result, linear regression likely underestimates true ECS (Gregory et al., 2004; Andrews et al., 2015; Knutti & Rugenstein, 2015; Gregory & Andrews, 2016; Knutti et al., 2017). Despite these limitations, the impact of estimation method is thought to be minor compared to intermodel ECS spread (Flato et al., 2013).

Our Experiment is one case where these two methods produce inconsistent estimates. Using linear regression (Gregory et al., 2004) to estimate ECS for the Experiment and LE (Frey & Kay, 2018) reduces the ECS difference between the two versions of the model compared to SOM ECS estimates (compare gray and green markers in Figure 3.1). We believe that our SOM ECS estimate is closer to the true ECS of our Experiment than ECS estimated with linear regression. This is in part because it compares favorably with Tan et al. (2016), who made modifications to CESM similar to our Experiment and found an ECS increase of 1.3 K compared to default CESM by running a fully coupled climate model with a full-depth ocean until the global top-of-atmosphere radiation budget was balanced with doubled CO₂. The large difference between SOM and linear regression ECS estimates for the Experiment suggests that the spatial differences in warming and feedback, which differentiate the Experiment from the LE, may impact the accuracy of ECS estimates (Gregory et al., 2004; Murphy, 2010; Armour et al., 2013; Andrews et al., 2015).

Our study is nominally limited by its design in that we completed only one RCP8.5 Experiment run to compare to 38 existing LE members. Thus, while we can show our Experiment falls outside of the internal variability-generated range of the LE (Figure 3.2a), we cannot show how a distribution of Experiment runs would compare. We consider this limitation to be second

order because the difference in 21st century warming between the Experiment and LE is so much smaller than the ECS difference. Assuming that the internal variability in an Experiment ensemble would be of the order of the LE, our main conclusions would be unchanged. Notwithstanding this limitation and the discussion above, the main result of this study stands. Observational constraints on cloud phase that imply a large increase in ECS (Tan et al., 2016; Frey & Kay, 2018) do not imply a large increase in 21st century warming.

3.6 Conclusion

Cloud phase improvements in a climate model that decrease radiation biases produce a large (1.5 K) increase in ECS via extratropical cloud feedback (Frey & Kay, 2018). Despite this, 21st century warming under the RCP8.5 forcing scenario increases by a small, though statistically significant, 0.3 K compared to the default model, an increase just above the warming range due to internal variability (Figure 3.2a). The shortwave cloud feedbacks that drive increased ECS occur in the extratropics where the ocean is most effective at taking up heat (Figure 3.4). As a consequence, in the RCP8.5 scenario, the ocean takes up a portion of the heat from more positive extratropical shortwave cloud feedbacks (Figures 3.3 and 3.4) and moves it to depth (Figure 3.5), slowing surface warming compared to the default model. These processes are demonstrated with a state-of-the-art global climate model including a full-depth dynamic ocean and a realistic forcing scenario complementing previous work, which has identified the impact of extratropical OHU using idealized model configurations (i.e., Rose et al., 2014; Rugenstein et al., 2016a; Trossman et al., 2016). The ability of extratropical oceans to take up heat implies that extratropical cloud biases may not be as important to 21st century warming as biases in other regions. Observational

constraints on cloud phase and shortwave radiation that produce a large ECS increase do not imply large changes in 21st century warming projections.

Acknowledgments

We thank Isla Simpson, Brian Rose, and Brian Medeiros for helpful conversations. We thank Dave Bailey and Gary Strand for help with model setup. Our “Experiment” model is archived on the NCAR High Performance Storage System Repository (/home/wfrey/csm/b.e11.B20TRC5CNBDRD.f09_g16.001_SCminus20 and /home/wfrey/csm/b.e11.BRCP85C5CNBDRD.f09_g16.001_SCminus20/) and available upon request from William Frey. We acknowledge high-performance computing support from Yellowstone (<ark:/85065/d7wd3xhc>) provided by NCAR’s Computational and Information Systems Laboratory, sponsored by the NSF. This work was supported by startup funds awarded to Jennifer Kay by the University of Colorado Cooperative Institute for Research in the Environmental Sciences and NSF award AGS1554659. William Frey is also supported by the Air Force Institute of Technology. The views expressed in this article are those of the authors and do not reflect the official policy or position of the United States Air Force, Department of Defense, or the U.S. Government.

Chapter 4

The Combined Influence of Observed Southern Ocean Clouds and Sea Ice on Top-of-Atmosphere Albedo

4.1 Abstract

When sea ice concentration decreases, surface albedo decreases. Yet, the impact of Southern Ocean sea ice concentration decreases on top-of-atmosphere albedo is uncertain. Why? The cloud cover and opacity response to Southern Ocean sea ice variability has been challenging to quantify. Here, we use observations to constrain the cloud response to Southern Ocean sea ice variability and assess the combined influence of sea ice and clouds on top-of-atmosphere albedo. We focus on the spring and summer seasons that dominate the high-latitude shortwave energy budget. To isolate the influence of sea ice concentration on clouds, we analyze space-borne lidar observations in regions where present-day sea ice concentration varies. During spring, low cloud cover is slightly (4%) higher over open water compared to sea ice. During summer, sea ice variability does not affect low cloud cover. During both spring and summer, cloud opacity is larger over open water than over sea ice due to a cloud phase shift from ice toward liquid with warming. Independent ship-based visual and radiosonde observations available during summer corroborate the lidar results. Even with the cloud response, satellite-observed top-of-atmosphere albedo is lower over open water than over sea ice. As a result, the observations show the cloud response to sea ice retreat with warming will not mask the surface albedo decrease. In other words, more shortwave radiation will be absorbed when Southern Ocean sea ice is lost.

4.2 Introduction

Both clouds and sea ice influence Earth's energy budget by reflecting incoming shortwave radiation back to space. Sea ice has a strong influence on surface albedo, as sea ice is much more reflective than open ocean. Changes in surface albedo account for more than half of the interannual variability in planetary albedo (Qu & Hall, 2005). As the climate warms, sea ice is expected to retreat exposing more open ocean and decreasing surface albedo. However, cloud changes occurring in the same region as sea ice changes also influence top-of-atmosphere albedo (e.g. Hartmann & Ceppi, 2014). If the cloud response to sea ice retreat cannot completely compensate for the surface albedo decrease, top-of-atmosphere albedo will decrease. As a result, more shortwave radiation will be absorbed and accelerate warming (Qu & Hall, 2005; Fitzpatrick & Warren, 2007; Morrison et al., 2018).

Sea ice interacts with clouds at both poles. Yet, the Arctic and the Southern Ocean sea ice zone (poleward of 60°S) differ in important ways. The Southern Ocean sea ice zone is confined to equatorward of ~70°S due to the presence of Antarctica. In contrast, the Arctic Ocean and Arctic sea ice zone cover the North Pole. When compared to the Arctic, Southern Ocean sea ice-cloud interactions are more strongly influenced by deep ocean circulation (Marshall & Speer, 2012) and an all-season mid-latitude storm track. Recent trends in Arctic and Southern Ocean sea ice extent are opposite, with decreased Arctic sea ice extent and increased Southern Ocean sea ice extent (Stammerjohn et al., 2012; Simmons, 2015). Finally, each hemisphere is expected to respond to climate change differently, with the Arctic warming faster than the global average (Serreze et al., 2009) while the Southern Ocean warms more slowly than the global average (Armour et al., 2016). Given these differences, the relationship between sea ice and clouds in the Arctic and over the Southern Ocean must be assessed separately.

In the Arctic, the impact of sea ice on clouds has been quantified and the underlying physical mechanisms have been identified (see review paper by Kay et al., 2016c). During spring and fall, cloud cover and optical depth are larger over open water compared to over sea ice (Schweiger et al. 2008; Kay & Gettelman, 2009; Eastman & Warren, 2010; Palm et al., 2010; Morrison et al., 2018). During summer, there is no significant difference in either cloud cover or optical depth over open water compared with sea ice (Kay & Gettelman, 2009; Kay & L'Ecuyer, 2013; Morrison et al., 2018). The relationship between clouds and Arctic sea ice may depend on atmospheric conditions (e.g. stability and subsidence) which influence air-sea coupling (Barton et al., 2012; Taylor et al., 2015). In fact, the seasonal difference in cloud response to sea ice is due to the strength of air-sea coupling which is weaker during summer than other seasons (Morrison et al., 2018).

Over the Southern Ocean, the impact of sea ice on clouds is known during Austral winter but less certain during Austral spring and summer. In winter, sea ice and clouds are strongly linked, with low cloud cover increasing by 20-30% over open water compared to sea ice (Wall et al., 2017a). Similarly, annual mean cloud cover is greater over open water than over sea ice (Bromwich et al., 2012). During spring and summer, relatively sparse ship-based observations of clouds and solar irradiance suggest that clouds are more prevalent and optically thicker over open water than over sea ice, though this finding could be influenced by latitudinal variation (Fitzpatrick & Warren, 2007). The impact of Southern Ocean sea ice variability on top-of-atmosphere albedo, which determines how much shortwave radiation is absorbed, depends strongly on the cloud response. If clouds remain unchanged as sea ice retreats more shortwave radiation is absorbed, but if cloud cover or opacity increase as sea ice retreats the amount of absorbed shortwave radiation may decrease (Fitzpatrick & Warren, 2007).

Building on previous work, the goal of this study is to constrain the cloud and top-of-atmosphere albedo response to Southern Ocean sea ice variability. We focus on Austral spring and summer which dominate the Southern Ocean shortwave energy budget (e.g. Fitzpatrick & Warren, 2007). The Southern Ocean shortwave energy budget is particularly important because the Southern Ocean, including the sea ice zone poleward of 60°S, is one of the only regions of the globe where models robustly predict a negative shortwave cloud radiative feedback (Zelinka et al., 2012a). The magnitude of this negative feedback has a large impact on climate sensitivity (Tan et al., 2016; Frey et al., 2017; Frey & Kay, 2018) and could be influenced by sea ice-cloud interactions.

Historically, research on Southern Ocean sea ice-cloud interactions has been limited by a lack of reliable observations. Reanalysis products contain large errors over the Southern Ocean due to the lack of observational constraints (Hines et al. 1999; Marshall 2002; Bromwich & Fogt 2004; Bromwich et al. 2007; Bromwich et al., 2011; Nicolas & Bromwich, 2011; Jones et al., 2016). Additionally, reliable cloud observations are limited because they must be independent of surface condition to identify the impact of sea ice on clouds. Passive satellite observations of clouds (e.g. from the Moderate Resolution Imaging Spectrometer (MODIS)) are not independent of surface condition (Liu et al., 2010; Kay & L'Ecuyer, 2013). Using reanalysis and passive satellite observations to identify sea ice-cloud interactions can produce results different from those arrived at with surface-independent observations (Kay & Gettelman, 2009; Eastman & Warren, 2010; Palm et al., 2010; Morrison et al., 2018).

With this study, we overcome the limitations of previous studies by using two independent observational datasets that are both independent of surface conditions: 1) space-borne LIDAR and 2) visual ship-based observations. Following Morrison et al. (2018), we restrict our analysis to

areas where sea ice concentration varies. Thus, we ensure that our findings are not an artifact of geographic (latitudinal) variations in cloud properties. We find similar cloud changes using the independent satellite and surface-based datasets. The observations we analyze suggest the cloud response to sea ice variability is not enough to compensate for the change in surface albedo. In other words, even when the cloud response is included, top-of-atmosphere albedo is lower and more shortwave radiation is absorbed over open water compared to over sea ice.

4.3 Data and Methods

4.3.1 Data

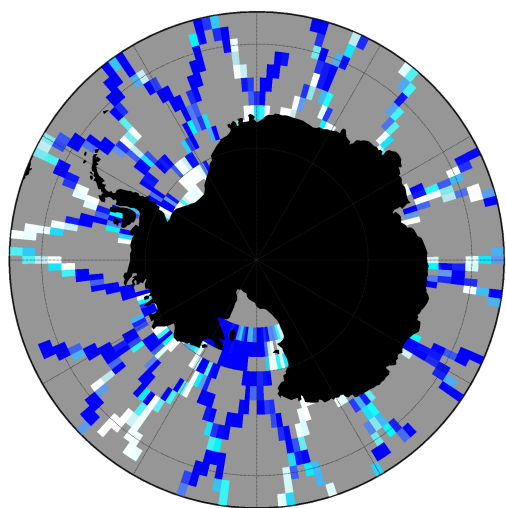
To isolate the relationship between sea ice and clouds we use observations that are independent of the underlying surface condition and available at daily or higher time frequency. We primarily use a decade (2006-2015) of observations from the Cloud-Aerosol LIDAR with Orthogonal Polarization (CALIOP) instrument (Winker et al., 2007) onboard the CALIPSO satellite. As an active sensor, CALIPSO cloud observations are not influenced by surface conditions. Our cloud cover analysis is based on the CALIPSO GCM-Oriented CALIPSO Cloud Product (CALIPSO-GOCCP) version 2.9 (Chepfer et al., 2010). CALIPSO-GOCCP provides daily cloud cover on a 2x2 degree grid with a 480m vertical resolution. Cloud cover is provided at low (Pressure>680 hPa), mid (680>Pressure>440 hPa), and high (Pressure<440 hPa) levels as well as total cloud cover. Clouds are detected for individual profiles taken every 333 m along-track in the CALIPSO footprint (70m diameter) (Winker et al., 2007). Cloud cover is defined for each grid cell and day as the number of cloudy profiles divided by the total number of profiles. CALIPSO data for any given day is relatively sparse and daily cloud cover in a grid cell is defined by a single satellite pass. Using daily data from a 10-year period provides full spatial coverage over the

Southern Ocean with multiple days of observations in each grid cell (Figure 4.1). In addition, our 10-year sample minimizes biases linked to the small CALIPSO footprint (Konsta et al., 2016) and allows us to identify relationships between clouds and sea ice.

To analyze cloud optical depth, we use daytime opaque and thin cloud cover from CALIPSO-GOCCP version 3.0 (Guzman et al., 2017). The opaque/thin product classifies clouds based on LIDAR attenuation. Clouds that fully-attenuate the LIDAR (optical depth $>\sim 3$, no surface echo detect) are classified as opaque while scenes where the LIDAR is not fully attenuated (optical depth < 3 , surface echo detected) are classified as thin. This definition of thin clouds includes both scenes which are covered with clouds with optical depth < 3 and scenes where the CALIPSO footprint (70m diameter) is partially filled with cloud such that the LIDAR is not fully attenuated even though the clouds that exist in the footprint may individually be optically thick (Leahy et al., 2012). We use these definitions to define opaque cloud fraction, or the opaque cloud cover divided by the total (opaque plus thin) cloud cover. The altitude of LIDAR attenuation is also provided. While the opaque/thin product is limited in that it only provides information on whether cloud optical depth is greater or less than ~ 3 , it is a direct measurement that is not influenced by surface condition. Cloud shortwave radiative properties change near an optical depth of 3 and continue to change with increasing optical depth (Zelinka et al., 2012b, Figure 1b). Therefore, the CALIPSO attenuation threshold does provide meaningful, if not complete, information about a cloud's impact on top-of-atmosphere albedo.

We pair CALIPSO cloud observations with coincident satellite-based observations of sea ice concentration and top-of-atmosphere albedo. Daily sea ice observations are from the National Snow and Ice Data Center (NSIDC) Climate Data Record of Passive Microwave Sea Ice

a) CALIPSO Low Cloud Cover on 1 December 2006



b) Number of CALIPSO Observations during summer (DJF) 2006-2015

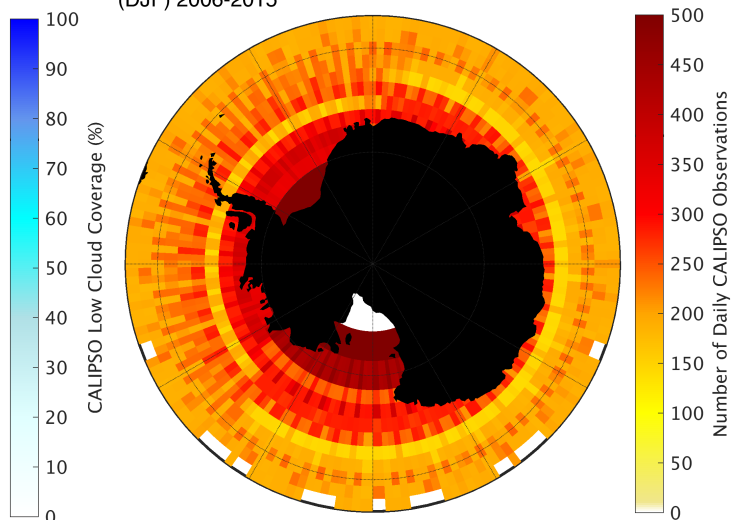


Figure 4.1: CALIPSO-GOCCP data demonstration. a) A single day (1 December 2006) of CALIPSO Low Cloud Cover data on the 2x2 degree GOCCP output grid (Chepfer et al., 2010). b) Number of daily CALIPSO Low Cloud Cover observations in each grid cell for summer (DJF) during our study period (2006-2015). Gray area in (a) shows grid cells with no CALIPSO data on 1 December 2006.

Concentration, version 3 (Peng et al., 2013; Meier et al., 2017). NSIDC sea ice data is published on a 25x25 km polar-stereographic grid and we re-gridded to a 2x2 degree grid to match CALIPSO-GOCCP. To assess the combined influence of sea ice and cloud changes on top-of-atmosphere albedo and absorbed shortwave radiation we use the Clouds and Earth's Radiant Energy System (CERES) Single Scanner Footprint 1-degree (SSF1deg) data set (Loeb et al., 2005) which provides daily observed all-sky top-of-atmosphere flux values from CERES along with solar insolation from SORCE TSI (Kopp et al., 2005) on a 1x1 degree latitude-longitude grid.

The satellite datasets outlined above provide extensive spatial and temporal cover, but also have limitations. Notably, CALIPSO LIDAR observations provide no information about clouds below the altitude of attenuation, which occurs near an optical depth of 3 (Chepfer et al., 2010). Ship-based observations provide an independent observation of clouds to compare to CALIPSO. We use ship-based visual sea ice and low cloud cover observations (König-Langlo et al., 2006)

along with soundings of temperature, pressure, and relative humidity (Driemel et al., 2016) taken during 13 cruises during Austral summer between 2002 – 2016 (Table 4.1). We limit our use of visual cloud observations to low cloud cover observations taken during daylight hours, the type of visual cloud observations shown to be most accurate (Town et al., 2007; Warren et al., 2007).

Cruise Label	Start Date dd-mm-yy	End Date dd-mm-yy	Location	Surface Meteorological Observations DOI	Meteorological Soundings DOI
ANT-XX/2	24-11-02	23-01-03	Weddell Sea	10.1594/PANGAEA. 269520	10.1594/PANGAEA. 849363
ANT-XXI/2	17-11-03	19-01-04	Weddell Sea	10.1594/PANGAEA. 269515	10.1594/PANGAEA. 849352
ANT-XXII/2	5-11-04	19-01-05	Weddell Sea	10.1594/PANGAEA. 267682	10.1594/PANGAEA. 849228
ANT-XXIII/2	18-11-05	13-01-06	Lazarev Sea	10.1594/PANGAEA. 544827	10.1594/PANGAEA. 849142
ANT-XXIII/8	23-11-06	30-01-07	Weddell Sea	10.1594/PANGAEA. 692881	10.1594/PANGAEA. 849135
ANT-XXIV/2	28-11-07	04-02-08	Weddell Sea	10.1594/PANGAEA. 692890	10.1594/PANGAEA. 845087
ANT-XXV/2	05-12-08	05-01-09	Lazarev Sea	10.1594/PANGAEA. 716896	10.1594/PANGAEA. 845089
ANT-XXVI/2	27-11-09	26-01-10	South Pacific	10.1594/PANGAEA. 743579	10.1594/PANGAEA. 849053
ANT-XXVII/2	28-11-10	05-02-11	South Atlantic	10.1594/PANGAEA. 760392	10.1594/PANGAEA. 849045
ANT-XXVIII/2	03-12-11	05-01-12	South Atlantic	10.1594/PANGAEA. 784458	10.1594/PANGAEA. 844866
ANT-XXIX/2	30-11-12	18-01-13	South Atlantic	10.1594/PANGAEA. 815476	10.1594/PANGAEA. 844856
ANT-XXIX/9	19-12-13	05-03-14	Weddell Sea	10.1594/PANGAEA. 832606	10.1594/PANGAEA. 844805
ANT-XXXI/2	06-12-15	14-02-16	Weddell Sea	10.1594/PANGAEA. 861438	10.1594/PANGAEA. 861658

Table 4.1: Summer cruises of the icebreaker Polarstern used in this study. While cruises include non-summer months, only data from summer months (December, January, February) were used. During each cruise, visual observations of sea ice and cloud cover were taken every three hours (König-Langlo et al., 2006) and meteorological soundings were launched daily near 10 UTC (Driemel et al., 2016).

4.3.2 Methods

Two methods are used to analyze how clouds respond to sea ice variability. In the first method, we follow Wall et al. (2017a). We composite low cloud cover based on meridional distance from the sea ice edge. Using daily data without interpolation, we define the sea ice edge for each longitude and day as the furthest equatorward grid cell with sea ice concentration $\geq 35\%$. We then bin cloud cover data poleward and equatorward of the sea ice edge ($\pm 6^\circ$ latitude). This process is repeated for each day and each longitude before results are averaged to produce mean low cloud cover as a function of meridional distance from the sea ice edge. As discussed below, this method could be influenced by latitudinal variations in clouds unrelated to sea.

In the second method, we follow Morrison et al. (2018). We focus on the grid-cell level and limit our analysis to areas where sea ice concentration changes. Unlike the first method, this second method removes the impact of latitudinal variations in cloud properties and isolates the cloud response to sea ice variability. Similar to Morrison et al. (2018) for the Arctic, we define an intermittent surface mask for the Southern Ocean. For each season, we consider the daily sea ice concentration over our ten-year sample (2006-2015) in a given grid cell and whether or not we have satellite cloud observations for that grid cell on a given day. A grid cell is included in the intermittent mask if both of the following conditions are met: 1) There are at least 10 days where the grid cell has sea ice concentration $< 15\%$ (defined as Open Water) and we have satellite observations in the grid cell and, 2) There are at least 10 days where the grid cell has sea ice concentration $> 80\%$ (defined as Sea Ice) and we have satellite observations in the grid cell. All grid cells that do not meet both criteria are excluded from the intermittent mask.

With the intermittent mask defined, we use it to diagnose how clouds respond to sea ice variability. To diagnose the low cloud cover response to sea ice variability, we compare mean low

cloud cover within the intermittent mask on days with open water with mean low cloud cover within the intermittent mask on days with sea ice. A similar comparison is done for opaque cloud fraction and top-of atmosphere albedo. Because our intermittent mask depends on both sea ice concentration and the availability of satellite data, it is slightly different for each satellite dataset (CALIPSO low cloud cover, CALIPSO opaque cloud fraction, and CERES top-of-atmosphere albedo) we consider. The diagnosed cloud response to sea ice variability does not depend on our choice to use 10 days as the requirement for sea ice and open water days within the intermittent mask. Different choices (i.e. 1 or 50 days) produce similar results with the primary impact being a change in size of the intermittent mask.

4.4 Results

4.4.1 Seasonal Sea Ice Concentration and Low Cloud Cover

We begin by assessing seasonal sea ice concentration and low cloud cover over the high-latitude Southern Ocean (poleward of 50°S). Sea ice varies seasonally (Figure 4.2 a-d) with concentration above 80% extending from Antarctica to near 60° S during winter (June, July, and August (JJA)) and spring (September, October, and November (SON)). During summer (December, January, February (DJF)) and fall (March, April, and May (MAM)) large sea ice concentrations are confined to the Ross and Weddell seas. The sea ice edge (defined as the furthest equatorward grid cell with sea ice concentration $\geq 35\%$ (Wall et al., 2017a)) exhibits considerable variability, especially in summer in the western hemisphere.

Low cloud cover also varies seasonally over the high-latitude Southern Ocean (Figure 4.2 e-h). Low cloud cover is highest in summer and lowest in winter. The relationship between clouds and sea ice also differs by season. In winter and fall, there is an apparent increase in low cloud

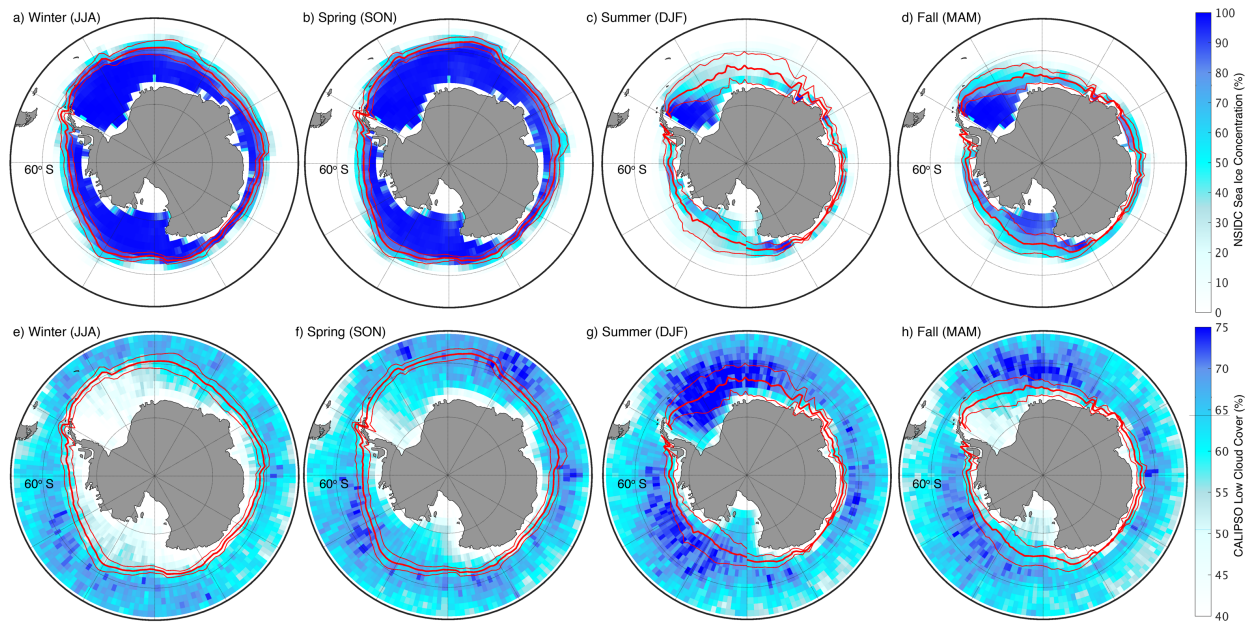


Figure 4.2: Seasonal Antarctic sea ice and low cloud cover. Mean NSIDC sea ice concentration (colored) (Peng et al., 2013) during winter (a), spring (b), summer (c) and fall (d). Mean CALIPSO-GOCCP Low Cloud Cover (colored) (Chepfer et al., 2010) during winter (e), spring (f), summer (g) and fall (h). Low cloud defined as cloud below 680 hPa. Bold red shows mean seasonal position of the sea ice edge, thin red lines show +/- one standard deviation for the sea ice edge. Sea ice edge defined for each day and longitude as the furthest-equatorward occurrence of sea ice concentration greater than or equal to 35% (Wall et al., 2017a). Data are from 2006-2015.

cover with decreasing sea ice concentration (as in Wall et al., 2017a). During spring and summer, low cloud cover does not appear as closely related to sea ice concentration.

4.4.2 Spring and Summer Low Cloud Cover across the Sea Ice Edge

One way to identify the relationship between sea ice and clouds is to composite cloud cover based on distance from the sea ice edge, as in Wall et al. (2017a) (method one in section 4.3.2). With this method, there is an apparent increase in low cloud cover equatorward of the sea ice edge compared with poleward of the sea ice edge during both spring and summer (Figure 4.3). We hypothesize that compositing data across the sea ice edge may be influenced by latitudinal

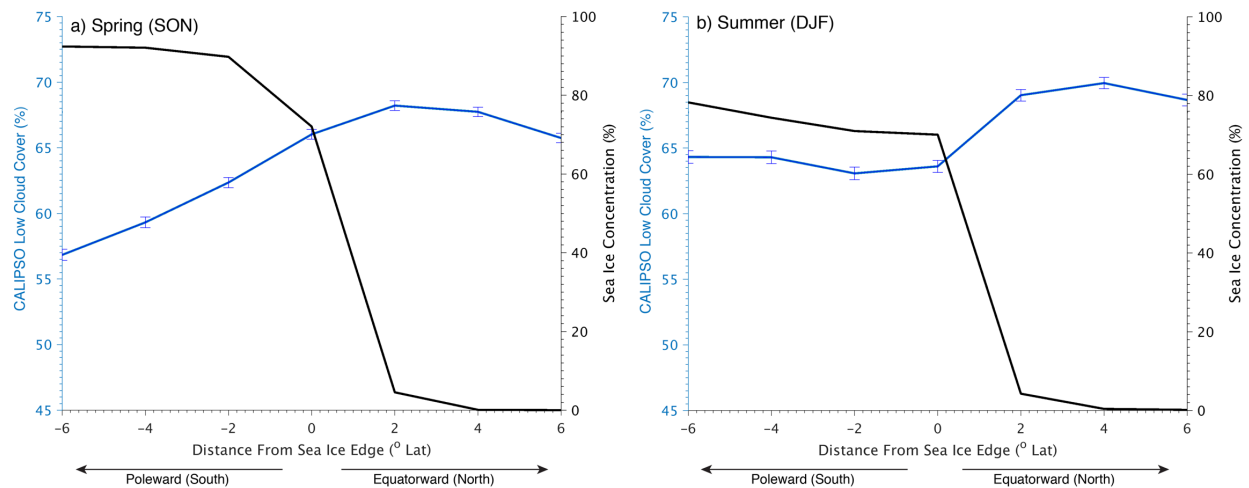


Figure 4.3: Spring and Summer Low Cloud Cover and Sea Ice Concentration as a function of meridional distance from the sea ice edge. Mean CALIPSO low cloud cover (blue) and mean NSIDC sea ice concentration (black) vs. meridional distance from the sea ice edge for spring (a) and summer (b). See section 2.2 method one for detailed methodology. Results shown are averages using daily data from 2006-2015. Error bars on low cloud cover show a 95% confidence interval using the t-distribution.

variations in cloud cover unrelated to sea ice. In Figure 4.3, moving from sea ice to open water always means moving from south to north. Low cloud cover also varies in this direction (increasing from south to north near Antarctica) in ways that may be unrelated to sea ice (Figure 4.2). For example, latitudinal variations in low cloud cover are caused by the Southern Hemisphere storm track (e.g. Hoskins & Hodges, 2005) and patterns of vertical velocity, stability and sea surface temperatures (Wall et al., 2017b) that are unrelated to sea ice.

4.4.3 Spring and Summer Low Cloud Cover Response to Sea Ice Variability

A second way to identify the relationship between sea ice and clouds is by using our intermittent mask (method two in section 4.3.2). Within the intermittent mask during summer (Figure 4.4 a-c) there is no significant change in low cloud cover over open water compared with sea ice. During spring (Figure 4.4 d-f) there is a small (4.5%) increase in low cloud cover over

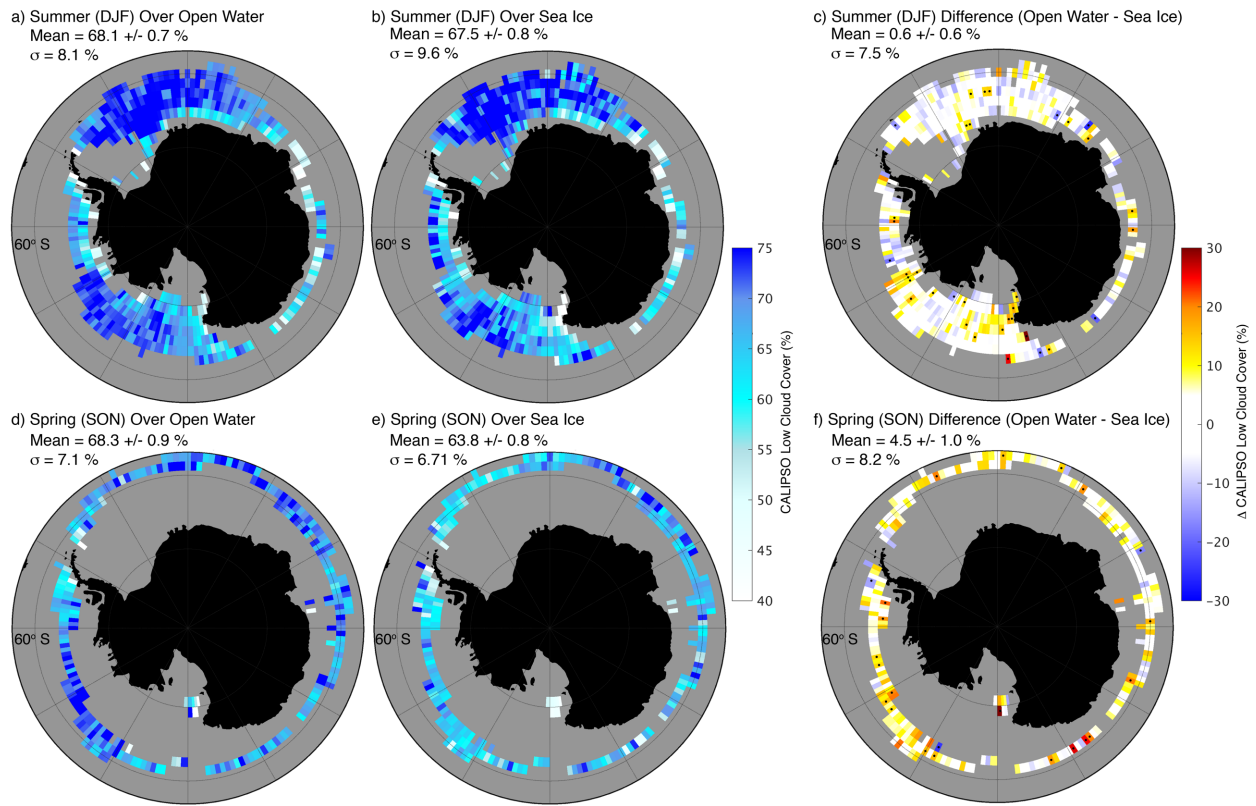


Figure 4.4: Low Cloud Cover within the intermittent mask. CALIPSO low cloud cover during summer over open water (sea ice concentration < 15%) (a), over sea ice (sea ice concentration > 80%) (b), and their difference (open water minus sea ice) (c). (d-f) as in (a-c) but for spring. Gray area in each panel shows ocean grid cells not included in the intermittent mask (section 2.2). The top left of each panel displays the mean (+/- 95% confidence interval using t-distribution) and standard deviation over the intermittent mask. Stippling in (c) and (f) show differences statistically significant at the 95% level using a Student's t-test. Mean of daily data shown (2006-2015).

open water compared to sea ice. During both seasons, the impact of sea ice on low cloud cover appears smaller when the intermittent mask is used compared with compositing data across the sea ice edge (Figure 4.3). We trust the intermittent mask result (Figure 4.4) because it more clearly reflects the low cloud cover response to sea ice variability independent of latitudinal variations of cloud properties. Yet, the intermittent mask is limited by use of LIDAR data which provides no information about clouds occurring below the altitude of attenuation (Chepfer et al., 2010). As a result, low cloud response to sea ice variability may be undetectable to space-borne LIDAR if it occurs below optically thick clouds.

Ship-based observations available during summer provide a totally independent dataset that we use to corroborate space-borne LIDAR observations. Ship-based visual cloud observations confirm the result found using space-borne LIDAR. During summer, there is no notable difference in low cloud cover over open water compared with sea ice (Figure 4.5a). In the western hemisphere, locations of ship-based observations (Figure 4.5b) overlap well with the intermittent mask used for CALIPSO observations (Figure 4.4). Though we have no ship-based observations over most of the eastern hemisphere, we do not consider this to be a serious limitation given that CALIPSO observations showed no hemispheric difference in cloud response (Figure 4.4).

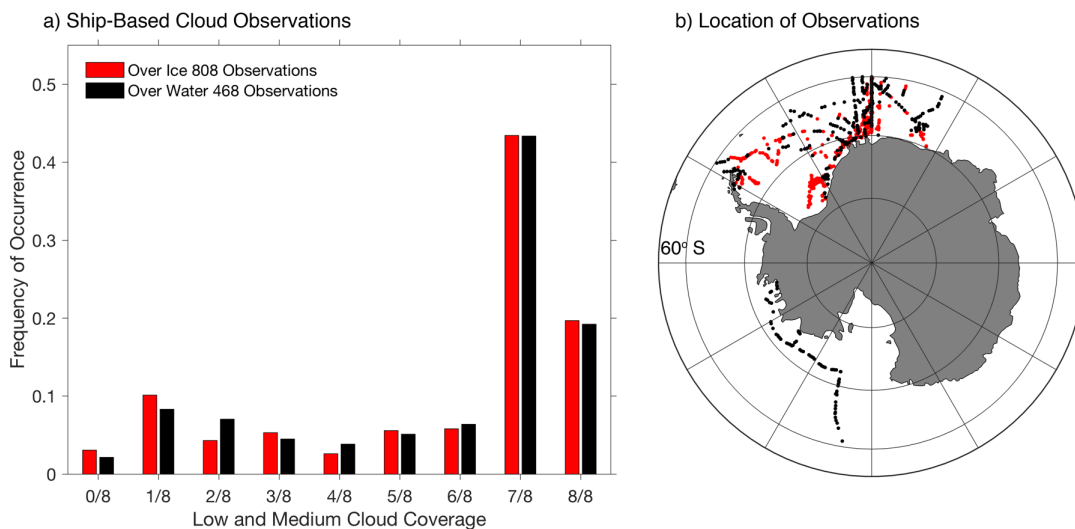


Figure 4.5: Ship-Based cloud observations. a) Histograms of summer low and medium cloud cover over sea ice (red) and over open water (black) created using visual sea ice and cloud observations (König-Langlo et al., 2006) from 13 research cruises (Table 4.1). b) Locations of observations taken over sea ice (red) and over open water (black). Cloud cover and sea ice arrangement and concentration reported using standard WMO reporting values (König-Langlo et al., 2006). A visual sea ice observation is defined as “open water” if sea ice is reported as “no ice in sight” or “sea ice present in concentration less than 3/10” while an observation is defined as “sea ice” if sea ice concentration is reported as “7/10 to 8/10” or “9/10 or more.” Low and medium cloud cover is reported in eighths of cover.

4.4.4 Spring and Summer Cloud Opacity Response to Sea Ice Variability

Though the cloud cover response to sea ice variability is small in spring and near zero in summer, cloud opacity also matters. For example, cloud optical depth increases in response to sea ice loss could lessen the magnitude of top-of-atmosphere albedo decreases, or the top-of-atmosphere albedo could even increase (Fitzpatrick & Warren, 2007). Vertical profiles of relative humidity and temperature taken during Polarstern research cruises (Table 4.1) suggest increased cloud optical depth over open water. Relative humidity is higher over open water compared to sea ice in the lowest 2km (Figure 4.6a). Additionally, temperature profiles over open water are warmer than those over sea ice (Figure 4.6b), which could suggest an increase in optical depth (see detailed discussion in section 4.5.2).

Consistent with ship-based profiles of relative humidity and temperature, CALIPSO observations also suggest an increase in optical depth over open water compared to sea ice. The fraction of opaque clouds (clouds that fully attenuate the LIDAR) is larger over open water compared to sea ice in both summer and spring (Figure 4.7). The increase in the opaque cloud fraction (defined as opaque cloud cover divided by total (opaque + thin) cloud cover) suggests that the overall optical depth of clouds and their shortwave radiative effect (Guzman et al., 2017) increase over open water compared with sea ice. The altitude of LIDAR attenuation in opaque clouds also changes over sea ice compared to open water. Near the surface, the altitude of full attenuation is higher over open water than it is over sea ice (Figure 4.8). When combined with relative humidity profiles (Figure 4.6) this higher altitude of attenuation is consistent with a thicker cloud layer over open water. In summary, changes in observed relative humidity and temperature (Figure 4.6), opaque cloud fraction (Figure 4.7), and the altitude of attenuation (Figure 4.8) all suggest that clouds are optically thicker over open water compared with sea ice.

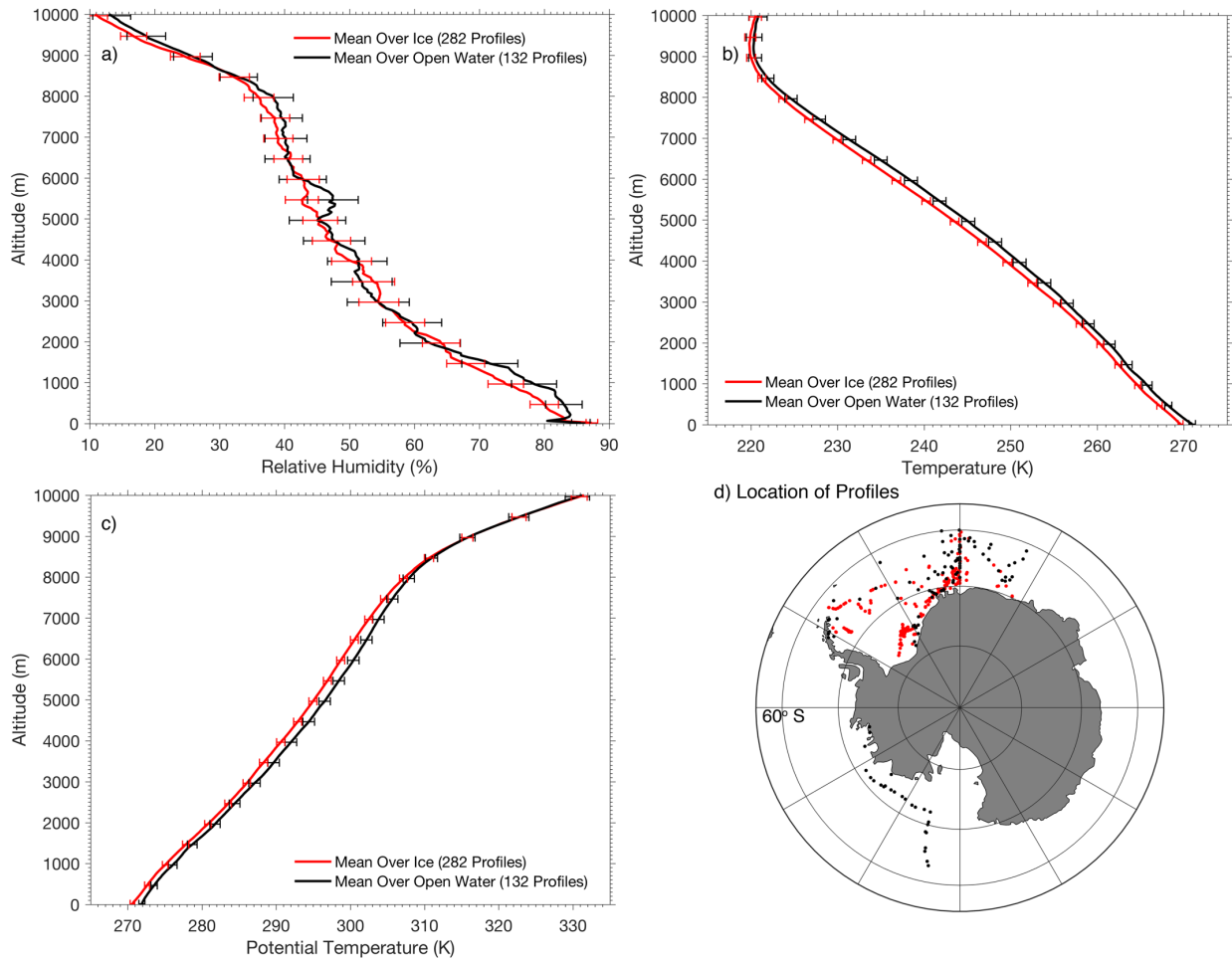


Figure 4.6: Ship-Based meteorological profiles. Vertical profiles of relative humidity (a), temperature (b), and potential temperature (c). Locations of the soundings used to produce profiles (d). Over sea ice (red) and over open water (black). Error bars show 95% confidence interval (t-distribution) every 500m. Sea ice concentration assessed using visual sea ice observations as in Figure 5. Profiles taken with a vertical resolution of 50 m during summer between 2002-2016 (Table 1). Soundings are not always launched at times coinciding with sea ice observations, and here we only use profiles taken within 3 hours of a visual sea ice observation.

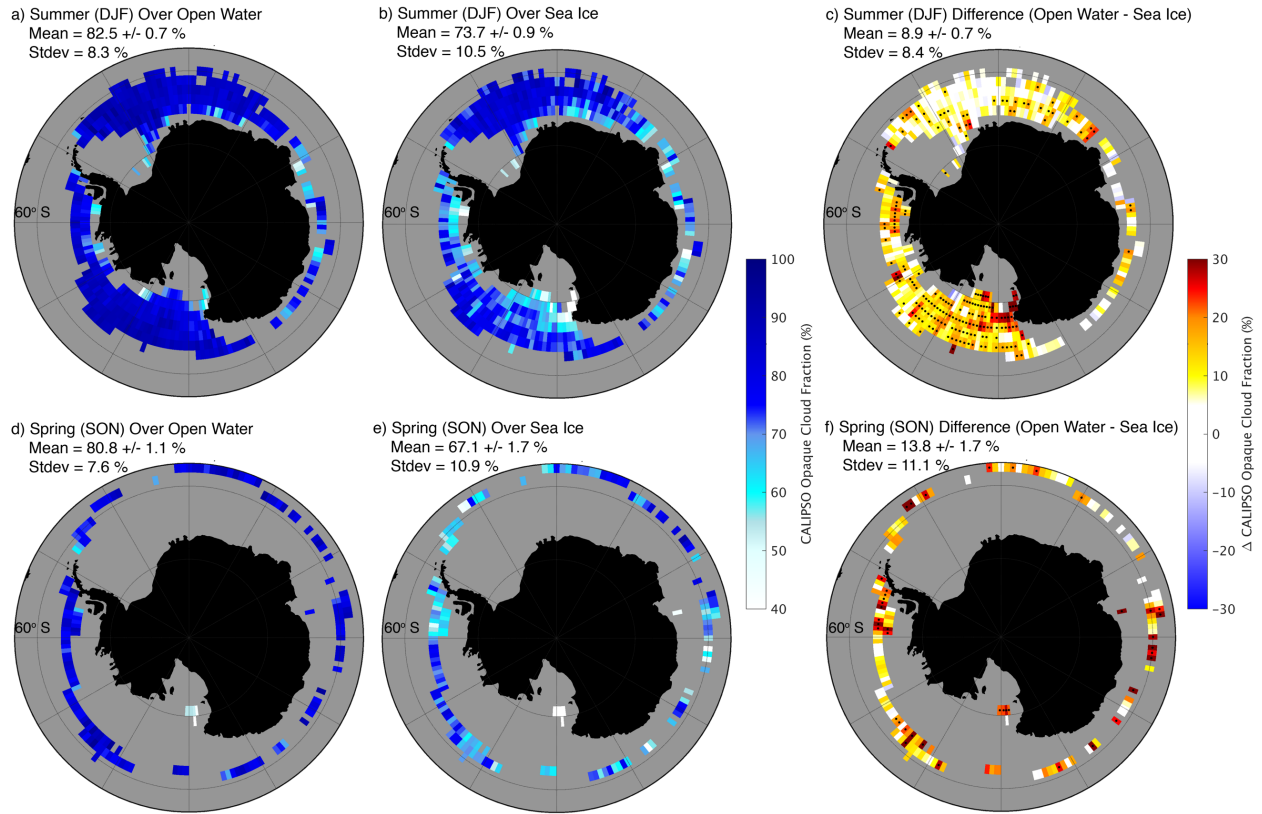


Figure 4.7: Opaque cloud fraction within the intermittent mask. As in Figure 4.4 but for opaque cloud fraction. Opaque cloud defined as clouds which fully attenuate the CALIPSO LIDAR (optical depth >3) (Guzman et al., 2017). Opaque cloud fraction defined as opaque cloud cover divided by total cloud cover. Mean of daily data shown (2007-2015).

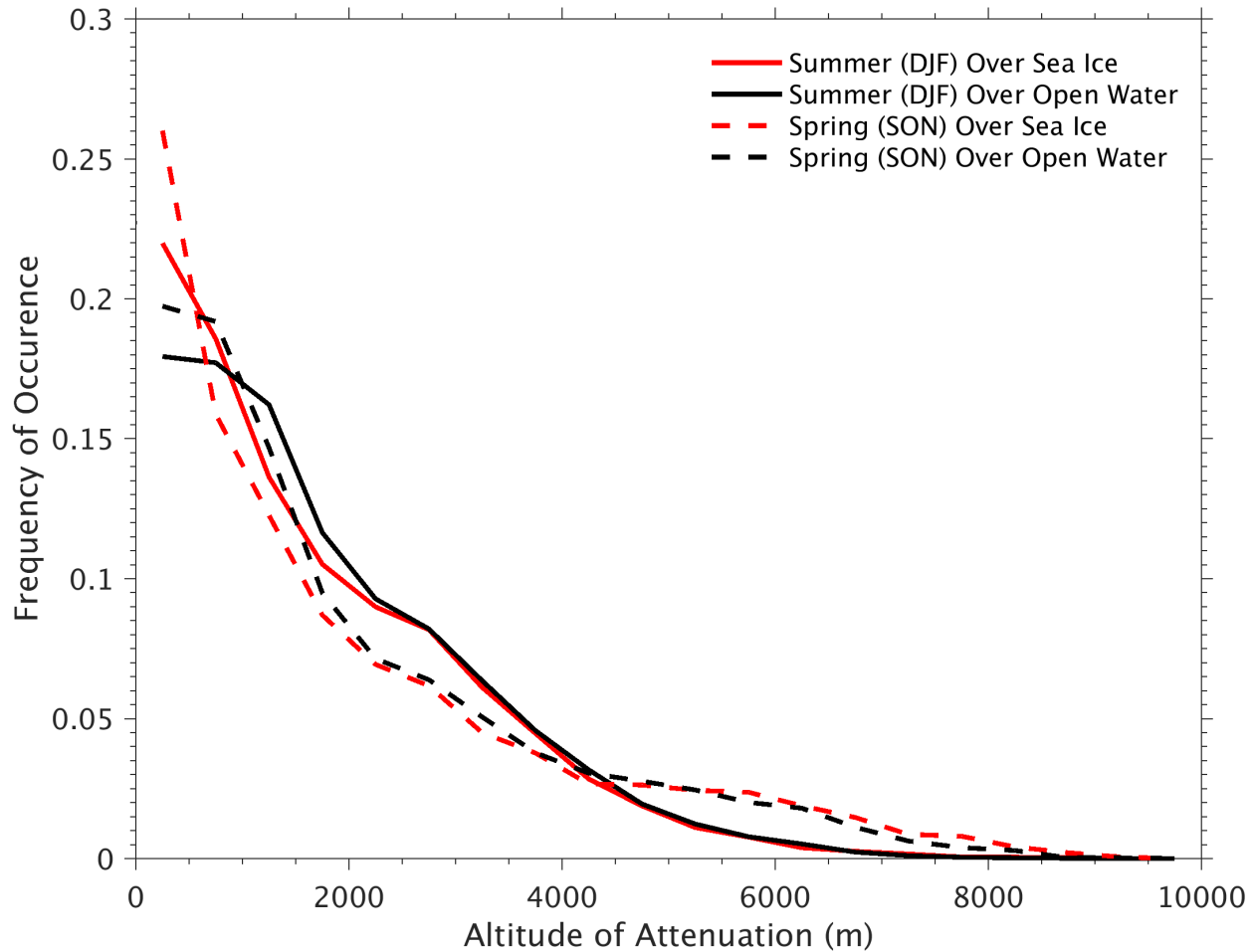


Figure 4.8: Probability density functions (PDF) of the altitude of CALIPSO LIDAR signal attenuation in opaque clouds over sea ice (red) and open water (black) during summer (solid) and spring (dashed). PDF created with daily CALIPSO-GOCCP data (Guzman et al., 2017) from 2007-2016 over the seasonal intermittent masks from Figure 4.7. PDF bin width is 500 meters.

4.4.5 Combined Impact of Sea Ice Variability and Cloud Response on Top-of-Atmosphere

Albedo

We next assess the joint influence of sea ice variability and clouds on top-of-atmosphere albedo. The cloud response to sea ice variability is not large enough to compensate for the decrease in surface albedo from sea ice to open water. CERES observations show that all-sky top-of-atmosphere albedo, which is influenced by both clouds and the surface, is lower over open water

than over sea ice within the intermittent mask during both spring and summer (Figure 4.9 and Table 4.2). As a result, in both spring and summer more shortwave radiation is absorbed over open water than over sea ice (Table 4.2). This is a significant advance over previous work where the sign of the absorbed shortwave radiation change in response to summer sea ice variability was uncertain (Fitzpatrick & Warren, 2007). Even though the difference in top-of-atmosphere albedo over open water compared to sea ice has a larger magnitude in spring than summer, the absorbed shortwave radiation increase is larger in summer compared to spring because solar insolation is larger during summer (Table 4.2).

4.4.6 Insensitivity of Results to the Definitions of Sea Ice and Open Water

Our results are robust to differing definitions of sea and open water. To show this, we bin data within the intermittent mask by sea ice concentration to show how low cloud cover, opaque cloud fraction, and top-of-atmosphere albedo vary across the whole range of sea ice concentration (Figure 4.10). For low cloud cover and opaque cloud fraction any difference between open water and sea ice appears driven by the highest (95-100%) and lowest (0-5%) sea ice concentration bins. Top-of-Atmosphere albedo increases with increasing sea ice concentration and is similar in spring and summer for sea ice concentration below 60%. Above 60% sea ice concentration, top-of-atmosphere albedo is higher in spring compared with summer which likely is driven by differences in the optical properties of sea ice and the associated snow cover (Massom et al., 2001). We performed a similar analysis of top-of-atmosphere albedo using CERES SSF Level2 data (Loeb et al., 2005) which provides albedo data at the instantaneous footprint level. The resulting albedo values and patterns (not shown) are similar to Figure 4.10c, indicating that the gridding algorithm used for the SSF1deg product does not impact our results.

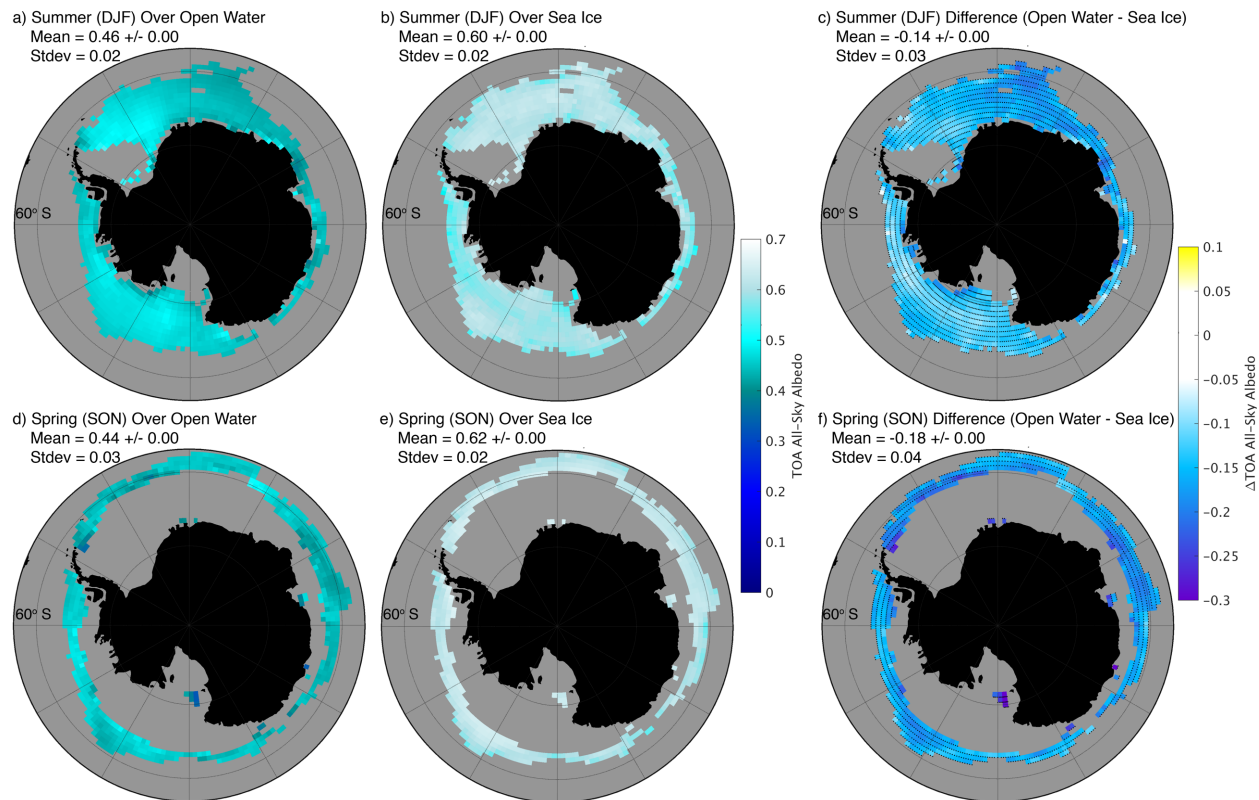


Figure 4.9: Top-of-Atmosphere (TOA) All-Sky Albedo within the intermittent mask. As in Figure 4.4 but for CERES TOA all-sky albedo. Mean of daily data shown (2006-2015).

	Over Open Water		Over Sea Ice		Difference (Open Water – Sea Ice)	
	Spring	Summer	Spring	Summer	Spring	Summer
CALIPSO Low Cloud Cover	68%	68%	64%	68%	+4%	+0%
CALIPSO Opaque Cloud Fraction	81%	83%	67%	74%	+14%	+9%
CERES Top-of-Atmosphere Albedo	0.44	0.46	0.62	0.60	-0.18	-0.14
Estimated Absorbed Shortwave Radiation	164 W m ⁻²	238 W m ⁻²	112 W m ⁻²	176 W m ⁻²	+53 W m ⁻²	+62 W m ⁻²

Table 4.2: Summary of main findings. Spring and summer mean values of CALIPSO low cloud cover, CALIPSO opaque cloud fraction, and CERES top-of-atmosphere albedo over the region (shown in Figures 4.4, 4.7, and 4.9, respectively) where sea ice concentration varies. Estimated absorbed shortwave radiation calculated by multiplying one minus the mean top-of-atmosphere albedo by the mean solar insolation for each season over the appropriate region.

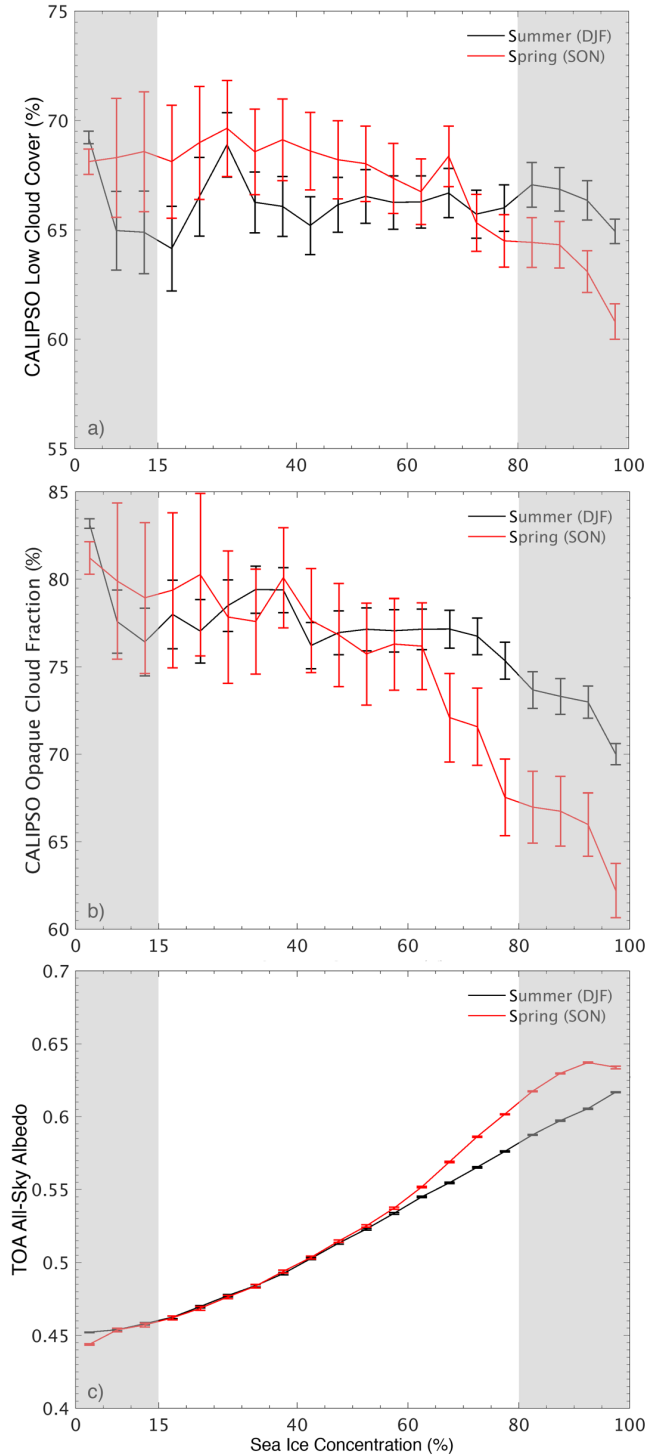


Figure 4.10: CALIPSO low cloud cover (a), CALIPSO opaque cloud fraction (b) and CERES top-of-atmosphere (TOA) all-sky albedo (c) as a function of NSIDC sea ice concentration within the intermittent masks shown in Figures 4.4, 4.7, and 4.9, respectively during summer (black) and spring (red). Data binned based on daily sea ice concentration (bin width 5%) and then averaged within each bin. Error bars show 95% confidence interval using a t-distribution. Shaded areas show definitions of open water and sea ice used for intermittent masks. Data from 2006-2015 in (a) and (c), (b) from 2007-2015.

4.5 Discussion

4.5.1 Cloud and Albedo Response to Sea Ice Variability Revealed with Surface-Independent Observations

The most important result of this study is isolating the cloud and top-of-atmosphere albedo response to varying sea ice conditions in the Southern Ocean. We found no change (a small increase) in low cloud cover during summer (spring) in response to decreased sea ice concentration (Figure 4.4). We also found more opaque cloud in summer and spring over open water compared to sea ice (Figure 4.7). Most importantly, even with the cloud response, top-of-atmosphere albedo is lower and more shortwave radiation is absorbed over open water than over sea ice (Figure 4.9). Because our results are based on observations that are independent of surface condition, they accurately reveal cloud changes occurring over open water compared to sea ice.

4.5.2 Potential Mechanisms for Increasing Opaque Cloud Fraction

Surface-independent observations of temperature and cloud phase help constrain potential mechanisms underlying the observed cloud response to varying sea ice conditions. One potential mechanism leading to increased cloud opacity when sea ice retreats is an increase in air-sea coupling strength (Kay & Gettelman, 2009; Wall et al. 2017a; Morrison et al., 2018). Air-sea coupling contributes to low-cloud formation and maintenance as moisture is transferred from the sea surface to the atmosphere to promote cloud formation (Klein & Hartmann, 1993). Interestingly, differences in air-sea coupling between open water and sea ice do not appear to drive the increase in summer opaque cloud fraction. We quantify the strength of air-sea coupling by assessing near-surface static stability, the difference in potential temperature between 850 hPa and the surface. Potential temperature profiles (Figure 4.6c) indicate no significant difference in near-surface static

stability over open water (5.3 K +/- 0.7K) compared with sea ice (5.6K +/- 0.4K) during summer. Further, the difference between surface air and sea temperature is small during summer (less than 1K) which limits fluxes of moisture and heat from the sea to the atmosphere (Kay & Gettelman, 2009; Morrison et al., 2018).

A second potential mechanism leading to increased cloud opacity over open water as compared to over sea ice is an increase in temperature (Figure 4.6b). Increased temperatures lead to increased cloud opacity in the clouds prevalent over the Southern Ocean via two processes. In the first process, increased temperatures increase overall cloud water content as a result of an increased moist adiabatic lapse rate (e.g., Somerville & Remer, 1984; Betts & Harshvardhan, 1987; Tselioudis et al., 1992; Gordon & Klein, 2014; Ceppi et al., 2016a). In the second process, increased temperatures result in more cloud liquid at the expense of cloud ice (e.g., Hu et al., 2010; McCoy et al., 2014; McCoy et al., 2015; Ceppi et al., 2016a). An increase in cloud liquid at the expense of ice increases optical depth even if overall water content is constant because cloud water droplets are much smaller than cloud ice crystals (Storelvmo et al., 2015). An increase in cloud liquid at the expense of ice also decreases precipitation efficiency which can increase cloud liquid water content (Senior & Mitchell, 1993; Tsushima et al., 2006; Ceppi et al., 2016a).

CALIPSO cloud phase classifications support the second mechanism for cloud opacity increase by indicating a cloud phase shift from ice toward liquid. CALIPSO-GOCCP classifies cloud as either liquid, ice, or undefined using the polarization of returns (Cesana & Chepfer, 2013). A classification of “undefined” most likely corresponds to mixed-phase clouds (Cesana et al., 2016). We use these classifications within the intermittent mask (as in Figure 4.4) to compare cloud phase over open water to sea ice. During summer, low liquid cloud cover is virtually unchanged over open water compared to sea ice while low ice cloud cover decreases by 1.5% and

the undefined low cloud cover increases by 2.1%. During spring, low liquid cloud cover and undefined low cloud cover both increase by 2.5% over open water compared with sea ice while low ice cloud cover decreases by 0.6%. In both seasons, we find a decrease in low ice cloud cover coupled with an increase in mixed-phase and liquid cloud cover. CALIPSO cloud phase classifications suggest that increased temperatures (Figure 4.6) lead to increased opaque cloud fraction (Figure 4.7) through a shift in cloud phase from ice toward liquid.

4.5.3 Influence of Sea Ice on Southern Ocean Shortwave Cloud Radiative Feedbacks

We conclude our discussion by considering the implications of the diagnosed cloud response to sea ice variability on Southern Ocean shortwave cloud radiative feedbacks. Models robustly predict a negative shortwave cloud feedback due to an optical depth increase with warming over the Southern Ocean sea ice zone (Mitchell et al., 1989; Klein et al., 2009; Zelinka et al., 2012a; McCoy et al., 2015; Ceppi et al., 2016a; Ceppi et al., 2016b; Terai et al., 2016). Our observational analysis indicates that sea ice does not directly impact this feedback. The same mechanism which drives the Southern Ocean negative shortwave feedback in models, increased temperatures leading to a shift in cloud phase from ice toward liquid (Ceppi et al., 2016a), also causes the observed increase in cloud opacity we show over open water compared to sea ice. Therefore, sea ice will likely contribute to Southern Ocean shortwave cloud radiative feedbacks only to the extent that decreased sea ice concentration is accompanied by increased temperatures.

4.6 Summary and Conclusions

Space-borne LIDAR observations are used to diagnose the spring and summer cloud response to Southern Ocean sea ice variability. Over the Southern Ocean region where surface condition varies between sea ice and open water, we find the following:

- During spring, there is a small increase in low cloud cover over open water compared to sea ice. During summer, sea ice variability does not impact low cloud cover (Figure 4.4).
- During both spring and summer, the fraction of optically thick clouds increases over open water compared to sea ice (Figure 4.7).
- During both spring and summer, top-of-atmosphere albedo is lower and more shortwave radiation is absorbed over open water compared to sea ice (Figure 4.9).

Entirely independent of the space-borne LIDAR observations, ship-based observations available during summer also show no cloud cover response to sea ice variability (Figure 4.5). Even when the cloud response to sea ice variability is included, top-of-atmosphere albedo is lower and more shortwave radiation is absorbed over open water compared to sea ice. The results imply the cloud response to sea ice loss accompanying warming in the future will only partly mask the positive surface ice albedo feedback. When sea ice is lost during spring and summer, the Southern Ocean will absorb more shortwave radiation, which will accelerate warming.

Acknowledgements

CALIPSO-GOCCP data are available from the ClimServ center (<http://climserv.ipsl.polytechnique.fr/cfmip-obs/>). CERES SSF1deg data are available at https://ceres.larc.nasa.gov/order_data.php. NSIDC sea ice data are available at <https://nsidc.org/data/g02202>. Ship-based observations from Polarstern research cruises are

available at <https://www.pangaea.de/expeditions/cr.php/Polarstern>. Code necessary to reproduce the results is available upon request from William Frey. This work was supported by startup funds awarded to Jennifer Kay by the University of Colorado Cooperative Institute for Research in the Environmental Sciences and NASA award NNX16AP18G. Rodrigo Guzman was supported by Centre National d'Etudes Spatiales (CNES). William Frey was supported by the Air Force Institute of Technology. The views expressed in this article are those of the authors and do not reflect the official policy or position of the United States Air Force, Department of Defense, or the U.S. Government.

Chapter 5

The Combined Influence of Southern Ocean Clouds and Sea Ice on Top-Of-Atmosphere Albedo in the Community Earth System Model

5.1 Introduction

Many climate models predict negative shortwave cloud optical depth feedbacks over the Southern Ocean region (Zelinka et al., 2012a), including the high latitude region (poleward of 60 ° S) seasonally covered by sea ice. These cloud feedbacks play an important role in model predictions of equilibrium climate sensitivity (Tan et al., 2016; Frey & Kay, 2018), though they appear less important for transient warming (Frey et al., 2017). Shortwave cloud optical depth feedbacks over the high-latitude Southern Ocean coincide in space and time with a transition from sea ice to open water as the climate warms. Therefore, it is important to assess how clouds might be impacted by changing sea ice.

Present-day observations show that during the spring and summer seasons which dominate the high-latitude shortwave radiation budget, there is only a small cloud response to sea ice variability. Low cloud cover and cloud opacity increase slightly in response to decreased sea ice concentration. Nevertheless, the combined impact of sea ice retreat and the cloud response is a decrease in top-of-atmosphere albedo over open water compared to sea ice (Table 4.2). The observed increase in cloud opacity likely results from increased air temperatures over open water compared to sea ice leading to a cloud phase shift from ice toward liquid. This same mechanism is responsible for negative cloud optical depth feedback predicted by climate models (e.g. Ceppi et al., 2016a). Importantly, observations show that clouds do not respond directly to sea ice

variability through changes in air-sea coupling which suggests that sea ice retreat with warming will not directly impact Southern Ocean shortwave cloud feedbacks.

In this chapter, we assess how well one widely-used climate model, the Community Earth System Model (CESM) version 1 (Hurrell et al., 2013), represents the relationship between Southern Ocean sea ice and clouds in the present-day climate. Consistent with observations, in CESM low cloud cover and cloud opacity increase and top-of-atmosphere albedo decreases in response to decreasing sea ice concentration during both spring and summer. However, compared to observations CESM overestimates the magnitude of the cloud and top-of-atmosphere albedo response to sea ice variability. In contrast to observations, air-sea coupling strength in CESM increases over open water compared to sea ice during both spring and summer. This increase in air-sea coupling strength, which is not observed, could impact the cloud feedbacks predicted by CESM with warming in the Southern Ocean region influenced by sea ice.

5.2 Model and Methods

5.2.1 Model Set Up

We assess the relationship between present-day (2006-2015) clouds and sea ice in the large ensemble (LE) version of CESM (Kay et al., 2015), based on CESM version one (Hurrell et al., 2013), at one-degree horizontal resolution. The model is forced with the RCP8.5 emissions scenario (Riahi et al., 2011). We run CESM with a LIDAR simulator (Chepfer et al., 2008) that provides diagnostics for cloud phase (Cesana & Chepfer, 2013) and opaque and thin clouds (Guzman et al., 2017) that can be directly compared to the same space-borne LIDAR observations (Chepfer et al., 2010) assessed in Chapter 4. Below, we refer to model output generated by the LIDAR simulator as “CALIPSO-simulated”. As with our observational analysis, we analyze

model output at a daily frequency. In contrast to our observational analysis, our model analysis is not limited by data availability. We have model output of sea ice concentration, LIDAR simulator-derived cloud cover and opacity, and atmospheric conditions (e.g. temperature, potential temperature, and relative humidity) at all grid points for all days from 2006-2015.

5.2.2 Methods

To identify the relationship between clouds and sea ice concentration in CESM we use the intermittent mask (method two in Chapter 4, Section 4.2.2) to isolate the region where sea ice concentration varies. We focus on spring and summer, which dominate the high-latitude Southern Ocean shortwave energy budget. The spatial extent of the spring and summer intermittent masks in CESM is very similar to the observed masks shown in Chapter 4. We find no notable geographic patterns in cloud cover, opaque cloud fraction, or top-of-atmosphere albedo within the intermittent masks in CESM (not shown). Therefore, we present model results as average values within the CESM intermittent masks (Table 5.1) for comparison with observed results (Table 4.2) rather than showing a full set of model figures.

5.3 Spring and Summer Cloud and Albedo Response to Sea Ice Variability in CESM Compared with Observations

5.3.1 Low Cloud Cover

We begin by assessing the low cloud cover response to sea ice variability in CESM. Low cloud cover is greater over open water than over sea ice during both spring and summer in CESM (Table 5.1). This modeled cloud response is in contrast to observations (Table 4.2), which showed

	Over Open Water		Over Sea Ice		Difference (Open Water – Sea Ice)	
	Spring	Summer	Spring	Summer	Spring	Summer
CESM CALIPSO Low Cloud Cover	60%	69%	49%	61%	+11%	+8%
CESM CALIPSO Opaque Cloud Fraction	51%	50%	33%	40%	+18%	+10%
CESM Top-of- Atmosphere Albedo	0.38	0.37	0.64	0.59	-0.26	-0.22
CESM Estimated Absorbed Shortwave Radiation	181 W m ⁻²	280 W m ⁻²	105 W m ⁻²	182 W m ⁻²	+76 W m ⁻²	+98 W m ⁻²

Table 5.1: CESM results within the intermittent mask. Spring and summer mean values of CESM CALIPSO-simulated low cloud cover, CESM CALIPSO-simulated opaque cloud fraction, and CESM top-of-atmosphere albedo over the region where sea ice concentration varies (the intermittent mask, see section 4.2.2). Estimated absorbed shortwave radiation calculated by multiplying one minus the mean top-of-atmosphere albedo by the mean solar insolation for each season over the appropriate region.

no low cloud cover response to sea ice variability during summer. In both spring and summer, CESM overestimates the low cloud cover response to sea ice variability compared to observations primarily because CESM low cloud cover is too small over sea ice. For sea ice concentrations less than 80%, CESM low cloud cover (Figure 5.1a) is within 10% of observations (Figure 4.10a). However, low cloud cover in CESM decreases sharply at sea ice concentrations greater than 80% (Figure 5.1a) in a way not seen in observations (Figure 4.10a). This disparity in low cloud cover over high sea ice concentrations in CESM compared to observations suggests problems with boundary layer structure over sea ice (e.g. Medeiros et al., 2011).

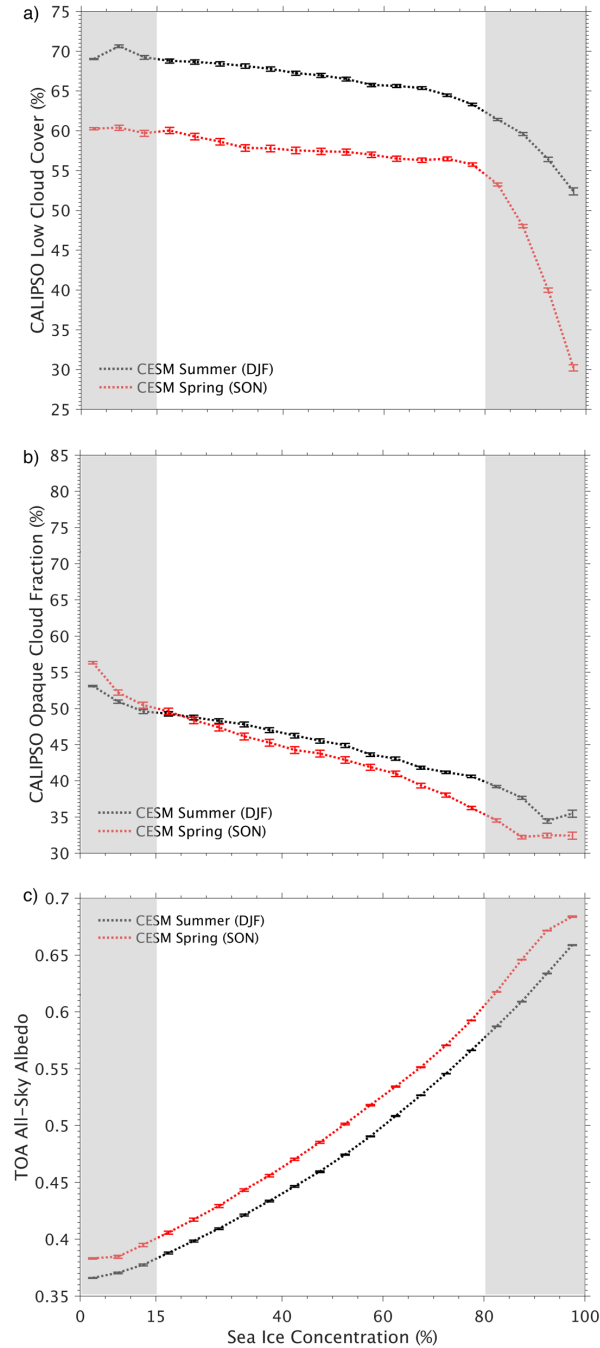


Figure 5.1: CESM CALIPSO-simulated low cloud cover (a), CESM CALIPSO-simulated opaque cloud fraction (b) and CESM top-of-atmosphere (TOA) all-sky albedo (c) as a function of sea ice concentration within the intermittent masks (see section 2.2) during summer (black) and spring (red). Data binned based on daily sea ice concentration (bin width 5%) and then averaged within each bin. Error bars show 95% confidence interval using a t-distribution. Shaded areas show definitions of open water and sea ice used for intermittent masks. Data from 2006-2015 in (a) and (c), (b) from 2007-2015, matching the time periods used for observations in Figure 4.10.

5.3.2 Opaque Cloud Fraction

In addition to cloud cover, cloud opacity is important in determining the top-of-atmosphere albedo change in response to sea ice variability. Consistent with observations, CESM shows an increase in opaque cloud fraction (defined as opaque cloud cover divided by total (opaque + thin) cloud cover) over open water compared to sea ice during both spring and summer (Table 5.1). During both seasons, CESM opaque cloud fraction (Figure 5.1b) is much lower than observations (Figure 4.10b) for all sea ice concentrations. This low bias in opaque cloud fraction is due to biases in CESM cloud phase over the Southern Ocean. Southern Ocean clouds in CESM contain too little supercooled liquid compared to observations (Kay et al., 2016a) which decreases their optical depth and causes opaque cloud fraction to be lower than observed. Despite the low bias over both open water and sea ice, the difference in opaque cloud fraction between open water and sea ice is similar in CESM (Table 5.1) and observations (Table 4.2).

5.3.3 Top-Of-Atmosphere Albedo

We next show how sea ice and clouds combine to impact top-of-atmosphere albedo in CESM. Consistent with observations, top-of-atmosphere albedo is lower over open water compared to sea ice in CESM during both spring and summer (Table 5.1). During both seasons, top-of-atmosphere albedo increases more strongly with increasing sea ice concentration in CESM (Figure 5.1c) than observed (Figure 4.10c). At low sea ice concentrations (below 15%), top-of-atmosphere albedo is lower in CESM than in observations during both spring and summer likely because Southern Ocean clouds in CESM are much less opaque than those observed. In contrast, at high sea ice concentrations (above 80%) top-of-atmosphere albedo is greater in CESM than in observations, even though CESM opaque cloud fraction and low cloud cover are both much less

than observed. Larger than observed top-of-atmosphere albedo despite smaller than observed cloud cover and opacity over high sea ice concentrations in CESM suggests that sea ice albedo in CESM is too large.

5.4 Discussion

5.4.1 Cloud and Albedo Response to Sea Ice Variability in CESM

In CESM, low cloud cover and cloud opacity increase and top-of-atmosphere albedo decreases with decreasing sea ice concentration during both spring and summer (Figure 5.1). Even though CESM clouds have significant biases (notably opaque cloud fraction is too small at all sea ice concentrations and low cloud cover is too small over sea ice), the cloud and top-of-atmosphere albedo response to sea ice variability in CESM has the same sign as the observed response. While the CESM top-of-atmosphere albedo sign change matches observations, compared to observations CESM overestimates the magnitude of the low cloud cover, opaque cloud fraction, and top-of-atmosphere albedo response to sea ice variability (Table 5.1 compared to Table 4.2). Next, we identify the mechanism behind the cloud opacity response to sea ice variability in CESM and discuss how sea ice retreat could impact cloud feedbacks predicted by CESM.

5.4.2 Mechanisms for Increasing Opaque Cloud Fraction in CESM Compared to Observations

Both observations and CESM show an increase in opaque cloud fraction over open water compared to sea ice in the present-day climate. However, the mechanism leading to increased cloud opacity in CESM is different from the observed mechanism. In observations, a shift in cloud phase from ice to liquid appears to increase optical depth over open water compared to sea ice

(Chapter 4, Section 4.4.2). This cloud opacity increase is consistent with a mechanism where increased temperatures result in more cloud liquid at the expense of cloud ice as sea ice transitions to open water (e.g. Hu et al., 2010; McCoy et al., 2014; McCoy et al., 2015; Ceppi et al., 2016a) even in the absence of changes in air-sea coupling.

In CESM, CALIPSO cloud phase diagnostics provide no evidence of a shift in cloud phase over open water compared to sea ice. Instead, in CESM overall cloud water content (liquid and ice) increases as temperatures increase over open water compared to sea ice. This is consistent with a mechanism where overall cloud water content increases with temperature (e.g., Somerville & Remer, 1984; Betts & Harshvardhan, 1987; Tselioudis et al., 1992; Gordon & Klein, 2014; Ceppi et al., 2016a). Such an increase in overall cloud water content could be related to increased air-sea coupling strength (Klein & Hartmann, 1993), which we quantify with near-surface static stability. In CESM, near-surface static stability over open water (3.9K spring, 3.8K summer) is lower than over sea ice (9.0K spring, 5.5K summer). This decrease in stability over open water compared to sea ice, which is not observed (Section 4.4.2), indicates an increase in air-sea coupling strength which could contribute to the increase in total cloud water content in CESM.

5.4.3 Influence of Sea Ice on Southern Ocean Shortwave Cloud Radiative Feedbacks in CESM

The finding that the increase in cloud opacity with decreasing sea ice concentration in CESM is likely due to changes in air-sea coupling and total cloud water content and not due to changes in cloud phase has potential implications for cloud feedbacks. As with many models (Zelinka et al., 2012a), CESM predicts a negative shortwave cloud feedback due to an optical depth increase with warming over the Southern Ocean (e.g. Kay et al., 2014; Frey & Kay, 2018).

Observations indicate that sea ice should not directly impact this feedback (Chapter 4, Section 4.4.3). However, when sea ice is replaced with open water in CESM air-sea coupling strength is increased, consistent with increased total cloud water content and cloud opacity. This increase in air-sea coupling strength, which is not observed (Chapter 4, Section 4.4.2), could contribute to the negative cloud optical depth feedback predicted by CESM in the future given that the feedback partly occurs in a region where sea ice is currently observed and expected to retreat as the climate warms. Further work is necessary to quantify how much changes in air-sea coupling strength contribute to the negative cloud optical depth feedback in CESM and disentangle the impacts of air-sea coupling from other cloud feedback processes relevant over the Southern Ocean (e.g. Kay et al., 2014; Frey & Kay, 2018).

5.5 Summary

A LIDAR simulator is used to diagnose the spring and summer cloud response to Southern Ocean sea ice-variability in the Community Earth System Model (CESM). Over the Southern Ocean region where the modeled surface condition varies between sea ice and open water, we find the following:

- During spring and summer, low cloud cover and cloud opacity increase over open water compared to sea ice.
- Even when the cloud response is included, spring and summer top-of-atmosphere albedo is lower and more shortwave radiation is absorbed over open water compared to sea ice.
- The cloud and top-of-atmosphere albedo response to sea ice variability in CESM is of the same sign but larger in magnitude than the observed response.

While both observations and CESM show increased cloud opacity over open water compared to sea ice, the mechanism leading to increased cloud opacity is different. In CESM, the increase in cloud opacity with decreasing sea ice concentration is likely due to changes in air-sea coupling and total cloud water content. This is a contrast to observations, which suggest increased cloud opacity with decreasing sea ice concentration is due to changes in cloud phase with increased temperatures. Because decreased sea ice concentration is directly linked to increased cloud opacity via air-sea coupling in CESM in a way not observed, sea ice loss with warming in CESM may contribute to cloud optical depth feedbacks in a way inconsistent with observations.

Acknowledgements

Thanks to Ariel Morrison who set up and ran the CESM model simulation analyzed in this chapter.

Chapter 6

Conclusions and Future Work

6.1 Synopsis

This dissertation has explored the influence of Southern Ocean cloud feedbacks on global climate change. This final chapter synthesizes the most important findings and provides suggestions for future research.

6.2 How Southern Ocean Cloud Phase Impacts Cloud Feedbacks and Climate Change Projections in a Global Climate Model.

In the first part of this dissertation (Chapters 2 and 3), we improved the Community Earth System model by modifying cloud phase parameterizations to reduce the magnitude of Southern Ocean absorbed shortwave radiation and cloud phase biases. We used the improved version of the model to establish how Southern Ocean cloud feedbacks influence climate change projections. The primary findings were:

- Improving absorbed shortwave radiation and cloud phase biases over the Southern Ocean in the Community Earth System Model (CESM) increases equilibrium climate sensitivity (ECS) by 1.5 K.
- The increase in ECS is due to two shortwave cloud feedbacks over the Southern Ocean. First, a weaker negative optical depth feedback at high latitudes increases warming. Second, warming is amplified by a positive cloud cover and cloud thinning feedback in the mid-latitudes.

- The same model improvements which increase ECS by 1.5 K hardly impact model projections of 21st century warming. Over the 21st century, ocean heat uptake moves heat input by extratropical shortwave cloud feedbacks to depth and delays transient surface warming.
- Because of the ability of extratropical oceans to take up heat, extratropical cloud biases and feedbacks are not as important for transient warming as cloud biases and feedbacks in other regions.

Next, we provide broader context and suggestions for future work based on Chapters 2 and 3. We found increased ECS in CESM is a robust response to improving the Southern Ocean shortwave radiation bias. Our targeted changes to Southern Ocean mixed-phase clouds (Frey & Kay, 2018) produce an ECS increase similar to one resulting from microphysical parameterization changes which impact mixed-phase clouds globally (Tan et al., 2016). We also show for the first time that increased ECS is not solely due to a changing negative optical depth feedback, but is in fact mostly caused by an increased positive cloud amount feedback in the Southern Hemisphere mid-latitudes. Future work is needed to assess whether fixing cloud phase biases over the Southern Ocean in other models produces large increases in ECS as we found in CESM.

Perhaps most importantly, we demonstrated that increased ECS caused by extratropical shortwave cloud feedbacks does not imply an increase in 21st Century warming in CESM because of extratropical ocean heat uptake. When extratropical cloud feedbacks drive an increase in ECS, 21st century warming does not increase in a way consistent with the CMIP5 ensemble. This result suggests that the current practice of using ECS as the parameter to quantify the magnitude of climate change in integrated assessment models (Calel & Stainforth, 2017) may be misleading because the idealized ECS metric does not always correlate well with 21st century climate change projections. A useful continuation of this work would be a detailed assessment of feedbacks and

ocean heat uptake among the CMIP5 ensemble to determine how and if the geographic distribution of cloud feedbacks and ocean heat uptake influences the relationship between ECS and 21st century warming.

Finally, working with two versions of CESM which differ primarily by their representation of Southern Ocean cloud phase highlighted interesting discrepancies in two commonly used methods of estimating ECS. In our modified version of CESM, ECS estimated with a slab ocean model was 1.2 K higher than ECS estimated with linear regression applied to a fully-coupled model (the method of Gregory et al., 2004; as applied in Frey et al., 2017). This is unexpected because the impact of estimation technique on ECS estimates is thought to be minor (Flato et al., 2013). In fact, with the default version of CESM, ECS estimated with a slab ocean model is only 0.2 K higher than ECS estimated with linear regression (Frey et al., 2017). Given that historically SOM and linear ECS estimates have been used interchangeably (e.g. IPCC AR4 used SOMs, IPCC AR5 used linear regression), it is important to understand when, how, and why these estimates differ. Assessing SOM and linear ECS estimates will require very long (3,000+ years) fully-coupled runs with multiple model set ups (for example, both the default CESM and our improved version) that reach a new equilibrium after a doubling of CO₂. Long fully-coupled runs to equilibrium will allow comparison of ECS estimates with true ECS and show when and how linear regression estimates of ECS converge to the true value.

6.3 The Observed and Modeled Influence of Sea Ice Variability on Southern Ocean Clouds and Top-of-Atmosphere Albedo.

Our conclusions from Chapters 2 and 3 show that Southern Ocean cloud feedbacks play an important role in climate change projections. Therefore, it is important to assess how realistically

models represent the processes that influence Southern Ocean cloud feedbacks. One such process is the interaction between changing sea ice concentrations and clouds. In the second part of this dissertation (Chapters 4 and 5), we isolated the impact of changing Southern Ocean sea ice concentration on clouds in both observations and a climate model. We show how the observed and modeled sea ice-cloud interactions differ and discuss how these differences could impact model-predicted cloud feedbacks. The primary findings were:

- In observations, low cloud cover is larger over open water compared to sea ice in spring but unchanged during summer. Cloud opacity is larger over open water compared to over sea ice during both spring and summer. Even when the cloud response is included, top-of-atmosphere albedo decreases and more shortwave radiation is absorbed as sea ice concentration decreases.
- In the Community Earth System Model, the low cloud cover, cloud opacity, and top-of-atmosphere albedo responses to present-day Southern Ocean sea ice variability have the same sign as observed. However, in CESM the magnitude of the response is larger than observed in each case.
- The mechanism leading to increased cloud opacity with decreasing sea ice concentration in CESM is different from the observed mechanism.
 - In observations, increased cloud opacity is the result of increased air temperatures which accompany sea ice retreat and lead to a shift in cloud phase from ice toward liquid. Observations show no change in air-sea coupling over open water compared to sea ice.
 - In CESM, total cloud water content increases with decreasing sea ice concentration consistent with an increase in model air-sea coupling strength. In CESM there is no evidence of a shift in cloud phase over open water compared to sea ice.

Next, we provide broader context and suggestions for future work based on Chapters 4 and 5. Our observational analysis of sea ice-cloud interactions is an important advance because we clearly show that even with the cloud response, top-of-atmosphere albedo is lower over open water compared to sea ice during spring and summer over the Southern Ocean. Because we use observations that are not impacted by surface condition, we are confident we clearly identify changes in clouds which occur over varying sea ice concentrations. Our work shows that as Southern Ocean sea ice is lost in the future, more shortwave radiation will be absorbed which will accelerate warming. Our observational analysis could be enhanced in the future if more surface-independent cloud observations become available. For example, observations of cloud optical depth, cloud liquid and ice water paths, and cloud particle effective radius which are accurate over both open water and sea ice would help even more clearly identify the cloud opacity response to sea ice variability and the mechanisms behind it.

Though both observations and CESM indicate that cloud opacity increases with decreasing sea ice concentration, the mechanism behind cloud opacity increase is different. In CESM, decreased sea ice concentration is accompanied by an increase in air-sea coupling strength. This increase in air-sea coupling strength could increase moisture fluxes to the atmosphere and result in the increase in total cloud water content seen in the model. Though the increase in air-sea coupling strength with decreasing sea ice concentration is not observed, it could impact the cloud optical depth feedback predicted by CESM in regions where sea ice is lost in the future. Future work is required to identify how much sea ice loss might contribute to cloud optical depth feedbacks in CESM. Additionally, a broader analysis of spring and summer sea ice-cloud interactions in other models would also be useful to determine how cloud optical depth feedbacks in general are impacted by sea ice loss.

6.4 Concluding Thoughts

In this dissertation, we modified a global climate model to “fix” a long-standing absorbed shortwave radiation bias linked to Southern Ocean cloud phase (Kay et al. 2016) and examined how these cloud phase modifications impact cloud radiative feedbacks. We identified the influence of Southern Ocean clouds and cloud feedbacks on global warming in idealized and realistic modeling scenarios and showed that Southern Ocean dynamics can reduce the warming caused by cloud feedbacks under transient climate change scenarios. We also isolated the impact of present-day Southern Ocean sea ice variability on clouds in both observations and a climate model and described how sea ice loss could impact cloud feedbacks in the future. Our results establish how local interactions between Southern Ocean clouds, ocean dynamics and sea ice impact the global coupled climate system. Ultimately, our work motivates continued efforts to observe, model, and understand the complex climate of the remote Southern Ocean region.

Bibliography

- Allen, M., Andronova, N., Booth, B., Dessai, S., Frame, D., Forest, C., et al. (2006). Observational constraints on climate sensitivity. In H. Schellnhuber, W. Cramer, N. Nakicenovic, T. Wigley, & G. Yohe (Eds.), *Avoiding dangerous climate change* (pp. 281–290). Cambridge, UK: Cambridge University Press.
- Allen, M. R., & Frame, D. J. (2007). Call off the quest. *Science*, 318(5850), 582–583. <https://doi.org/10.1126/science.1149988>
- Andrews, T., Gregory, J. M., & Webb, M. J. (2015). The dependence of radiative forcing and feedback on evolving patterns of surface temperature change in climate models. *Journal of Climate*, 28(4), 1630–1648. <https://doi.org/10.1175/JCLI-D-14-00545.1>
- Andrews, T., Gregory, J. M., Webb, M. J., & Taylor, K. E. (2012). Forcing, feedbacks and climate sensitivity in CMIP5 coupled atmosphere-ocean climate models. *Geophysical Research Letters*, 39, L09712. <https://doi.org/10.1029/2012GL051607>
- Armour, K. C., Bitz, C. M., & Roe, G. H. (2013). Time-varying climate sensitivity from regional feedbacks. *Journal of Climate*, 26(13), 4518–4534. <https://doi.org/10.1175/JCLI-D-12-00544.1>
- Armour, K. C., Marshall, J., Scott, J. R., Donohoe, A., & Newsom, E. R. (2016). Southern Ocean warming delayed by circumpolar upwelling and equatorward transport. *Nature Geoscience*, 9(7), 549–554. <https://doi.org/10.1038/ngeo2731>
- Baker, A. H., Hammerling, D. M., Mickelson, S. A., Xu, H., Stolpe, M. B., Naveau, P., et al. (2016). Evaluating lossy data compression on climate simulation data within a large ensemble. *Geoscientific Model Development*, 9(12), 4381–4403. <https://doi.org/10.5194/gmd-9-4381-2016>
- Banks, H. T., & Gregory, J. M. (2006). Mechanisms of ocean heat uptake in a coupled climate model and the implications for tracer based predictions of ocean heat uptake. *Geophysical Research Letters*, 33, L07608. <https://doi.org/10.1029/2005GL025352>
- Barton, N.P., Klein, S.A., Boyle, J. S., & Zhang, Y. Y. (2012). Arctic synoptic regimes: Comparing domain-wide Arctic cloud observations with CAM4 and CAM5 during similar dynamics. *Journal of Geophysical Research*, 117, D15205. <https://doi.org/10.1029/2012JD017589>
- Betts, A. K., and Harshvardhan (1987), Thermodynamic constraint on the cloud liquid water feedback in climate models, *Journal of Geophysical Research*, 92(D7), 8483–8485. <https://doi.org/10.1029/JD092iD07p08483>

- Bitz, C. M., Shell, K. M., Gent, P. R., Bailey, D. A., Danabasoglu, G., & Armour, K. C. (2012). Climate sensitivity of the Community Climate System Model, Version 4. *Journal of Climate*, 25(9), 3053–3070. <https://doi.org/10.1175/JCLI-D-11-00290.1>
- Bodas-Salcedo A., Williams K. D., Field P. R., & Lock A. P. (2012). The surface downwelling solar radiation surplus over the Southern Ocean in the met office model: The role of midlatitude cyclone clouds. *Journal of Climate*, 25, 7467–7486. <https://doi.org/10.1175/JCLI-D-11-00702.1>
- Bodas-Salcedo, A., Hill, G., Furtado, K., Williams, K. D., Field, P. R., Manners, J. C., et al. (2016). Large contribution of supercooled liquid clouds to the solar radiation budget of the Southern Ocean. *Journal of Climate*, 29, 4213-4228. <https://doi.org/10.1175/JCLI-D-15-0564.1>
- Bodas-Salcedo, A., Williams, K. D., Ringer, M. A., Beau, I., Cole, J. N. S., et al. (2014). Origins of the solar radiation biases over the Southern Ocean in CFMIP2 models. *Journal of Climate*, 27, 41–56. <https://doi.org/10.1175/JCLI-D-13-00169.1>
- Boer, G. J., & Yu, B. (2003). Dynamical aspects of climate sensitivity. *Geophysical Research Letters*, 30(3), 1135. <https://doi.org/10.1029/2002GL016549>
- Bony, S., Dufresne, J. L., Le Treut, H., Morcrette, J.J., & Senior, C. (2004). On dynamic and thermodynamic components of cloud changes. *Climate Dynamics*, 22, 71–86. <https://doi.org/10.1007/s00382-003-0369-6>
- Bony, S., & Dufresne, J. L. (2005). Marine boundary layer clouds at the heart of tropical cloud feedback uncertainties in climate models. *Geophysical Research Letters*, 32, 1–4. <https://doi.org/10.1029/2005GL023851>
- Boucher, O., Randall, D., Artaxo, P., Bretherton, C., Feingold, G., Forster, P., et al. (2013). Clouds and Aerosols. In: *Climate Change 2013: The Physical Science Basis. Contribution of Working Group I to the Fifth Assessment Report of the Intergovernmental Panel on Climate Change* [Stocker T. F., Qin D., Plattner G. K., Tignor M., Allen S. K., Boschung J., Nauels A., Xia Y., Bex V., Midgley P. M. (eds.)] pp 571-657. Cambridge University Press, Cambridge, United Kingdom and New York, NY, USA. <https://doi.org/10.1017/CBO9781107415324.016>
- Bretherton, C. S., & Blossey, P. N. (2014). Low cloud reduction in a greenhouse-warmed climate: Results from Lagrangian LES of a subtropical marine cloudiness transition. *Journal of Advances in Modeling Earth Systems*, 6, 91-114, <https://doi.org/10.1002/2013MS000250>
- Bretherton, C. S. (2015). Insights into low-latitude cloud feedbacks from high-resolution models. *Philosophical Transactions of the Royal Society A*, 373, 3354–3360. <https://doi.org/10.1098/rsta.2014.0415>
- Brient, F., & Bony, S. (2013). Interpretation of the positive low-cloud feedback predicted by a climate model under global warming. *Climate Dynamics*, 40, 2415–2431. <https://doi.org/10.1007/s00382-011-1279-7>

- Bromwich, D. H., & Fogt, R. L. (2004). Strong trends in the skill of the ERA-40 and NCEP-NCAR Reanalysis in the high and midlatitudes of the southern hemisphere, 1958-2001. *Journal of Climate*, 17, 4603-4619. <https://doi.org/10.1175/3241.1>
- Bromwich, D. H., Fogt, R. L., Hodges, K. I., & Walsh, J. E. (2007). A tropospheric assessment of the ERA-40, NCEP, and JRA-25 global reanalyses in the polar regions. *Journal of Geophysical Research*, 112, D10111. <https://doi.org/10.1029/2006JD007859>
- Bromwich, D. H., Nicolas, J. P., Hines, K. M., Kay, J. E., Key, E. L., Lazzara, M. A., et al. (2012). Tropospheric clouds in Antarctica. *Reviews of Geophysics*, 50, RG1004. <https://doi.org/10.1029/2011RG000363>
- Bromwich, D. H., Nicolas, J. P., & Monaghan, A. J. (2011). An assessment of precipitation changes over Antarctica and the Southern Ocean since 1989 in contemporary global reanalyses. *Journal of Climate*, 24, 4189-4209. <https://doi.org/10.1175/2011JCLI4074.1>
- Budyko, M. I. (1969). The effect of solar radiation variations on the climate of the Earth. *Tellus*, 21(5), 611–619. <https://doi.org/10.1111/j.2153-3490.1969.tb00466.x>
- Calel, R., & Stainforth, D. A. (2017). On the physics of three integrated assessment models. *Bulletin of the American Meteorological Society*, 1199–1216. <https://doi.org/10.1175/BAMS-D-16-0034.1>
- Ceppi, P., Hartmann, D. L., & Webb, M. J. (2016a). Mechanisms of the negative shortwave cloud feedback in high latitudes. *Journal of Climate*, 139–157. <https://doi.org/10.1175/JCLI-D-15-0327.1>
- Ceppi, P., McCoy, D. T., & Hartmann, D. L. (2016b). Observational evidence for a negative shortwave cloud feedback in mid to high latitudes. *Geophysical Research Letters*, 43, 1331-1339. <https://doi.org/10.1002/2015GL067499>
- Cesana, G., & Chepfer, H., (2013). Evaluation of the cloud thermodynamic phase in a climate model using CALIPSO-GOCCP, *Journal of Geophysical Research - Atmospheres*, 118, 7922–7937, <https://doi.org/10.1002/jgrd.50376>
- Cesana, G., Chepfer, H., Winker, D., Getzewich, B., Cai, X., Jourdan, O., et al. (2016). Using in situ airborne measurements to evaluate three cloud phase products derived from CALIPSO. *Journal of Geophysical Research: Atmospheres*, 121, 5788-5808. <https://doi.org/10.1002/2015JD024334>
- Charney, J. G., Arakawa, A., Baker, D. J., Bolin, B., Dickinson, R. E., Goody, R. M., et al. (1979). Carbon dioxide and climate: a scientific assessment. Washington, DC: National Academy of Sciences.

- Chepfer, H., Bony, S., Winker, D., Cesana, G., Dufresne, J. L., Minnis, P., et al. (2010). The GCM-Oriented CALIPSO Cloud Product (CALIPSO-GOCCP). *Journal of Geophysical Research*, 115, D00H16. <https://doi.org/10.1029/2009JD012251>
- Chepfer, H., Bony, S., Winker, D., Chiriaco, M., Dufresne, J.-L., & Sèze, G. (2008). Use of CALIPSO lidar observations to evaluate the cloudiness simulated by a climate model. *Geophysical Research Letters*, 35, L15704. <https://doi.org/10.1029/2008GL034207>
- Choi, Y.-S., Ho, C.-H., Park, C.-E., Storelvmo, T., & Tan, I. (2014). Influence of cloud phase composition on climate feedbacks. *Journal of Geophysical Research – Atmospheres*, 119, 3687–3700. <https://doi.org/10.1002/2013JD020582>
- Christensen, M. W. , Carrió, G. G., Stephens, G. L., & Cotton, W. R. (2013). Radiative impacts of free-tropospheric clouds on the properties of marine stratocumulus. *Journal of Atmospheric Science*, 70, 3102-3118. <https://doi.org/10.1175/JAS-D-12-0287.1>
- Chubb, T. H., Jensen, J. B., Siems, S. T., & Manton, M. J. (2013). In situ observations of supercooled liquid clouds over the Southern Ocean during the HIAPER Pole-to-Pole Observation campaigns. *Geophysical Research Letters*, 40, 5280-5285. <https://doi.org/10.1002/grl.50986>
- Clement, A. C., Seager, R., Cane, M. A., & Zebiak, S. E. (1996). An ocean dynamical thermostat. *Journal of Climate*, 9(9), 2190–2196. [https://doi.org/10.1175/1520-442\(1996\)009%3C2190:AODT%3E2.0.CO;2](https://doi.org/10.1175/1520-442(1996)009%3C2190:AODT%3E2.0.CO;2)
- Coleman, R. (2003). A comparison of climate feedbacks in general circulation models. *Climate Dynamics*, 20, 865-873. <https://doi.org/10.1007/s00382-003-0310-z>
- Cubasch, U., Meehl, G. A., Boer, G. J., Stouffer, R. J., Dix, M., Noda, A., et al. (2001). Projections of future climate change. In J. T. Houghton, et al. (Eds.), *Climate change 2001: The scientific basis. Contribution of Working Group I to the Third Assessment Report of the Intergovernmental Panel on Climate Change* (pp. 525–582). Cambridge, UK and New York: Cambridge University Press.
- Danabasoglu, G., & Gent, P. R. (2009). Equilibrium climate sensitivity: Is it accurate to use a slab ocean model? *Journal of Climate*, 22(9), 2494–2499. <https://doi.org/10.1175/2008JCLI2596.1>
- Deser, C., Sun, L., Tomas, R. A., & Screen, J. (2016). Does ocean coupling matter for the northern extratropical response to projected Arctic sea ice loss? *Geophysical Research Letters*, 43, 2149–2157. <https://doi.org/10.1002/2016GL067792>
- Dessler, A. E., Zhang, Z., & Yang, P. (2008). Water-vapor climate feedback inferred from climate fluctuations, 2003-2008. *Geophysical Research Letters*, 35, L20704. <https://doi.org/10.1029/2008GL035333>
- Driemel, A., Loose, Bernd, Grobe, H., Rainer, S., and König-Langlo, G. (2016). 30 years of upper

- air soundings on board of R/V POLARSTERN. *Earth System Science Data*, 8, 213-220. <https://doi.org/10.5194/essd-8-213-2016>.
- Eastman, R., & Warren, S. G. (2010). Interannual variations of Arctic cloud types in relation to sea ice. *Journal of Climate*, 23, 4216-4232. <https://doi.org/10.1175/2010JCLI3492.1>.
- Fitzpatrick, M. F., & Warren, S. G. (2007). The relative importance of clouds and sea ice for the solar energy budget of the Southern Ocean. *Journal of Climate*, 20, 941-954. <https://doi.org/10.1175/JCLI4040.1>
- Flato, G. M. (2011). Earth system models: an overview, *WIREs Climate Change*, 2, 783-800. <https://doi.org/10.1002/wcc.148>
- Flato, G., Marotzke, J., Abiodun, B., Braconnot, P., Chou, S. C., Collins, W., et al. (2013). Evaluation of climate models. In T. F. Stocker, et al. (Eds.), *Climate change 2013: The physical science basis. Contribution of Working Group I to the Fifth Assessment Report of the Intergovernmental Panel on Climate Change* (pp. 741–866). Cambridge, UK and New York: Cambridge University Press.
- Forster, P. M., Andrews, T., Good, P., Gregory, J. M., Jackson, L. S., & Zelinka, M. (2013). Evaluating adjusted forcing and model spread for historical and future scenarios in the CMIP5 generation of climate models. *Geophysical Research Letters*, 118, 1139–1150. <https://doi.org/10.1002/jgrd.50174>
- Frey, W. R., & Kay, J. E. (2018). The influence of extratropical cloud phase and amount feedbacks on climate sensitivity. *Climate Dynamics*, 50, 3097-3116. <https://doi.org/10.1007/s00382-017-3796-5>
- Frey, W. R., Maroon, E. A., Pendergrass, A. G., & Kay, J. E. (2017). Do Southern Ocean cloud feedbacks matter for 21st century warming? *Geophysical Research Letters*, 44, 12,447–12,456. <https://doi.org/10.1002/2017GL076339>
- Frey, W. R., Morrison, A. L., Kay, J. E., Guzman, R., & Chepfer, H. (Revised). The combined influence of observed Southern Ocean clouds and sea ice on top-of-atmosphere albedo. *Journal of Geophysical Research – Atmospheres*
- Friedlingstein, P., Cox, P., Betters, R., Bopp, L., von Bloh, W., Brovkin, V., et al. (2006). Climate-Carbon cycle feedback analysis: Results from the C4MIP model intercomparison, *Journal of Climate*, 19, 3337-3353. <https://doi.org/10.1175/JCLI3800.1>
- Frölicher, T. L., Sarmiento, J. L., Paynter, D. J., Dunne, J. P., Krasting, J. P., & Winton, M. (2015). Dominance of the Southern Ocean in anthropogenic carbon and heat uptake in CMIP5 models. *Journal of Climate*, 28, 862-886. <https://doi.org/10.1175/JCLI-D-14-00117.1>
- Gettelman, A., Kay, J. E., & Shell, K. M. (2012). The evolution of climate sensitivity and climate feedbacks in the Community Atmosphere Model. *Journal of Climate*, 25(5), 1453–1469.

<https://doi.org/10.1175/JCLI-D-11-00197.1>

- Gettelman, A., & Sherwood, S. C. (2016). Processes responsible for cloud feedback. *Current Climate Change Reports*, 2, 179-189 <https://doi.org/10.1007/s40641-016-0052-8>
- Gordon, N. D., & Klein, S. A. (2014). Low-cloud optical depth feedback in climate models. *Journal of Geophysical Research – Atmospheres*, 119, 6052–6065. <https://doi.org/10.1002/2013JD021052>
- Gregory, J. M. (2000). Vertical heat transports in the ocean and their effect on time-dependent climate change. *Climate Dynamics*, 16(7), 501–515. <https://doi.org/10.1007/s003820000059>
- Gregory, J. M., & Andrews, T. (2016). Variation in climate sensitivity and feedback parameters during the historical period. *Geophysical Research Letters*, 43, 3911–3920. <https://doi.org/10.1002/2016GL068406>
- Gregory, J. M., Andrews, T., & Good, P. (2015). The inconstancy of the transient climate response parameter under increasing CO₂. *Philosophical Transactions of the Royal Society A*, 373(2054), 20140417. <https://doi.org/10.1098/rsta.2014.0417>
- Gregory, J. M., Dixon, K. W., Stouffer, R. J., Weaver, A. J., Driesschaert, E., Eby, M., et al. (2005). A model intercomparison of changes in the Atlantic thermohaline circulation in response to increasing atmospheric CO₂ concentration. *Geophysical Research Letters*, 32, L12703. <https://doi.org/10.1029/2005GL023209>
- Gregory, J. M., Ingram, W. J., Palmer, M. A., Jones, G. S., Stott, P. A., Thorpe, R. B., et al. (2004). A new method for diagnosing radiative forcing and sensitivity. *Geophysical Research Letters*, 31, L03205. <https://doi.org/10.1029/2003GL018747>
- Grise, K. M., Polvani, L. M., & Fasullo, J. T. (2015). Reexamining the relationship between climate sensitivity and Southern Hemisphere radiation budget in CMIP models. *Journal of Climate*, 28, 9298-9312. <https://doi.org/10.1175/JCLI-D-15-0031.1>
- Guzman, R., Chepfer, H., Noel, V., Vaillant de Guelis, T., Kay, J. E., Raberanto, P., et al. (2017). Direct atmosphere opacity observations from CALIPSO provide new constraints on cloud-radiation interactions. *Journal of Geophysical Research: Atmospheres*, 122, 1066-1085. <https://doi.org/10.1002/2016JD025946>
- Hall, A. (2004). The role of surface albedo feedback in climate. *Journal of Climate*, 17, 1550-1568. [https://doi.org/10.1175/1520-0442\(2004\)017<1550:TROSAF>2.0.CO;2](https://doi.org/10.1175/1520-0442(2004)017<1550:TROSAF>2.0.CO;2)
- Hansen, J., Lacis, A., Rind, D., & Russell, G. (1984). Climate sensitivity: Analysis of feedback mechanisms. In J.E. Hansen & Y Takahashi (Eds.), *Climate Processes and Climate Sensitivity*, AGU Geophysical Monograph 29, Maurice Ewing Volume 5, pp 130-163, American Geophysical Union.

- Hansen, J., Ruedy, R., Sato, M., & Lo, K. (2010). Global surface temperature change. *Reviews of Geophysics*, 48, RG4004. <https://doi.org/10.1029/2010RG000345>
- Hartmann, D. L., & Ceppi, P. (2014). Trends in the CERES Dataset, 2000-13: The effects of sea ice and jet shifts and comparison to climate models. *Journal of Climate*, 27, 2444-2456. <https://doi.org/10.1175/JCLI-D-13-00411.1>
- Hartmann, D. L., & Larson, K. (2002). An important constraint on tropical cloud-climate feedback. *Geophysical Research Letters*, 29 (20), 1951. <https://doi.org/10.1029/2002GL015835>
- Hawcroft, M., Haywood, J. M., Collins, M., Jones, A., Jones, A. C., & Stephens, G. (2016) Southern Ocean albedo, inter-hemispheric energy transports and the double ITCZ: Global impacts of biases in a coupled model. *Climate Dynamics*, 48, 2279-2295. <https://doi.org/10.1007/s00382-016-3205-5>
- Held, I. M., Winton, M., Takahashi, K., Delworth, T., Zeng, F., & Vallis, G. K. (2010). Probing the fast and slow components of global warming by returning abruptly to preindustrial forcing. *Journal of Climate*, 23(9), 2418–2427. <https://doi.org/10.1175/2009JCLI3466.1>
- Hines, K. M., Grumbine, R. W., Bromwich, D. H., & Cullather, R. I. (1999). Surface energy balance of the NCEP MRF and NCEP-NCAR Reanalysis in Antarctic latitudes during FROST. *Journal of Climate*, 14, 851-866. [https://doi.org/10.1175/1520-0434\(1999\)014<0851:SEBOTN>2.0.CO;2](https://doi.org/10.1175/1520-0434(1999)014<0851:SEBOTN>2.0.CO;2)
- Hoffert, M. I., Callegari, A. J., & Hsieh, C. T. (1980). The role of deep sea heat storage in the secular response to climatic forcing. *Journal of Geophysical Research*, 85(C11), 6667–6679. <https://doi.org/10.1029/JC085iC11p06667>
- Hoskins, B. J., & Hodges, K. I. (2005). A new perspective on Southern Hemisphere storm tracks. *Journal of Climate*, 18, 4108-4129. [https://doi.org/10.1175/1520-0469\(1991\)048<2159:STITSH>2.0.CO;2](https://doi.org/10.1175/1520-0469(1991)048<2159:STITSH>2.0.CO;2)
- Hu, Y., Rodier, S., Xu, K., Sun, W., Huang, J., Lin, B., Zhai, P., & Josset, D. (2010). Occurrence, liquid water content, and fraction of supercooled water clouds from combined CALIOP/IIR/MODIS measurements. *Journal of Geophysical Research*, 115, D00H34, <https://doi.org/10.1029/2009JD012384>
- Huang, Y., Siems, S. T., Manton, M. J., Protat, A., & Delanoë, J. (2012). A study on the low-altitude clouds over the Southern Ocean using the DARDAR-MASK. *Journal of Geophysical Research*, 117, D18204. <https://doi.org/10.1029/2012JD017800>
- Hunke, E. C., & Lipscomb, W. H. (2010). CICE: The Los Alamos Sea Ice Model documentation and software user's manual, version 4.1. Doc. LA-CC-06-012, 76 pp. http://csdms.colorado.edu/w/images/CICE_documentation_and_software_user's_manual.pdf

- Hurrell, J. W., Holland, M. M., Gent, P. R., Ghan, S., Kay, J. E., Kushner, P. J., et al. (2013). The Community Earth System Model: A framework for collaborative research. *Bulletin of the American Meteorological Society*, 94(9), 1339–1360. <https://doi.org/10.1175/BAMS-D-12-00121.1>
- Hwang, Y.-T., & Frierson, D. M. W. (2013). Link between the double-Intertropical Convergence Zone problem and cloud biases over the Southern Ocean. *Proceedings of the National Academy of Sciences*, 110, 4935–40. <https://doi.org/10.1073/pnas.1213302110>
- Jahn, A., & Holland, M. M. (2013). Implications of Arctic sea ice changes for North Atlantic deep convection and the meridional overturning circulation in CCSM4-CMIP5 simulations. *Geophysical Research Letters*, 40, 1206–1211. <https://doi.org/10.1002/grl.50183>
- Jones, R. W., Renfrew, I. A., Orr, A., Webber, B. G. M., Holland, D. M., & Lazzara, M. A. (2016). Evaluation of four global reanalysis products using in situ observations in the Amundsen Sea Embayment, Antarctica. *Journal of Geophysical Research: Atmospheres*, 121. <https://doi.org/10.1002/2015JD024680>
- Jonko, A. K., Shell, K. M., Sanderson, B. M., & Danabasoglu, G. (2013). Climate feedbacks in CCSM3 under changing CO₂ forcing. Part II: Variation of climate feedbacks and sensitivity with forcing. *Journal of Climate*, 26(9), 2784–2795. <https://doi.org/10.1175/JCLI-D-12-00479.1>
- Kamae, Y., & Watanabe, M. (2012). On the robustness of tropospheric adjustment in CMIP5 models. *Geophysical Research Letters*, 39, L23808. <https://doi.org/10.1029/2012GL054275>
- Kay, J. E., Bourdages, L., Miller, N. B., Morrison, A., Yettella, V., Chepfer, H., & Eaton, B. (2016a). Evaluating and improving cloud phase in the Community Atmosphere Model version 5 using spaceborne LIDAR observations. *Journal of Geophysical Research – Atmospheres*, 121, 4162–4176. <https://doi.org/10.1002/2015JD024699>
- Kay, J. E., Deser, C., Phillips, A., Mai, A., Hannay, C., Strand, G., et al. (2015). The Community Earth System Model (CESM) large ensemble project: A community resource for studying climate change in the presence of internal climate variability. *Bulletin of the American Meteorological Society*, 96(8), 1333–1349. <https://doi.org/10.1175/BAMS-D-13-00255.1>
- Kay, J. E. & Gettelman, A. (2009). Cloud influence on and response to seasonal Arctic sea ice loss. *Journal of Geophysical Research*, 114, D18204. <https://doi.org/10.1029/2009JD011773>
- Kay, J. E., Holland, M. M., Bitz, C. C., Blanchard-Wrigglesworth, E., Gettelman, A., Conley, A., & Bailey, D. (2012). The influence of local feedbacks and northward heat transport on the equilibrium Arctic climate response to increased greenhouse gas forcing. *Journal of Climate*, 25, 5433–5450. <https://doi.org/10.1175/JCLI-D-11-00622.1>

- Kay, J. E. and L'Ecuyer, T. (2013). Observational constraints on Arctic Ocean clouds and radiative fluxes during the early 21st century, *Journal of Geophysical Research*, 118, 7219-7236. <https://doi.org/10.1002/jgrd.50489>
- Kay, J. E., L'Ecuyer, T., Chepfer, H., Loeb, N., Morrison, A., & Cesana G. (2016c). Recent advances in Arctic cloud and climate research, *Current Climate Change Reports*, 2:159, <https://doi.org/10.1007/s40641-016-0051-9>
- Kay, J. E., Medeiros, B., Hwang, Y. T., Gettelman, A., Perket, J., & Flanner, M. G. (2014). Processes controlling Southern Ocean shortwave climate feedbacks in CESM, *Geophysical Research Letters*, 41, <https://doi.org/10.1002/2013GL058315>
- Kay, J. E., Wall, C., Yettella, V., Medeiros, B., Hannay, C., Caldwell, P., & Bitz, C. (2016b). Global climate impacts of fixing the Southern Ocean shortwave radiation bias in the Community Earth System Model (CESM). *Journal of Climate*, 29(12), 4617–4636. <https://doi.org/10.1175/JCLI-D-15-0358.1>
- Kaya, T., Yamaguchi, M., & Akimoto, K. (2016). The uncertainty of climate sensitivity and its implication for the Paris negotiation. *Sustainability Science*, 11(3), 515–518. <https://doi.org/10.1007/s11625-015-0339-z>
- Khatriwala, S., Primeau F., & Hall, T. (2009). Reconstruction of the history of anthropogenic CO₂ concentrations in the ocean. *Nature*, 462, 346-350. <https://doi.org/10.1038/nature08526>.
- Klein, S. A., & Hartmann, D. L. (1993). The seasonal cycle of low stratiform clouds. *Journal of Climate*, 6, 1587-1606. [https://doi.org/10.1175/1520-0442\(1993\)006](https://doi.org/10.1175/1520-0442(1993)006)
- Klein, S. A., McCoy, R. B., Morrison, H., Ackerman, A. S., Avramov, A., de Boer, G., et al. (2009). Intercomparison of model simulations of mixed-phase clouds observed during the ARM mixed-phase Arctic cloud experiment. I: single-layer cloud. *Quarterly Journal of the Royal Meteorological Society*, 135 (641), 979-1002. <https://doi.org/10.1002/qj.416>
- Knutti, R., Joos, F., Müller, S. A., Plattner, G.-K., & Stocker, T. F. (2005). Probabilistic climate change projections for CO₂ stabilization profiles. *Geophysical Research Letters*, 32, L20707. <https://doi.org/10.1029/2005GL023294>
- Knutti, R., & Rugenstein, M. M. A. (2015). Feedbacks, climate sensitivity and the limits of linear models. *Philosophical Transactions of the Royal Society A*, 373(2054), 20150146. <https://doi.org/10.1098/rsta.2015.0146>
- Knutti, R., Rugenstein, M. A. A., & Hegerl, G. C. (2017). Beyond equilibrium climate sensitivity. *Nature Geoscience*, 10(10), 727–736. <https://doi.org/10.1038/ngeo3017>
- König-Langlo, G., Loose, B., & Bräuer, B. (2006). 25 years of Polarstern Meteorology (1982-2006). *WDC-MARE Reports*, 1-137. <https://doi.org/10.2312/wdc-mare.2006.4>

- Konsta, D., Dufresne, J.-L., Chepfer, H., Idelkadi, A., & Cesana, G. (2016). Use of A-train satellite observations (CALIPSO-PARASOL) to evaluate tropical cloud properties in the LMDZ5 GCM. *Climate Dynamics*, 47, 1263-1284. <https://doi.org/10.1007/s00382-015-2900-y>
- Kopp G., Lawrence G., & Rottman G. (2005) The Total Irradiance Monitor (TIM): Science Results. In: Rottman G., Woods T., George V. (eds) *The Solar Radiation and Climate Experiment (SORCE)*. Springer, New York, NY
- Lawrence, D. M., Oleson, K. W., Flanner, M. G., Thornton, P. E., Swenson, S. C., Lawrence, P. J., et al. (2011). Parameterization improvements and functional and structural advances in version 4 of the Community Land Model. *Journal of Advances in Modeling Earth Systems*, 3, M03001. <https://doi.org/10.1029/2011MS000045>
- Leahy, L. V., Wood, R., Charlson, R. J., Hostetler, C. A., Rogers, R. R., Vaughan, M. A., & Winker, D. M. (2012). On the nature and extent of optically thin marine low clouds. *Journal of Geophysical Research*, 117, D22201. <https://doi.org/10.1029/2012JD017929>
- Li, C., von Storch, J.-S., & Marotzke, J. (2013). Deep-ocean heat uptake and equilibrium climate response. *Climate Dynamics*, 40(5-6), 1071–1086. <https://doi.org/10.1007/s00382-012-1350-z>
- Li, Z. X., & Le Treut, H. (1992). Cloud-radiation feedbacks in a general circulation model and their dependence on cloud modelling assumptions. *Climate Dynamics*, 7, 133–139. <https://doi.org/10.1007/BF00211155>
- Liu, Y., Ackerman, S. A., Maddux, B. C., Key, J. R., & Frey, R. A. (2010). Errors in cloud detection over the Arctic using a satellite imager and implications for observing feedback mechanisms. *Journal of Climate*, 23, 1894-1907. <https://doi.org/10.1175/2009JCLI3386.1>
- Loeb, N. G., Kato, S., Loukachine K., & Manalo-Smith, N. (2005). Angular distribution models for top-of-atmosphere radiative flux estimation from the clouds and the earth's radiant energy system instrument on the Terra satellite. Part I: Methodology. *Journal of Atmospheric and Oceanic Technology*, 22, 338-351. <https://doi.org/10.1175/JTECH1712.1>
- Loeb, N. G., Wielicki, B. A., Doelling, D. R., Smith, G. L., Keyes, D. F., Kato, S., et al. (2009). Toward optimal closure of the Earth's top-of-atmosphere radiation budget. *Journal of Climate*, 22, 748–766. <https://doi.org/10.1175/2008JCLI2637.1>
- Lu, J., Vecchi, G. A., & Reichler, T. (2007). Expansion of the Hadley cell under global warming. *Geophysical Research Letters*, 34, L06805. <https://doi.org/10.1029/2006GL028443>
- Manabe, S., & Bryan, K. (1969). Climate calculations with a combined ocean-atmosphere model. *Journal of Atmospheric Sciences*, 26, 786-789. [https://doi.org/10.1175/1520-0469\(1969\)026<0786:CCWACO>2.0.CO;2](https://doi.org/10.1175/1520-0469(1969)026<0786:CCWACO>2.0.CO;2)
- Manabe, S., & Stouffer, R. J. (2007). Role of ocean in global warming. *Journal of the Meteorological Society of Japan*, 85B, 385–403. <https://doi.org/10.2151/jmsj.85B.385>

- Manabe, S., & Wetherald, R. T. (1967). Thermal equilibrium of the atmosphere with a given distribution of relative humidity, *Journal of Atmospheric Sciences*, 24 (3), 241-259. [https://doi.org/10.1175/1520-0469\(1967\)024<0241:TEOTAW>2.0.CO;2](https://doi.org/10.1175/1520-0469(1967)024<0241:TEOTAW>2.0.CO;2)
- Manabe, S., & Wetherald, R. T. (1975). The effects of doubling the CO₂ concentration on the climate of a general circulation model, *Journal of Atmospheric Sciences*, 32 (1), 3-14. [https://doi.org/10.1175/1520-0469\(1975\)032<0003:TEODTC>2.0.CO;2](https://doi.org/10.1175/1520-0469(1975)032<0003:TEODTC>2.0.CO;2)
- Marshall, G. J. (2002). Trends in Antarctic geopotential height and temperature: A comparison between radiosonde and NCEP-NCAR Reanalysis data. *Journal of Climate*, 15, 659-674. [https://doi.org/10.1175/1520-0442\(2002\)015<0659:TIAGHA>2.0.CO;2](https://doi.org/10.1175/1520-0442(2002)015<0659:TIAGHA>2.0.CO;2)
- Marshall, J., Scott, J. R., Armour, K. C., Campin, J.-M., Kelley, M., & Romanou, A. (2015). The ocean's role in the transient response of climate to abrupt greenhouse forcing. *Climate Dynamics*, 44(7-8), 2287–2299. <https://doi.org/10.1007/s00382-014-2308-0>
- Marshall, J., & Speer, K. (2012). Closure of the meridional overturning circulation through Southern Ocean upwelling. *Nature Geoscience*, 5(3), 171–180. <https://doi.org/10.1038/NGEO1391>
- Massom, R. AA., Eicken, H., Haas, C., Jeffries, M. O., Drinkwater, M. R., Sturm, M., et al. (2001). Snow on Antarctic Sea Ice. *Reviews of Geophysics*, 39 (3), 413-445. <https://doi.org/10.1029/2000RG000085>
- Mauritsen, T., Gravensén, R. G., Klocke, D., Langen, P. L., Stevens, B., & Tomassini, L. (2013). Climate feedback efficiency and synergy, *Climate Dynamics*, 41, 2539-2554. <https://doi.org/10.1007/s00382-013-1808-7>
- McCoy, D. T., Eastman, R., Hartmann, D. L., & Wood, R. (2017). The change in low cloud cover in a warmed climate inferred from AIRS, MODIS and ECMWF-Interim reanalysis. *Journal of Climate*, 30, 3609-3620. <https://doi.org/10.1175/JCLI-D-15-0734.1>
- McCoy, D. T., Hartmann, D. L., & Grosvenor, D. P. (2014). Observed Southern Ocean cloud properties and shortwave reflection. Part II: phase changes and low cloud feedback. *Journal of Climate*, 27, 8858–8868. <https://doi.org/10.1175/JCLI-D-14-00288.1>
- McCoy, D. T., Hartmann, D. L., Zelinka, M. D., Ceppi, P., & Grosvenor, D. P. (2015). Mixed-phase cloud physics and Southern Ocean cloud feedback in climate models. *Journal of Geophysical Research – Atmospheres*, 120, 9539–9554. <https://doi.org/10.1002/2015JD023603>
- McCoy, D. T., Tan, I., Hartmann, D. L., Zelinka, M. D., & Storelvmo, T. (2016). On the relationships among cloud cover, mixed-phase partitioning, and planetary albedo in GCMs. *Journal of Advances in Modeling Earth Systems*, 8 (2), 650-668. <https://doi.org/10.1002/2015MS000589>

- Medeiros, B., Deser, C., Tomas, R. A., & Kay, J. E. (2011). Arctic inversion strength in climate models. *Journal of Climate*, 24, 4733–4740. <https://doi.org/10.1175/2011JCLI3968.1>
- Meehl, G. A., Stocker, T. F., Collins, W. D., Friedlingstein, P., Gaye, A. T., Gregory, J. M., et al. (2007). Global climate projections. In S. Solomon, et al. (Eds.), *Climate change 2007: The physical science basis. Contribution of Working Group I to the Fourth Assessment Report of the Intergovernmental Panel on Climate Change* (pp. 747–845). Cambridge, UK and New York: Cambridge University Press.
- Meier, W., Fetterer, F., Savoie, M., Mallory, S., Duerr, R., & Stroeve, J. (2017). NOAA/NSIDC Climate Data Record of Passive Microwave Sea Ice Concentration, Version 3. Boulder, Colorado USA. NSIDC: National Snow and Ice Data Center. <https://dx.doi.org/10.7265/N59P2ZTG>
- Meinshausen, M., Smith, S. J., Calvin, K., Daniel, J. S., Kainuma, M. L. T., Lamarque, J. F., et al. (2011). The RCP greenhouse gas concentrations and their extensions from 1765 to 2300. *Climate Change*, 109(1-2), 213–241. <https://doi.org/10.1007/s10584-011-0156-z>
- Mikaloff-Fletcher, S. E., Gruber, N., Jacobson, A. R., Doney, S. C., Dutkiewicz, S., Gerber, M., et al. (2006). Inverse estimates of anthropogenic CO₂ uptake, transport, and storage by the ocean. *Global Biogeochemical Cycles*, 20, GB2002. <https://doi.org/10.1029/2005GB002530>
- Millar, R. J., Otto, A., Forster, P. M., Lowe, J. A., Ingram, W. J., & Allen, M. R. (2015). Model structure in observational constraints on transient climate response. *Climate Change*, 131(2), 199–211. <https://doi.org/10.1007/s10584-015-1384-4>
- Mitchell, J. F. B., Senior, C. A., & Ingram, W. J. (1989). CO₂ and climate: a missing feedback? *Nature*, 341, 132–134. <https://doi.org/10.1038/341132a0>
- Morrison, A. L., Kay, J. E., Chepfer, H., Guzman, R. & Yettella, V. (2018). Isolating the liquid cloud response to recent Arctic sea ice variability using spaceborne lidar observations. *Journal of Geophysical Research: Atmospheres*, 123, 473–490. <https://doi.org/10.1002/2017JD027248>
- Morrison, A. E., Siems, S. T., Manton, M. J. (2011). A three-year climatology of cloud-top phase over the Southern Ocean and North Pacific. *Journal of Climate*, 24, 2405–2418. <https://doi.org/10.1175/2010JCLI3842.1>
- Morrison, H., & Gettelman, A. (2008) A new two-moment bulk stratiform cloud microphysics scheme in the Community Atmosphere Model, Version 3 (CAM3). Part I: Description and numerical tests. *Journal of Climate*, 21, 3642–3659. <https://doi.org/10.1175/2008JCLI2105.1>
- Murphy, D. M. (2010). Constraining climate sensitivity with linear fits to outgoing radiation. *Geophysical Research Letters*, 37, L09704. <https://doi.org/10.1029/2010GL042911>

- Myers, T. A., & Norris, J. R. (2013). Observational evidence that enhanced subsidence reduces subtropical marine boundary layer cloudiness. *Journal of Climate*, 26, 7507–7524. <https://doi.org/10.1175/JCLI-D-12-00736.1>
- Nicolas, J. P., & Bromwich, D. H. (2011). Precipitation changes in high southern latitudes from global reanalyses: A cautionary tale. *Surveys of Geophysics*, 32, 475–494. <https://doi.org/10.1007/s10712-011-9114-6>
- Palm, S. P., Strey, S. T., Spinhirne, J., & Markus, T. (2010). Influence of Arctic sea ice extent on polar cloud fraction and vertical structure and implications for regional climate. *Journal of Geophysical Research*, 115, D21209. <https://doi.org/10.1029/2010JD013900>
- Park, S., & Bretherton, C. S. (2009). The University of Washington shallow convection and moist turbulence schemes and their impact on climate simulations with the Community Atmosphere Model. *Journal of Climate*, 22, 3449–3469. <https://doi.org/10.1175/2008JCLI2557.1>
- Park, S., Bretherton, C. S., & Rasch, P. J. (2014). Integrating cloud processes in the Community Atmosphere Model, version 5. *Journal of Climate*, 27, 6821–6856. <https://doi.org/10.1175/JCLI-D-14-00087.1>
- Pendergrass, A. P., Conley, A., & Witt, F. (2017). Surface and top-of-atmosphere radiative feedback kernels for CESM-CAM5. *Earth System Science Data*, 1–14. <https://doi.org/10.5194/essd-2017-108>
- Peng, G., Meier, W. N., Scott, D. J., & Savoie, M. H. (2013). A long-term and reproducible passive microwave sea ice concentration data record for climate studies and monitoring. *Earth System Science Data*, 5, 311–318. <https://doi.org/10.5194/essd-5-311-2013>
- Qu, X., Hall, A. (2005). Surface contribution to planetary albedo variability in cryosphere regions. *Journal of Climate*, 18, 5239–5252. <https://doi.org/10.1175/JCLI3555.1>
- Qu, X., Hall, A., Klein, S. A., & Caldwell, P. M. (2014) On the spread of changes in marine low cloud cover in climate model simulations of the 21st century. *Climate Dynamics*, 42, 2603–2626. <https://doi.org/10.1007/s00382-013-1945-z>
- Raper, S. C. B., Gregory, J. M., & Stouffer, R. J. (2002). The role of climate sensitivity and ocean heat uptake on AOGCM transient temperature response. *Journal of Climate*, 15(1), 124–130. [https://doi.org/10.1175/1520-0442\(2002\)15\(1\), 124–130.](https://doi.org/10.1175/1520-0442(2002)15<124:RSCBGR>2.0.CO;2)
- Riahi, K., Rao, S., Krey, V., Cho, C., Chirkov, V., Fischer, G., et al. (2011). RCP8.5 – A scenario of comparatively high greenhouse gas emissions. *Climate Change*, 109(1-2), 33–57. <https://doi.org/10.1007/s10584-011-0149-y>
- Rieck, M., Nuijens, L., & Stevens, B. (2012). Marine boundary layer cloud feedbacks in a constant relative humidity atmosphere. *Journal of Atmospheric Science*, 69, 2538–2550. <https://doi.org/10.1175/JAS-D-11-0203.1>

- Roeckner, E., Schlese, U., Biercamp, J., & Loewe, P. (1987). Cloud optical depth feedbacks and climate modeling, *Nature*, 329, 138-140. <https://doi.org/10.1038/329138a0>
- Rogelj, J., Meinshausen, M., Sedlacek, J., & Knutti, R. (2014). Implications of potentially lower climate sensitivity on climate projections and policy. *Environmental Research Letters*, 9. <https://doi.org/10.1008/1748-9326/9/3/031003>
- Rose, B. E. J., Armour, K. C., Battisti, D. S., Feldl, N., & Koll, D. D. B. (2014). The dependence of transient climate sensitivity and radiative feedbacks on the spatial pattern of ocean heat uptake. *Geophysical Research Letters*, 41, 1071–1078. <https://doi.org/10.1002/2013GL058955>
- Rose, B. E. J., & Rayborn, L. (2016). The effects of ocean heat uptake on transient climate sensitivity. *Current Climate Change Reports*, 2(4), 190–201. <https://doi.org/10.1007/s40641-016-0048-4>
- Rugenstein, M. A. A., Caldeira, K., & Knutti, R. (2016a). Dependence of global radiative feedbacks on evolving patterns of surface heat fluxes. *Geophysical Research Letters*, 43, 9877–9885. <https://doi.org/10.1002/2016GL070907>
- Rugenstein, M. A. A., Sedlacek, J., & Knutti, R. (2016b). Nonlinearities in patterns of long-term ocean warming. *Geophysical Research Letters*, 43, 3380–3388. <https://doi.org/10.1002/2016GL068041>
- Rugenstein, M. A. A., Winton, M., Stouffer, R. J., Griffies, S. M., & Halleberg, R. (2013). Northern high-latitude heat budget decomposition and transient warming. *Journal of Climate*, 26(2), 609–621. <https://doi.org/10.1175/JCLI-D-11-00695.1>
- Schneider, S. H. (1972). Cloudiness as a global climatic feedback mechanism: The effects on the radiation balance and surface temperature of variations in cloudiness. *Journal of Atmospheric Sciences*, 29, 1413-1422. [https://doi.org/10.1175/1520-0469\(1972\)029<1413:CAAGCF>2.0.CO;2](https://doi.org/10.1175/1520-0469(1972)029<1413:CAAGCF>2.0.CO;2)
- Schneider, S. H., Dickinson, R. E. (1974). Climate Modeling. *Reviews of Geophysics and Space Physics*. 12 (3), 447-493. <https://doi.org/10.1029/RG012i003p00447>
- Schweiger, A. J., Lindsay, R. W., Vavrus, S., & Francis, J. A. (2008). Relationships between Arctic sea ice and clouds during autumn. *Journal of Climate*, 21, 4799-4810. <https://doi.org/10.1175/2008JCLI2156.1>
- Sellers, W. D. (1969). A global climatic model based on the energy balance of the Earth-atmosphere system, *Journal of Applied Meteorology*, 8, 392-400. [https://doi.org/10.1175/1520-0450\(1969\)008<0392:AGCMBO>2.0.CO;2](https://doi.org/10.1175/1520-0450(1969)008<0392:AGCMBO>2.0.CO;2)
- Senior, C. A., & Mitchell, J. F. B. (1993). Carbon dioxide and climate: The impact of cloud parameterization. *Journal of Climate*, 6, 393-418. [https://doi.org/10.1175/1520-0442\(1993\)006<0393:CDACTI>2.0.CO;2](https://doi.org/10.1175/1520-0442(1993)006<0393:CDACTI>2.0.CO;2)

- Senior, C. A., & Mitchell, J. F. B. (2000). The time-dependence of climate sensitivity. *Geophysical Research Letters*, 27(17), 2685–2688. <https://doi.org/10.1029/2000GL011373>
- Serreze, M. C., Barrett, A. P., Stroeve, J. C., Kindig, D. N., & Holland, M. M. (2009). The emergence of surface-based Arctic amplification. *The Cryosphere*, 3, 11-19. <https://doi.org/10.5194/tc-3-11-2009>
- Sherwood, S. C., Bony, S., & Dufresne, J.-L. (2014). Spread in model climate sensitivity traced to atmospheric convective mixing. *Nature*, 505(7481), 37–42. <https://doi.org/10.1038/nature12829>
- Simmons, I. (2015). Comparing and contrasting the behavior of Arctic and Antarctic sea ice over the 35 year period 1979-2013. *Annals of Glaciology*, 56 (69), 18-28. <https://doi.org/10.3189/2015AoG69A909>
- Smith, R., Jones, P., Briegleb, B., Bryan, F., Danabasoglu, G., Dennis, J., et al. (2010). The Parallel Ocean Program (POP) reference manual: Ocean component of the Community Climate System Model (CCSM) and Community Earth System Model (CESM). *Los Alamos National Laboratory Tech. Rep.* LAUR-10-01853, 141 pp. www.cesm.ucar.edu/models/cesm1.0/pop2/doc/sci/POPRefManual.pdf.
- Soden, B. J., Broccoli, A. J., & Hemler, R. S. (2004). On the use of cloud forcing to estimate cloud feedback. *Journal of Climate*, 17 (19), 3661–3665. [https://doi.org/10.1175/1520-0442\(2004\)17<3661:OUCF>2.0.CO;2](https://doi.org/10.1175/1520-0442(2004)17<3661:OUCF>2.0.CO;2)
- Soden, B. J., & Held, I. M. (2006). An assessment of climate feedbacks in coupled ocean-atmosphere models. *Journal of Climate*, 19(14), 3354–3360. <https://doi.org/10.1175/JCLI3799.1>
- Somerville, R. C. J., & Remer, L. (1984). Cloud optical thickness feedbacks in the CO₂ climate problem. *Journal of Geophysical Research*, 89 (ND6), 9668–9672. <https://doi.org/10.1029/JD089iD06p09668>.
- Stammerjohn, S., Massom, R., Rind, D., & Martinson, D. (2012). Regions of rapid sea ice change: An inter-hemispheric seasonal comparison. *Geophysical Research Letters*, 39, L06501. <https://doi.org/10.1029/2012GL050874>
- Storelvmo, T., Tan, I., & Korolev, A. V. (2015). Cloud phase changes induced by CO₂ warming—a powerful yet poorly constrained cloud-climate feedback. *Current Climate Change Reports*, 1, 288–296. <https://doi.org/10.1007/s40641-015-0026-2>
- Stouffer, R. J., & Manabe, S. (2003). Equilibrium response of thermohaline circulation to large changes in atmospheric CO₂ concentration. *Climate Dynamics*, 20(7-8), 759–773. <https://doi.org/10.1007/s00382-002-0302-4>

- Tan, I., Storelvmo, T., & Zelinka, M. D. (2016). Observational constraints on mixed-phase clouds imply higher climate sensitivity. *Science*, 352(6282), 224–227. <https://doi.org/10.1126/science.aad5300>
- Taylor, K. E., Crucifix, M., Braconnot, P., Hewitt, C. D., Doutriaux, C., Broccoli, A. J., et al. (2007). Estimating shortwave radiative forcing and response in climate models. *Journal of Climate*, 20(11), 2530–2543. <https://doi.org/10.1175/JCLI4143.1>
- Taylor, K. E., Stouffer, R. J., & Meehl, G. A. (2012). An overview of CMIP5 and the experiment design. *Bulletin of the American Meteorological Society*, 93, 485–498. <https://doi.org/10.1175/BAMS-D-11-00094.1>
- Taylor, P. C., Kato, S., Xu, K.-M., & Cai, M. (2015). Covariance between Arctic sea ice and clouds within atmospheric state regimes at the satellite footprint level. *Journal of Geophysical Research: Atmospheres*, 120, 12656–12678. <https://doi.org/10.1002/2015JD023520>
- Terai, C. R., Klein, S. A., & Zelinka, M. D. (2016). Constraining the low-cloud optical depth feedback at middle and high latitudes using satellite observations. *Journal of Geophysical Research: Atmospheres*, 121, 9696–9716. <https://doi.org/doi:10.1002/2016JD025233>.
- Tian, B. (2015). Spread of model climate sensitivity linked to double-intertropical convergence zone bias. *Geophysical Research Letters*, 42, 4133–4141. <https://doi.org/10.1002/2015GL064119>
- Town, M. S., Walden, V. P., & Warren, S. G. (2007). Cloud cover over the South Pole from visual observations, satellite retrievals, and surface-based infrared radiation measurements. *Journal of Climate*, 20, 544–559. <https://doi.org/10.1175/JCLI4005.1>
- Trenberth, K. E., & Fasullo, J. T. (2010). Simulation of present-day and twenty-first-century energy budgets of the Southern Oceans. *Journal of Climate*, 23(2), 440–454. <https://doi.org/10.1175/2009JCLI3152.1>
- Trossman, D. S., Palter, J. B., Merlis, T. M., Huang, Y., & Xia, Y. (2016). Large-scale ocean circulation–cloud interactions reduce the pace of transient climate change. *Geophysical Research Letters*, 43, 3935–3943. <https://doi.org/10.1002/2016GL067931>
- Tselioudis, G., Lipat, B. R., Konsta, D., Grise, K. M., & Polvani, L. M. (2016). Midlatitude cloud shifts, their primary link to the Hadley cell, and their diverse radiative effects. *Geophysical Research Letters*, 43, 4594–4601. <https://doi.org/10.1002/2016GL068242>
- Tselioudis, G., Rossow, W. B., & Rind, D. (1992). Global patterns of cloud optical thickness variation with temperature. *Journal of Climate*, 5, 1484–1495. [https://doi.org/10.1175/1520-0442\(1992\)005<1484:GPOCOT>2.0.CO;2](https://doi.org/10.1175/1520-0442(1992)005<1484:GPOCOT>2.0.CO;2)
- Tsushima, Y., Emori, S., Ogura, T., Kimoto, M., Webb, M. J., Williams, K. D., et al. (2006). Importance of the mixed-phase cloud distribution in the control climate for assessing the

- response of clouds to carbon dioxide increase: a multi-model study. *Climate Dynamics*, 27, 113–126. <https://doi.org/10.1007/s00382-006-0127-7>
- Tsutsui, J. (2017). Quantification of temperature response to CO₂ forcing in atmosphere-ocean general circulation models. *Climate Change*, 140(2), 287–305. <https://doi.org/10.1007/s10584-016-1832-9>
- Vial, J., Dufresne, J.-L., & Bony, S. (2013). On the interpretation of inter-model spread in CMIP5 climate sensitivity estimates. *Climate Dynamics*, 41(11-12), 3339–3362. <https://doi.org/10.1007/s00382-013-1725-9>
- Wall, C. J., Hartmann, D. L., & Ma, P.-L. (2017b). Instantaneous linkages between clouds and large-scale meteorology over the Southern Ocean in observations and a climate model. *Journal of Climate*, 30, 9455-9474. <https://doi.org/10.1175/JCLI-D-17-0156.1>
- Wall, C. J., Kohyama, T., & Hartmann, D. L. (2017a) Low-cloud, boundary layer, and sea ice interactions over the Southern Ocean during winter. *Journal of Climate*, 30, 4857-4871. <https://doi.org/10.1175/JCLI-D-16-0483.1>
- Warren, S. G., Eastman, R. M., & Hahn, C. J. (2007). A survey of changes in cloud cover and cloud types over land from surface observations, 1971-96. *Journal of Climate*, 20, 717-738, <https://doi.org/10.1175/JCLI4031.1>
- Weaver, A. J., Dedlacek, J., Eby, M., Alexander, K., Crespin, E., Fichet, T., et al. (2012). Stability of the Atlantic meridional overturning circulation: A model intercomparison. *Geophysical Research Letters*, 39, L20709. <https://doi.org/10.1029/2012GL053763>
- Webb, M. J., Lambert, F. H., & Gregory, J. M. (2013). Origins of differences in climate sensitivity, forcing and feedbacks in climate models. *Climate Dynamics*, 40(3-4), 677–707. <https://doi.org/10.1007/s00382-012-1336-x>
- Webb, M. J., Senior, C. A., Sexton, D. M. H., Ingram, W. J., Williams, K. D., Ringer, M. A., et al. (2006) On the contribution of local feedback mechanisms to the range of climate sensitivity in two GCM ensembles. *Climate Dynamics*, 27, 17–38. <https://doi.org/10.1007/s00382-006-0111-2>
- Wetherald, R. T., & Manabe, S. (1988). Cloud feedback processes in a general circulation model, *Journal of Atmospheric Sciences*, 45 (8), 1397-1415. [https://doi.org/10.1175/1520-0469\(1988\)045<1397:CFPIAG>2.0.CO;2](https://doi.org/10.1175/1520-0469(1988)045<1397:CFPIAG>2.0.CO;2)
- Wigley, R. M. L., & Schlesinger, M. E. (1985). Analytical solution for the effect of increasing CO₂ on global mean temperature. *Nature*, 315(6021), 649–652. <https://doi.org/10.1038/315649a0>
- Wilks, D. S. (2016). “The stippling shows statistically significant grid points”: How research results are routinely overstated and overinterpreted, and what to do about it. *Bulletin of the*

- American Meteorological Society*, 97(12), 2263–2273. <https://doi.org/10.1175/BAMS-D-15-00267.1>
- Williams, K. D., Bodas-Salcedo, A., Déqué, M., Fermepin, S., Medeiros, B., Watanabe, M., et al. (2013). The transpose-AMIP II experiment and its application to the understanding of southern ocean cloud biases in climate models. *Journal of Climate*, 26, 3258–3274. <https://doi.org/10.1175/JCLI-D-12-00429.1>
- Williams, K. D., Ingram, W. J., & Gregory, J. M. (2008). Time variation of effective climate sensitivity in GCMs. *Journal of Climate*, 21(19), 5076–5090. <https://doi.org/10.1175/2008JCLI2371.1>
- Winker, D. M., Hunt, W. H., & McGill, M. J. (2007). Initial performance assessment of CALIOP. *Geophysical Research Letters*, 34, L19803. <https://doi.org/10.1029/2007GL030135>
- Winton, M., Griffies, S. M., Samuels, B. L., Sarmiento, J. L., & Frolicker, T. L. (2013). Connecting changing ocean circulation with changing climate. *Journal of Climate*, 26(7), 2268–2278. <https://doi.org/10.1175/JCLI-D-12-00296.1>
- Winton, M., Takahasi, K., & Held, I. M. (2010). Importance of ocean heat uptake efficacy to transient climate change. *Journal of Climate*, 23(9), 2333–2344. <https://doi.org/10.1175/2009JCLI3139.1>
- Wood, R., & Bretherton, C. S. (2006). On the relationship between stratiform low cloud cover and lower-tropospheric stability. *Journal of Climate*, 19, 6425–6432. <https://doi.org/10.1175/JCLI3988.1>
- Xie, P., & Vallis, G. K. (2012). The passive and active nature of ocean heat uptake in idealized climate change experiments. *Climate Dynamics*, 28, 667–684. <https://doi.org/10.1007/s00382-011-1063-8>
- Zelinka, M. D., & Hartmann, D. L. (2010). Why is the longwave cloud feedback positive? *Journal of Geophysical Research – Atmospheres*, 115, D16117. <https://doi.org/10.1027/2010JD013817>
- Zelinka, M. D., Klein, S. A., Hartmann, D. L. (2012a). Computing and partitioning cloud feedbacks using cloud property histograms part II: attribution to changes in cloud amount, altitude, and optical depth. *Journal of Climate*, 25, 3736–3754. <https://doi.org/10.1175/JCLI-D-11-00249.1>
- Zelinka, M. D., Klein, S. A., & Hartmann, D. L. (2012b). Computing and partitioning cloud feedbacks using cloud property histograms. Part I: Cloud radiative kernels. *Journal of Climate*, 25, 3715–3735. <https://doi.org/10.1175/JCLI-D-11-00248.1>
- Zhou, C., Zelinka, M. D., & Klein, S. A. (2016). Impact of decadal cloud variations on the Earth's energy budget. *Nature Geoscience*, 9(12), 871–874. <https://doi.org/10.1038/NGEO2828>